

In compliance with the
Canadian Privacy Legislation
some supporting forms
may have been removed from
this dissertation.

While these forms may be included
in the document page count,
their removal does not represent
any loss of content from the dissertation.

**COMPUTATIONAL ANALYSIS OF MAGNETIC
RESONANCE DATA ASSISTS IN PRE-SURGICAL
EVALUATION OF EPILEPSY PATIENTS**

by

Samson Antel

Department of Biomedical Engineering
McGill University, Montreal

November 2002

A thesis submitted to the Faculty of Graduate Studies and Research in partial fulfillment
of the requirements for the degree of

Doctor of Philosophy

Copyright

© Samson Antel, 2002



National Library
of Canada

Bibliothèque nationale
du Canada

Acquisitions and
Bibliographic Services

Acquisitions et
services bibliographiques

395 Wellington Street
Ottawa ON K1A 0N4
Canada

395, rue Wellington
Ottawa ON K1A 0N4
Canada

Your file *Votre référence*
ISBN: 0-612-88413-9
Our file *Notre référence*
ISBN: 0-612-88413-9

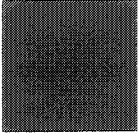
The author has granted a non-exclusive licence allowing the National Library of Canada to reproduce, loan, distribute or sell copies of this thesis in microform, paper or electronic formats.

L'auteur a accordé une licence non exclusive permettant à la Bibliothèque nationale du Canada de reproduire, prêter, distribuer ou vendre des copies de cette thèse sous la forme de microfiche/film, de reproduction sur papier ou sur format électronique.

The author retains ownership of the copyright in this thesis. Neither the thesis nor substantial extracts from it may be printed or otherwise reproduced without the author's permission.

L'auteur conserve la propriété du droit d'auteur qui protège cette thèse. Ni la thèse ni des extraits substantiels de celle-ci ne doivent être imprimés ou autrement reproduits sans son autorisation.

Canada



Abstract

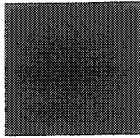
This dissertation presents a series of studies aimed at applying machine learning methods to information derived from magnetic resonance (MR) based examinations in order to aid in the pre-surgical evaluation of patients with epilepsy. Two forms of epilepsy were studied: non-lesional temporal lobe epilepsy (TLE) and extra-temporal lobe epilepsy (ETLE) due to malformations of cortical development (MCD).

Regarding patients with TLE, our aim was to predict outcome, in terms of reduction of seizure frequency, following surgical resection. To this end, we trained a Bayesian classifier on results from volumetric magnetic resonance imaging (MRI) and magnetic resonance spectroscopic imaging (MRSI), which allow rapid, non-invasive measurement of structural and metabolic data, respectively. We demonstrated that the pattern of MR markers can predict whether or not a patient with TLE will benefit from surgery.

In our studies of patients with ETLE, we focused on patients whose epilepsy was due to focal cortical dysplasia (FCD), a common form of MCD. In these patients, the identification of FCD lesions is critical in helping to direct the site of surgical resection. This is commonly performed by visual analysis of conventional MRI. The MRI characteristics of FCD are well known; however, in many patients, lesions of FCD are characterized by minor structural abnormalities that go unrecognized or are too subtle to

be detected by standard radiological analysis. Thus, the objective of this part of the dissertation was to use mathematical models of the MRI characteristics of FCD as a basis for automated detection of FCD lesions. The mathematical models included first-order statistical and morphological operators which can help measure visually discernable MRI characteristics of FCD lesions, and second-order texture analysis, which can quantify information regarding tissue structure or organization not readily accessible through visual analysis. A Bayesian classifier trained on these models demonstrated a significantly increased sensitivity in lesion detection compared to standard analysis of conventional MRI.

Both components of this thesis present clinically useful techniques for applying machine learning methods to MR data to assist in the pre-surgical evaluation of epilepsy patients. These methods are intended to be used in conjunction with conventional approaches.



Résumé

L'objectif de cette thèse est d'améliorer l'évaluation préchirurgicale des patients avec des épilepsies focales pharmacorésistantes à l'aide d'une série d'études dédiées à l'application d'algorithmes de classification automatique de données d'imagerie par résonance magnétique (IRM). Nous avons étudié deux formes d'épilepsie: l'épilepsie temporale non-lésionnelle et l'épilepsie extra-temporale due à des malformations du développement cortical (MDC).

En ce qui concerne l'épilepsie du lobe temporal, la forme la plus fréquente d'épilepsie focale, notre objectif était de prédire, en termes de réduction de nombre de crises, le résultat chirurgical. Nous avons utilisé un classificateur Bayésien sur des données d'IRM spectroscopique (IRMS) et d'IRM volumétrique qui permettent, respectivement, une quantification non-invasive de l'anatomie et du métabolisme cérébral. Nous avons démontré que des combinaisons particulières de ces données peuvent prédire les patients pour lesquels la chirurgie de l'épilepsie sera efficace.

Pour l'épilepsie extra-temporale, nous nous sommes concentrés sur l'étude de la dysplasie focale corticale (DFC), qui en est souvent la cause. L'identification d'une lésion de DFC facilite la localisation du foyer épileptique pouvant être traité chirurgicalement. La plupart du temps l'identification de DFC se fait par l'analyse visuelle de l'IRM. Bien que les caractéristiques radiologiques des lésions de DFC soient

connues, dans beaucoup de cas, ces lésions sont caractérisées par des anomalies structurelles mineures, qui peuvent passer inaperçues à l'analyse radiologique standard.

Notre objectif était d'utiliser des modèles mathématiques des caractéristiques IRM de la DFC dans le but de développer une méthode automatique de détection de ces lésions. Différents modèles sont utilisés. D'une part, des analyses statistiques de premier ordre et des opérateurs morphologiques permettent une mesure quantitative des caractéristiques IRM visibles de la DFC. D'autre part, des analyses de texture de deuxième ordre permettent la quantification de la structure et l'organisation tissulaire inaccessible à l'analyse purement visuelle. L'utilisation d'un classificateur automatique basé sur ces modèles nous a permis d'augmenter le nombre de lésions détectées par rapport à l'analyse visuelle standard des images IRM.

Les méthodes présentées dans cette thèse ont une utilité clinique dans l'évaluation préchirurgicale de l'épilepsie pharmacorésistante et peuvent être utilisées conjointement avec l'approche conventionnelle.

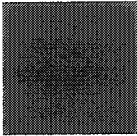


Table of Contents

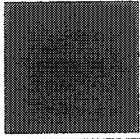
ABSTRACT.....	ii
RESUME.....	iv
ACKNOWLEDGEMENTS.....	xi
CONTRIBUTIONS TO ORIGINAL KNOWLEDGE.....	xiv
CONTRIBUTIONS OF AUTHORS.....	xvi
CHAPTER 1: INTRODUCTION	1
CHAPTER 2: REVIEW OF THE LITERATURE.....	4
2.1 TEMPORAL LOBE EPILEPSY.....	4
2.1.1 Epidemiology and surgical treatment.....	4
2.1.2 Lateralization of seizure focus using MR markers.....	5
2.1.3 MR markers as prognostic indicators of surgical outcome.....	6
2.1.4 Outcome prediction.....	7
2.2 FOCAL CORTICAL DYSPLASIA.....	8
2.2.1 Etiology and surgical treatment.....	8
2.2.2 Lesion detection on MRI.....	8
2.3 MODELING MRI CHARACTERISTICS OF FCD.....	9
2.3.1 Cortical thickness.....	9
2.3.2 GM/WM interface.....	11
2.3.3 Hyperintense T1 signal.....	12
2.4 TEXTURE ANALYSIS.....	12
2.4.1 Approaches to texture analysis.....	12

2.4.2	Applications to the medical domain.....	13
2.4.2.1	Texture analysis of brain MRI.....	14
2.4.2.2	Texture analysis of brain MRI: single ROI approach..	14
2.4.2.3	Texture analysis of brain MRI: mapping approach....	15
2.5	BAYESIAN CLASSIFICATION.....	15
2.5.1	Theory.....	16
2.5.2	Medical applications.....	17
CHAPTER 3: ASSISTING PRE-SURGICAL EVALUATION OF TLE		18
3.1.	Preface.....	18
3.2	Manuscript 1: Predicting surgical outcome in temporal lobe epilepsy patients using MRI and MRSI.....	19
	Abstract.....	20
	Introduction.....	21
	Methods.....	22
	Patients.....	22
	MRI acquisition and volumetric analysis.....	24
	MRSI acquisition and data analysis.....	26
	Design of Bayesian classifiers and statistical analysis..	28
	Results.....	29
	Worthwhile improvement vs. no worthwhile improvement.....	29
	Seizure free vs. not seizure-free.....	30
	Discussion.....	32

	References.....	38
CHAPTER 4: ASSISTING DETECTION OF FCD LESIONS.....		43
4.1	Preface.....	43
4.2	Manuscript 2: Texture analysis and morphological processing of MRI assist detection of focal cortical dysplasia in extra-temporal partial epilepsy.....	45
	Abstract.....	46
	Introduction.....	46
	Methods.....	48
	Subjects.....	48
	MRI acquisition.....	48
	Image preparation.....	49
	Image processing.....	49
	Assessment of the performance of diagnostic tests and inter-rater agreement.....	53
	Results.....	54
	Discussion.....	55
	First order texture analysis.....	56
	Morphological processing.....	57
	References.....	58
4.3	Manuscript 3: Computational models of MRI characteristics of focal cortical dysplasia improve lesion detection.....	62
	Abstract.....	63

Introduction.....	63
Methods.....	65
Patients and MRI acquisition.....	65
Image preparation.....	65
Image processing.....	66
Cortical thickness model.....	66
Blurred GM-WM interface model.....	67
Hyperintense GM model.....	68
Composite maps and contrast measurement.....	68
Statistical analysis.....	70
Results.....	70
Discussion.....	72
References.....	75
4.4 Manuscript 4: Automated detection of focal cortical dysplasia lesions using computational models of their MRI characteristics and texture analysis.....	78
Abstract.....	79
Introduction.....	80
Methods.....	82
Subjects.....	82
MRI acquisition.....	83
Image preparation.....	83
Tissue segmentation.....	84

Calculation of computational models of MRI characteristics of FCD.....	84
Cortical thickness measurement.....	85
Gradient magnitude.....	85
Relative intensity.....	88
Texture analysis.....	88
Classifier design.....	92
Analysis.....	95
Results.....	97
Discussion.....	98
References.....	104
Appendix A.....	107
CHAPTER 5: SUMMARY AND CONCLUSIONS.....	108
5.1 Predicting surgical outcome in TLE patients based on MR data..	109
5.2 Assisting lesion detection in FCD.....	110
5.3 Conclusion.....	111
BIBLIOGRAPHY.....	112



Acknowledgements

This thesis would not have been possible without the support, encouragement, and guidance of many people. Thus, the utmost appreciation is extended to:

My supervisor, Dr. Douglas L. Arnold, for always being supportive of and me and my research. He has taught me so much; not just about MR spectroscopy and the clinical issues related to my research, but also how to critically evaluate ideas and information.

Dr. Rajjan Shinghal, for his friendly encouragement and his readiness to answer any questions I had, big or small.

Dr. Robert Kearney, for his patience as I found my footing, guidance and for ensuring that, despite my best efforts to the contrary, the steps to completing this thesis were completed anywhere near on schedule.

My committee members: Dr. Louis Collins, for answering all of my image-processing questions and his assistance in reviewing all my manuscripts, and Dr. William Feindel, for his contributing his vast expertise and invaluable neurosurgical perspective.

Drs. Neda & Andrea Bernasconi, without whom this thesis would have followed a vastly different course. Their readily offered insights, guidance, and support have greatly improved the work that constitutes this thesis. I have greatly enjoyed our partnership that's developed over the course of this work and hope it will continue. Special thanks for translating the abstract into French.

Drs. Li Li Min and Fernando Cendes, for teaching me about the application of MR spectroscopy to epilepsy, and for their support as the project went along.

My friends and colleagues in the MR spectroscopy lab, past and present. Their friendship made this work enjoyable, and all their help made it possible. In alphabetical order: Zografos Caramanos, Jacqueline Chen, Dr. Nicola DeStefano, Simon Francis, Dr. Sanjay Kalra, Dr. Yevgeniy Kuznetsov, Dr. Sridar Narayanan, Dr. Wolfgang Serles, Dr. Carmela Tartaglia, Ellie Tobman, and Robin Wong. Additional appreciation goes to those in the lab who endured all the involuntary beta-testing of AVIS and AVIS_IDL.

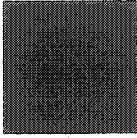
Dr. Sylvain Prima, for help in translating the abstract into French.

Dr. Joe Cousins, for introducing me to MR spectroscopy. His mentorship provided a foundation for me to undertake this thesis.

My parents, for their help, support, encouragement, and advice. And all the rides home.

My wife, Dr. Daisy Antel, for her constant support and encouragement. And for finishing her thesis first, allowing me to use her experience as a guide through the process.

And my sons: Ryan, thanks to whom I worked the “night shift” at the lab twice a week (which turned out to be my most productive hours), and Adam, who was co-operative enough to delay his arrival into the world until until one week after the thesis submission deadline.



Contributions to Original Knowledge

This thesis contains four manuscripts. Three have already been published in internationally known, peer-reviewed journals; the fourth has been submitted. The important and original contributions to scientific knowledge are outlined below.

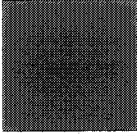
Manuscript 1: *Predicting surgical outcome in temporal lobe epilepsy using MRI and MRSI.* In this study, we applied a Bayesian classifier to pre-operative MR volumetric and MRSI data and demonstrated that the pattern across these markers can predict surgical outcome. We were the first to develop a classifier based solely on MR data for the purpose of identifying all surgical candidates, including patients achieving partial but worthwhile improvement, rather than just those likely to achieve complete freedom from seizures.

Manuscript 2: *Texture analysis and morphological processing of MRI assist detection of focal cortical dysplasia in extra-temporal partial epilepsy.* Lesions of focal cortical dysplasia can be difficult to detect on MRI, even for experienced observers. However, the primary MRI characteristics of FCD lesions (cortical thickening, blurred gray matter/white matter interface, hyperintense T1 signal) are known. Thus, we hypothesized that the implementation of computational models of these characteristics and the creation of 3D maps based on these models would assist in lesion detection. This study was the

first to propose modeling the MRI characteristics of FCD. Using our methods, lesion sensitivity was increased by 50% relative to visual analysis of conventional MRI. As lesion localization is often a prerequisite to surgical treatment of epilepsy of extra-temporal lobe origin, these results suggest that our technique may be valuable for the pre-surgical evaluation of such patients.

Manuscript 3: *Computational models of MRI characteristics of focal cortical dysplasia improve lesion detection.* Based on the success in improving lesion detection in our previous study, we hypothesized that further improvements could be achieved through the use of sophisticated techniques to better model the MRI characteristics of FCD pathology. In particular, this study was the first to apply a recently developed technique for cortical thickness measurement¹ to a clinical problem, thereby providing the first clinical validation of the technique. The results of this study demonstrated a further increase in FCD lesion visibility.

Manuscript 4: *Automated detection of focal cortical dysplasia lesions using computational models of their MRI characteristics and texture analysis.* Upon establishing the utility of computational models of MRI characteristics of FCD lesions with respect to lesion detection, we hypothesized that they, in conjunction with second order texture analysis, could be used as the basis for an automated classifier to perform automated lesion detection. This study was the first to apply texture analysis to MRI of focal cortical dysplasia patients, and the first study to perform automated detection of FCD lesions.



Contributions of Authors

In accordance with the Guidelines for Thesis Preparation of the Faculty of Graduate Studies and Research of McGill University, the contributions of individual authors to the work described in each manuscript contained in this thesis is described below.

Manuscript 1: *Predicting surgical outcome in temporal lobe epilepsy using MRI and MRSI.*

Authors: Samson B. Antel MSc, Li Li Min MD,PhD, Fernando Cendes MD,PhD, D. Louis Collins PhD, Robert E. Kearney PhD, Rajjan Shinghal PhD, Douglas L. Arnold MD.

Contributions: This study used a Bayesian classifier to analyze MR volumetric data and MRSI data acquired by Drs. Cendes and Li. The study was conceptualized through discussions between Dr. Arnold, Dr. Shinghal, and myself. I designed and implemented the Bayesian classifier, and analyzed the results. I also performed initial data interpretation and wrote the manuscript. Dr. Li assisted in the clinical interpretations of the results. All co-authors critically reviewed the manuscript.

Manuscript 2: *Texture analysis and morphological processing of MRI assist detection of focal cortical dysplasia in extra-temporal partial epilepsy.*

Authors: Andrea Bernasconi MD, Samson B. Antel MSc, D. Louis Collins PhD, Neda Bernasconi MD, Andre Olivier MD, PhD, Francois Dubeau MD, G. Bruce Pike PhD, Frederick Andermann MD, Douglas L. Arnold MD.

Contributions: This and all subsequent manuscripts in this thesis reflect a close collaboration between myself and Dr. Andrea Bernasconi. The general nature of our collaboration consisted of a shared conceptualization of the projects. I handled the development and/or implementation of image processing routines and related analysis tasks, and Dr. Bernasconi providing insight as to how to make the work clinically useful and assisting in clinical interpretation of the results.

In this particular manuscript, we implemented computational models of MRI characteristics of FCD pathology to assist in lesion detection. The project was conceived jointly by myself and Dr. Andrea Bernasconi. I performed the necessary image preparatory steps and developed and/or implemented the computational models used in the study. Drs. Andrea and Neda Bernasconi performed the MRI scans, and carried out the visual analysis of conventional MRI and the computational maps, including the manual labeling of the FCD lesions. I performed the statistical analysis, and the manuscript was written jointly by myself and Dr. Andrea Bernasconi. Drs. Andermann, Dubeau, and Olivier were involved in the clinical care of the patients. Dr. Pike provided insight on some technical issues, and Drs. Neda Bernasconi and Arnold critically reviewed the manuscript.

Manuscript 3: *Computational models of MRI characteristics of focal cortical dysplasia improve lesion detection.*

Authors: Samson B. Antel MSc, Andrea Bernasconi MD, Neda Bernasconi MD, D. Louis Collins PhD, Robert E. Kearney PhD, Rajjan Shinghal PhD, Douglas L. Arnold MD.

Contributions: This study was conceived jointly by myself and Drs. Andrea and Neda Bernasconi. I performed the necessary image preparatory steps and implemented the image-processing routines. I also performed the statistical analysis and wrote the manuscript. Drs. Andrea and Neda Bernasconi provided the manual labeling of FCD lesions on conventional MRI, and along with the rest of the authors, critically reviewed the manuscript.

Manuscript 4: *Automated detection of FCD lesions based on computational models of their MRI characteristics and texture analysis.*

Authors: Samson B. Antel MSc, D. Louis Collins PhD, Neda Bernasconi MD, Robert E. Kearney PhD, Rajjan Shinghal PhD, Douglas L. Arnold MD, Andrea Bernasconi MD

Contributions: The general idea to develop an automated classifier for FCD lesion detection was conceived jointly by myself and Dr. Andrea Bernasconi. I was responsible for the design of the classifier and the overall design of the study. I also performed the necessary image preparatory steps and implemented the image-processing routines, including the development of a library of routines to perform texture analysis on MINC volumes. Additionally, I performed the statistical analysis and wrote the manuscript. Drs. Andrea and Neda Bernasconi provided the manual labels of FCD lesions on conventional MRI, contributed clinical and neuroanatomical insights, and along with the rest of the authors, critically reviewed the manuscript.

1 ■ Introduction

The use of magnetic resonance (MR) techniques has dramatically transformed the study of epilepsy. By allowing in-vivo, non-invasive analysis of anatomical structure (in the case of magnetic resonance imaging, abbreviated as MRI) and metabolic function (through the use of magnetic resonance spectroscopic imaging, abbreviated as MRSI), MR techniques have provided previously unattainable insights into the disease, both from a research and a clinical perspective.

MR techniques can take on particular importance during pre-surgical investigation of epilepsy patients. For surgery to be a viable treatment option, a necessary (though not sufficient) step is the determination of the focus or foci of epileptic seizures. MRI and MRSI have provided crucial insight for this task.

The overall goal of this thesis is to develop computer-based classifiers which use patterns of MR data to assist in pre-surgical evaluation of epilepsy patients. Specifically, we examine two types of epilepsy: apparently non-lesional temporal lobe epilepsy (TLE), and focal cortical dysplasia (FCD), an extra-temporal epileptic disorder.

Currently, identification of surgical candidates among TLE patients proceeds via consensus evaluation of multiple modalities, including electroencephalography (EEG), MRI, neuropsychological tests and clinical examinations in order to determine if seizures

are originating predominantly from the left temporal lobe, the right temporal lobe, or both. In the case of FCD, identification of surgical candidates is largely dependent on the localization of the epileptogenic region or lesion. This task is most often carried out via careful visual examination of MRI as well as EEG evaluation.

These techniques have been well-developed over the last few years. However, 10-20% of TLE patients who undergo surgery after an extensive pre-surgical work-up do not experience a worthwhile reduction in seizure frequency following surgery. In FCD, up to 40% of lesions can go undetected during standard radiological examination, reducing the likelihood that surgery can offer help in these cases.

It is hypothesized that the application of machine learning techniques to MR data may assist in the presurgical evaluation of these patients. Thus, the specific goals of the thesis are to:

- i) assist in the identification of surgical candidates among TLE patients by developing a computer-based classifier to analyze a pattern of MR markers for a given patient and to predict whether the patient will experience a worthwhile surgical outcome (in terms of a reduction in seizure frequency).

- ii) assist in the detection of FCD lesions by (a) applying computational models of MRI characteristics of FCD pathology to enhance visual detection of FCD lesions, and (b) by combining the computational models with texture analysis of MRI to develop a computer-based classifier to locate FCD lesions.

This thesis is organized as follows. Chapter 2 provides an overview and a review of the literature pertaining to the epileptic syndromes studied in this thesis, with particular emphasis on the role played by MR modalities as part of the pre-surgical evaluation process. Chapter 2 also provides an overview and literature review of the technical methods used in the thesis, including techniques for modeling the MRI characteristics of FCD, texture analysis, and Bayesian classification theory. For the latter two techniques, emphasis is placed on their use in medical applications, particularly MRI of the brain.

Chapter 3 concerns the first goal set out above, concerning the identification of surgical candidates among TLE patients, and consists of a manuscript which describes the study we designed to address this issue.

Chapter 4 relates to computer-assisted identification of lesions of FCD, and consists of manuscripts 2, 3, and 4. Taken together, these papers trace the development of a technique for enhancing FCD lesion detection from its preliminary form as an aid for lesion detection by visual exploration through the construction of a computer-based classifier which performs automatic FCD lesion detection.

Chapter 5 presents a summary and conclusion.

2 ■ **Review of the Literature**

2.1 TEMPORAL LOBE EPILEPSY

2.1.1 Epidemiology and surgical treatment

Epilepsy is a relatively common disorder, affecting approximately 1% of the general population.^{2,3} Temporal lobe epilepsy (TLE) is one of the most common forms of epilepsy.⁴ Most cases, approximately 80%, are treated effectively with anti-epileptic medications.⁵ A recent randomized controlled study of surgery for TLE demonstrated the increased effectiveness of surgery relative to prolonged medical therapy.⁶ Nevertheless, surgery has been primarily targeted to the 20% of patients who are refractory to pharmacological treatment⁷. Studies have reported that 60-90% of patients experience a good outcome following surgery, defined as either complete or worthwhile reduction in seizure frequency⁶⁻⁹.

The two common surgical approaches to TLE are an anterior temporal lobectomy, which, as the name implies, involves the removal of the anterior portion of the temporal lobe, and a selective amygdalohippocampectomy, a more conservative resection in which all or part of the amygdala and hippocampus are removed. Arruda et al.⁹ found no difference in outcome (in terms of reduction of seizure frequency) between the two procedures.

2.1.2 Lateralization of seizure focus using MR markers

A prerequisite for surgical intervention is the lateralization of the seizure focus. Lateralization is critical for determining on which side the resection will be performed, and also to determine if contralateral abnormalities exist that may contraindicate surgery. Lateralization is generally achieved through the consensus of several methodologies, including EEG, MRI, MRSI, clinical findings, and neuropsychological testing. While EEG is often used as a gold standard for this task, much research has been done on the use of MR markers for the same purpose.

A frequent target of MR study is the hippocampus, because it is thought to play a central role in the origin and propagation of seizures^{10,11}. Multiple studies have demonstrated that mesial temporal sclerosis or hippocampal atrophy as detected on MRI can help lateralize the seizure focus in TLE.^{9,12-17}

Other structures have been examined with MRI for lateralizing efficacy. Bernasconi et al.¹⁸ demonstrated that the volume of the entorhinal cortex can help lateralize the seizure focus, while Cendes et al.¹⁹ found the same for the volume of the amygdala.

Several studies have concluded that MRSI can contribute to the lateralization of seizure focus.²⁰⁻²⁸ These studies focused on levels of N-acetyl-aspartate (NAA), a marker of neuronal integrity^{29,30}, within the temporal lobe. Connelly et al.²⁸ demonstrated the utility of MRSI in lateralizing the seizure focus in cases where MRI is inconclusive.

Perhaps the benchmark study regarding the use of MR markers to lateralize seizure focus was reported by Cendes et al.¹⁹, in which hippocampal atrophy, amygdaloid atrophy, NAA in the mid and posterior temporal lobes were analyzed together to correctly lateralize seizure focus in 98/100 patients.

2.1.3 MR markers as prognostic indicators of surgical outcome

Lateralization of the seizure focus is in itself an important predictor of surgical outcome. The more localized the epileptogenic region, the more likely it is to be completely resected. Many studies have focused on examining the prognostic value of specific MR markers. Their findings support the intuitive notion that highly localized abnormalities are correlated with a positive outcome, while more diffuse abnormalities are associated with a poorer outcome. In the review that follows, unilateral will be assumed to mean both unilateral and ipsilateral to side of maximum EEG abnormality.

Multiple studies have demonstrated that unilateral hippocampal atrophy is associated with a good surgical outcome^{9,12,31-33}. Several studies have demonstrated that in cases with bilateral hippocampal atrophy, a greater degree of abnormality within the ipsilateral hippocampus correlates with a good outcome, while symmetrical bilateral atrophy is associated with poorer outcome^{9,32}.

Ho et al.³⁴ found that patients with unilateral ipsilateral abnormalities in both the amygdala and the hippocampus fared worse following surgery compared to patient with unilateral hippocampal atrophy alone. Similarly, Kuzniecky et al.³⁵ found that patients with bilateral hippocampal atrophy and bilateral amygdaloid atrophy fared worse than patient with bilateral hippocampal atrophy alone.

Various studies have addressed the prognostic value of MRSI data. Kuzniecky et al.³⁵ found that higher NAA levels within the contralateral temporal lobe were associated with positive outcome. Ende et al.²⁰ noted that an ipsilateral decrease in NAA is correlated with a positive outcome. Li et al.³⁶ found that an absence of NAA reduction in the contralateral temporal lobe predicted good outcome in patients with bilateral hippocampal atrophy.

2.1.4 Outcome prediction

The studies just described deal primarily with group differences. What is missing is an attempt to apply these findings to individual patients. Several groups have developed computer-based classifiers to predict surgical outcome in TLE, relying heavily (but not always exclusively) upon MR markers. Arle et al.³⁷ developed a series of neural networks trained on combinations of EEG, MR, neuropsychological and pathological data to predict freedom from seizures following surgery. Grigsby et al.³⁸ developed neural network based on EEG and IQ testing to predict seizure freedom. Berg et al.³⁹ used multiple logistic regression to predict seizure freedom, using intraoperative data as input variables rather than MR data. While these classifiers were generally successful in terms of assigning patients to the correct target class, various issues limit their clinical utility, discussed in manuscript 1.

2.2 FOCAL CORTICAL DYSPLASIA

2.2.1 Etiology and surgical treatment

Focal cortical dysplasia (FCD) is one of a variety of malformations of cortical development (MCD). It was first reported by Taylor et al.⁴⁰ in 1971. FCD is characterized by a localized disruption of the normal cortical lamination associated with an excess of large, aberrant neurons, an increase in cortical thickness, and often, abnormal neuroglial elements in the underlying white matter. The dysplastic tissue retains sufficient connectivity to produce seizures.^{41,42} FCD is the most common form of developmental disorder in patients with pharmacologically intractable partial epilepsy referred for presurgical evaluation⁴³.

Localization of the FCD lesion(s) is necessary if surgical resection is to be considered. Whether additional tissue needs to be resected is a subject of much debate in the literature.⁴⁴⁻⁵³ A meta-analysis by Sisodiya⁴³ of approximately 60 studies found that 40% of FCD patients became seizure free after surgery.

2.2.2 Lesion detection on MRI

High-resolution MRI of the brain has made it possible to identify FCD in an increasing number of patients.⁵⁴ Lee et al.⁵⁵ and Chan et al.⁵⁶ described three common characteristics exhibited by FCD on MRI: i) variable degrees of cortical thickening, due to a proliferation of neurons in the affected cortical layers; ii) a poorly defined transition between gray matter and white matter, reflective of abnormal neuronal proliferation and positioning in this area; and iii) a hyperintense signal on T1-weighted MRI.

In many patients, however, lesions of FCD are characterized by minor structural abnormalities or are too subtle to be detected by standard radiological evaluation. Hence, visual analysis of conventional MRI may miss a significant proportion of FCD lesions. Thus, several techniques have been developed to assist in lesion detection. Chan et al. 1998 showed that the use of T2-weighted fast multiplanar inversion recovery images can assist visualization on conventional MRI. Bastos et al.⁵⁷ used curvilinear reconstruction (an alternative method of presenting of 3D MRI data that can improve the display of complex gyral structures of the hemispheres) to help visually identify lesions in 4 of 5 patients who had been classified as normal based on analysis of conventional MRI. Montenegro et al.⁵⁸ applied curvilinear reconstruction to improve lesion visualization in 33% of subjects. Woermann et al.⁵⁹ and Kassubek et al.⁶⁰ used statistical parametric mapping, based on voxelwise comparisons of gray level intensity in FCD patients relative to healthy controls, to help locate lesions.

2.3 Modeling MRI characteristics of FCD

One hypothesis explored in this thesis is that lesion visualization can be improved through the use of computational models of the characteristics of FCD evident on T1-weighted MRI: increased cortical thickness, blurring of the interface between gray matter (GM) and white matter (WM), and hyperintense T1 signal. Methods applied to each one are described here.

2.3.1 Measuring Cortical Thickness on MRI

Accurate measurement of cortical thickness on MRI is a challenging problem. The first step in most studies is to segment the cortex. This can be done to a good first approximation using segmentation techniques to separate the brain into its GM, WM, and cerebrospinal fluid (CSF) (and perhaps partial volume) components. Multi-channel approaches require information from two or more MRI acquisitions (e.g., T1, T2, and PD). The intensity profile across the different scans at each voxel is used to classify the voxel by tissue type. This approach was adopted in several studies.⁶¹⁻⁶⁴

Single-echo approaches rely on a single (usually T1 weighted) MRI acquisition. Some single-echo approaches rely upon analysis of the gray level intensity histogram. Momenan et al.⁶⁵ combined information from the histogram with a clustering technique to segment the brain into GM, WM, and CSF. Schnack et al.⁶⁶ described a simple method wherein polynomial curves were fitted to the intensity histogram of a T1 volume to determine an intensity threshold separating GM from WM. Other single-echo segmentation studies have relied upon the estimation of the statistical distribution of intensity for each tissue class: Shattuck et al.⁶⁷ developed statistical models of intensity distribution for tissue classes within T1 MRI, enabling tissue classification via a Bayesian classifier, while Rajapakse et al.⁶⁸ and Ruan et al.⁶⁹ combined statistical models of intensity distribution for each tissue class on T1 MRI with Markov random field models to perform tissue segmentation.

Isolating GM tissue using methods such as those described above can provide an adequate approximation of the cortex for some applications. However, such techniques generally do not address issues such as non-separation of adjacent gyri which can be an impediment to more accurate cortical extraction. Thus, more sophisticated, surface-based

techniques for cortical extraction have been developed. MacDonald et al.⁷⁰, Fischl et al.⁷¹, and Dale et al.⁷² have developed techniques incorporating anatomical constraints to achieve more accurate gyral separation. Magnotta et al.⁷³ approached the problem using a technique based on the erosion of cortical GM. Jones et al.¹ relied upon edge thinning and gradient information.

Once cortical extraction has been accomplished, most methods of measuring cortical thickness proceed by selecting a point on either the inner or outer cortical surface, using an algorithm to determine a corresponding point on the other surface, and then measuring the length of the straight line connecting the two.^{70,71,73} One drawback to this approach is that thickness is defined only for voxels along the internal and external surfaces of gyri. Further, this approach can lead to solutions that are incongruent with the structure and organization of the cortex. For instance, lines can intersect, or multiple lines can start or end at a particular voxel. To avoid such problems, a recent study by Jones et al.¹ borrows a tool from mathematical physics. The method models the cortex as an equipotential surface with boundary conditions set on both surfaces. Laplace's equation is then solved over the cortex, creating a series of "equipotential surfaces". Thickness at a given voxel is determined by the length of the path that passes through the voxel and is perpendicular to each equipotential surface. This approach avoids the problems described above. Recent studies by Yezzi et al.^{74,75} have expanded on Jones's method, using a pair of linear, first-order partial differential equations to compute path lengths after solving Laplace's equation.

2.3.2 GM/WM interface

FCD lesions often exhibit a blurred GM/WM interface, reflective of abnormal neuronal proliferation and positioning. Extraction of the GM/WM interface on MRI has been addressed largely as a by-product of cortical and WM surface extraction.^{70,76} Cook et al.⁷⁷ applied fractal analysis to MRI and found differences in fractal dimension of the GM/WM interface in patients with frontal lobe epilepsy compared to controls.

2.3.3 Hyperintense T₁ signal

This property is easily quantified through the use of first order statistics. Therefore no studies have focused on developing techniques to model this MRI characteristic of FCD.

2.4 TEXTURE ANALYSIS

The final hypothesis presented in this thesis is that combining the aforementioned computational models of MRI characteristics of FCD with texture analysis of MRI can enable automated FCD lesion identification. Texture is an important property of an image, yet it has no precise definition. In an intuitive or qualitative sense, texture can be taken to represent image properties such as shading variations, coarseness and regularity. Texture analysis seeks to quantify these patterns in a systematic way.

2.4.1 Approaches to texture analysis

There are several approaches to texture analysis. Statistical methods examine the distribution of intensity levels within an image. First order statistical methods involve analysis of the gray-level histogram. Second order statistical methods consider the spatial distribution of gray level intensities. Julesz carried out much research regarding

the discrimination of different textures based on the properties of their spatial statistics.⁷⁸⁻

⁸³ The most widely used method of analyzing second-order statistical properties was first proposed by Haralick ⁸⁴. This study described an approach to quantifying image texture by i) calculating gray-level co-occurrence matrices (GLCMs), which store information on the spatial relationship between gray-level intensity pairs by tallying the occurrences of pairs of voxels exhibiting particular intensities and separated by a given distance in a given direction, and ii) applying various texture operators to these co-occurrence matrices in an attempt to capture different aspects of the information contained therein. In the context of GLCM-based texture analysis, texture operators are mathematical functions that are calculated over the GLCM and are designed to quantify a particular aspect of the distribution of entries in the GLCM, such as the degree of clustering along the diagonal. Unless otherwise noted, in the remainder of this work it will be assumed that the term texture analysis refers to GLCM-based approach.

2.4.2 Applications to the medical domain

Although texture analysis was originally developed for non-medical applications such as satellite imagery⁸⁴, it has been employed in a variety of medical applications. Multiple studies have applied texture analysis to digital mammograms to help detect microcalcifications ⁹⁵⁻⁹⁷ or to differentiate between benign and malignant masses.⁹⁸⁻¹⁰⁴ Other applications that have been studied are the discrimination of benign moles from malignant skin cancer ^{105,106}, staging of cervical lesions ¹⁰⁷, bone loss ^{108,109}, detection of myocarditis^{110,111}, detection of diseased skeletal muscle¹¹², checking for abnormal testicular growth¹¹³, discrimination of soft-tissue tumors¹¹⁴, analysis of colorectal

tissue^{115,116}, discrimination of cirrhotic livers from normals¹¹⁷, detection of prostate cancer¹¹⁸, and detection of abnormalities within chest radiographs¹¹⁹.

2.4.2.1 Texture analysis of brain MRI

A collaboration among several research centers in Europe (the COST B11 European Community project) has focused on the application of texture analysis to MRI^{120,121}. The major output of this project has been the development of a software package (MaZda). Relatively few studies in general have reported on the application of texture analysis to brain MRI. The studies that have been published can be divided into two groups based on the way in which texture analysis is applied.

2.4.2.2 Texture analysis of brain MRI: single ROI approach

In this approach, texture analysis is applied to one or more isolated regions of interest (ROI) such as a 2D MRI slice or a brain tumor. In most studies of this nature, the object is to perform differential diagnosis or to characterize disease progression. Freeborough & Fox¹²² were able to discriminate between brains of Alzheimer's patient and normal controls using texture analysis. They also report using texture analysis to track the progress of the disease. Mathias et al.¹²³ could differentiate between spinal cord cross-sections of controls and MS patients, as well as monitor changes associated with the course of MS. Yu et al.¹²⁴ used texture analysis to distinguish between active and non-active MS plaques. Schad et al.¹²⁵ and Lerski et al.¹²⁶ were able to differentiate between edema and tumors. Yu et al.¹²⁷ revealed abnormalities in apparently normal hippocampi contralateral to hippocampal sclerosis.

2.4.2.3 Texture analysis of brain MRI: mapping approach

To perform texture mapping, a small region of interest (ROI) is centered on each voxel within an image. Texture analysis is then performed over each ROI, and the resulting texture property mapped to the location of the center voxel to create the texture map. The few studies applying this technique to MRI have been concerned with lesion or tissue segmentation.

Kjaer et al.¹²⁸ achieved success in segmenting brain tumors using texture mapping. As well, they were able to distinguish between edema and tumours. Kovalev¹²⁹ used texture mapping based on a six-dimensional co-occurrence matrix to distinguish between patients with mild cognitive disturbances and healthy older control subjects. They were also successful in segmenting regions exhibiting diffuse white matter hypointensities. The six dimensional co-occurrence matrix was arrived at by considering the co-occurrences of gradient magnitude and direction for voxel pairs in addition to gray level intensity.

2.5 BAYESIAN CLASSIFICATION

The two main components of this thesis are computer-assisted prediction of surgical outcome in TLE patients and computer-assisted identification of lesions on T1-MRI of FCD patients. Bayesian classifiers trained on MR data were used as tools to accomplish these tasks and were not themselves the focus of the research. Further, Bayesian theory and classification are well-developed and widely used concepts, and current research in this area is outside the scope of this thesis. Thus this section will be

limited to the presentation of an overview of Bayesian theory and some examples of its application to the medical domain.

2.5.1 Theory

A Bayesian classifier is a machine learning technique which employs Bayesian decision theory to assign a previously unseen instance (e.g., a patient, a voxel, etc.) into a target category given a training sample. The eponymous Bayesian decision theory was developed by the mathematician Thomas Bayes¹³⁰. More recent treatments are given by Mitchell¹³¹ and Duda et al.¹³². Bayesian decision theory rests upon the relationship known as Bayes theorem of conditional probability: $P(A|B)=P(B|A)P(A)/P(B)$, where $P(A|B)$ is termed conditional probability, i.e., the probability of observing A given that B is true. The basic classification task is to assign an instance into the most likely class $c_i \in \{c_1, \dots, c_n\}$, based on a set of data values \mathbf{X} ; that is, to find the c_i that maximizes $P(c_i|\mathbf{X})$. $P(c_i|\mathbf{X})$ is termed the posterior probability. While the posterior probability is generally difficult to determine experimentally, the class-conditional probability $P(\mathbf{X}|c_i)$ can often be estimated from experimental data. Bayes theory allows the computation of the posterior probability based on the class-conditional probability as follows:

$$P(c_i|\mathbf{X})=P(\mathbf{X}|c_i)P(c_i)/P(\mathbf{X})$$

where $P(c_i)$ is termed the prior probability and represents the likelihood of an instance belonging to class c_i given the absence of any other data, i.e. it's prevalence in nature, and $P(\mathbf{X})$ indicates the probability of observing the particular set of data values. Once $P(c_i|\mathbf{X})$ is calculated for all i , the Bayes decision rule can be used to classify the instance: classify as c_i if $P(c_i|\mathbf{X}) > P(c_j|\mathbf{X})$ for all $j \neq i$.

When X consists of multiple attribute values $[x_1, x_2, \dots, x_n]$, the covariance amongst the various attributes needs to be calculated to determine $P(X|c_i)$. For some applications such as text processing, this is not feasible and necessitates the assumption of conditional independence amongst attributes. The result is the naïve, or simple, Bayes classifier¹³¹:
decide c_i if $P(c_i)\prod P(x_k|c_i) > P(c_j)\prod P(x_k|c_j)$ for all $j \neq i$ and $k=1:n$. The assumption of conditional independence is not always justified in some applications. However, Domingos and Pizzani¹³³ have demonstrated that the simple Bayes classifier can perform at or near optimal levels even if the independence assumption is violated. For continuously valued data such those used in this thesis, the covariance between attributes is readily calculated, and thus the full Bayesian classifier was used.

2.5.2 Medical applications

Medical applications of Bayesian classifiers are numerous and include skin lesion detection¹³⁴, identification of patients at risk for femoral neck fractures¹³⁵, prognosis of patients with femoral neck fracture¹³⁶, diagnosis of sports injuries¹³⁷, diagnosis of hypertension based on heart rate variability¹³⁸, detection of contraction in the gastrointestinal tract¹³⁹, detection of EEG patterns related to nocturnal hypoglycemia¹⁴⁰, staging of astrocytomas¹⁴¹, and classification of sleep stage based on EEG¹⁴².

3

Assisting pre-surgical evaluation of TLE

3.1 Preface

The inclusion of MR methods as part of the pre-surgical evaluation of TLE has lowered the costs and risks associated with this monitoring by reducing reliance on techniques such as video-EEG which require prolonged hospitalization in highly specialized units. Many studies have demonstrated the role of MR markers in lateralizing seizure focus and have examined the relationship of these markers to surgical outcome in TLE patients. Most of these studies, however, have focused on group differences; few have attempted to predict outcome for a particular patient based on MR or other data. Further, the outcome-predictor studies published to date present classifiers that have been trained to predict freedom from seizures, rather than to identify all patients likely to achieve a worthwhile or better reduction in seizure frequency.

Given the non-invasiveness and reduced costs associated with MR investigations, and the evidence of correlation of MR markers with surgical outcome, we undertook the following study to train a classifier on MR data to help identify TLE patients likely to benefit from surgery.

3.2 Manuscript 1

Presented in part at the:

•Joint European Conference on Artificial Intelligence in Medicine and Medical Decision Making, 1999.

•American Epilepsy Society annual meeting, 2000.

•3rd International Magnetic Resonance and Epilepsy Symposium, 2000.

Published in *Neurology* 2002;58(10):1505-1512.

Predicting Surgical Outcome in Temporal Lobe Epilepsy Patients Using MRI and MRSI.

Antel SB, M.Sc.^{1,3}; Li LM, MD, PhD^{2,3}; Cendes F, MD, PhD^{2,3}; Collins DL, PhD^{1,2}; Kearney RE, PhD¹; Shinghal R, PhD⁴; Arnold DL, MD, FRCP(C)^{2,3}

¹Departments of Biomedical Engineering, and ²Neurology and Neurosurgery, McGill University.

³MR Spectroscopy Unit, Montreal Neurological Institute and Hospital.

⁴Department of Computer Science, Concordia University.
Montreal, Canada

Address for Correspondence:

Douglas Arnold, MD
Montreal Neurological Institute
3801 University St.
Montreal, PQ H3A 2B4
Canada
Phone: (514)-398-8185
Fax: (514)-398-2975
doug@mrs.mni.mcgill.ca

ABSTRACT

Objective: To develop a classifier which uses magnetic resonance data to predict surgical outcome in patients with temporal lobe epilepsy (TLE).

Methods: Eighty-one patients with medically refractory TLE who underwent surgical treatment were studied. Patients underwent comprehensive pre-surgical investigation, including ictal video EEG recording, proton magnetic resonance spectroscopic imaging, and volumetric MRI. Outcome was measured using Engel's classification system, condensed into two outcome groups. Two approaches were taken. First, outcome was defined as experiencing worthwhile improvement with > 90% reduction of seizure frequency (Classes I, II, & III) or not (class IV). A second approach was to define outcome as experiencing freedom from seizure following surgery (Class I) or not (Classes II, III, & IV). For each approach, we constructed a Bayesian classifier to predict outcome by calculating the probability of a patient's pattern of results from spectroscopic analysis of the temporal lobes and volumetric analysis of the amygdala and hippocampus being associated with the various outcome groups.

Results: The worthwhile improvement classifier correctly predicted the surgical outcomes of 60/65 (92%) of patients who experienced worthwhile improvement, and 10/16 (63%) of patients who did not. The seizure-free classifier correctly predicted the surgical outcomes of 39/52 (75%) of patients who became seizure-free, and 21/29 (72%) of patients who did not.

Conclusions: Magnetic resonance features are important markers of surgical outcome in temporal lobe epilepsy patients and can provide assistance in identifying surgical candidates.

INTRODUCTION

Surgical treatment of refractory temporal lobe epilepsy (TLE) via a selective amygdalohippocampectomy or an anterior temporal lobe resection has been shown to be an effective means of seizure control for about 70-80% of patients.¹ Pre-surgical assessment of prognosis is based on the convergence of results from multiple pre-surgical investigations, including prolonged video-EEG monitoring, neuroimaging, and neuropsychological tests. Video-EEG remains the most widely accepted standard for definition of the epileptogenic area; however, such examination is costly and inconvenient, requiring prolonged hospitalization in highly specialized units. Even after this extensive examination, a proportion (20-30%) of patients do poorly after surgery.^{2,3} Improved methods for lateralization of TLE and predicting surgical outcome could greatly facilitate the selection of patients for surgery. Towards this end, we have developed a statistical model to predict surgical outcome, based on data from proton magnetic resonance spectroscopic imaging (MRSI) and volumetric MRI.

MRSI and MRI allow rapid, non-invasive measurement of structural and metabolic data from the brain, in vivo. Studies have demonstrated the utility of MRSI and volumetric MRI in the lateralization of seizure focus.⁴⁻⁸ {77 /id Kuzniecky, Hugg, et al. 1998} Furthermore, results from MRSI and volumetric MRI have been shown to correlate with surgical outcome. In particular, unilateral ipsilateral hippocampal atrophy has been correlated with good surgical outcome⁹⁻¹³, whereas bilateral hippocampal atrophy has been associated with poorer surgical outcome.¹¹ Hippocampal atrophy in conjunction with amygdaloid atrophy¹⁴, and decreased levels of N-acetyl-aspartate

(NAA) in the contralateral posterior temporal lobe^{15, 16} decrease the odds of a good surgical outcome. Such results, however, do not provide a quantitative prediction of an individual patient's chances for a good outcome from surgical intervention.

Few studies have attempted to generate predictions for surgical outcomes for individual patients based on pre-surgical evaluations. Neural network models have been proposed^{17, 18} which achieve a high rate of success at predicting freedom from seizures following surgery. However, the clinical utility of neural networks is diminished by the difficulty of interpreting the highly complex relationship between the input data and the outcome prediction. With this in mind, we have constructed Bayesian classifiers^{19, 20} based on pre-surgical MRI volumetry and MRSI to predict surgical outcome in TLE patients. A Bayesian classifier produces a quantitative assessment of an individual patient's chances of a worthwhile surgical outcome, and is robust to noisy data. The relationship between the input data and the outcome prediction is straightforward. A set of a priori class-conditional probabilities (the probability of observing some input data given a particular class) are transformed into a posteriori probabilities (the probability of an instance belonging to a given class given its input data) through the application of Bayes's theorem of conditional probability. The classifiers developed in this paper are based on MR data that can be acquired rapidly, non-invasively, and on an outpatient basis.

METHODS

Patients

Subjects for this study were drawn from 318 consecutive patients with pharmacologically refractive suspected TLE seen by the epilepsy service at the Montreal Neurological Hospital between 1994 and 1998. Of these 318 patients, 201 patients were not operated, either because they were on a surgical waiting list, or were still undergoing investigation, or a consensus assessment (of neurosurgeons, neurologists, and neuropsychologists) was not reached during conventional pre-surgical evaluation. Of the remaining 117 patients who did undergo surgery, 36 were excluded from the study due to either extra-temporal involvement (n=9), the presence of a space occupying lesion (e.g., tumor, vascular malformation, n=12), lack of pre-operative volumetric MRI or MRSI data (n=5), or lack of follow-up data (n=10).

Thus, the patient database for this study consisted of 81 individuals (50 women, 31 men) with "non-lesional" TLE (mean age 35 +/- 11.2 years). All patients underwent surgical treatment for TLE; 41 patients underwent anterior temporal lobe resection, and 40 patients underwent a selective amygdalo-hippocampectomy. No significant differences were found between these two patient groups on any of the variables utilized in this study. All patients underwent prolonged video-EEG monitoring, using the International 10-20 system including sphenoidal electrodes, and were operated on the side of maximum EEG abnormality. The determination of side of maximum EEG abnormality reflected the overall prolonged EEG analysis. For patients in whom lateralization by ictal onset was not congruent with lateralization by inter-ictal EEG, or in

whom a seizure onset on one side was followed by intra-ictal activity that predominated on the opposite side, the ictal findings and the side of initial ictal changes were accorded greater influence for the purpose of lateralization. The mean follow-up was 38.1 months (range from 9.2 to 78.2 months; 18 patients had less than a 2-year follow up). Surgical outcomes were assessed using Engel's modified classification scheme.²¹ The breakdown of the patients' surgical outcomes was as follows: 52 patients with Class I outcome (free of seizures or residual auras), 1 with Class II outcome (less than 3 seizures per year), 12 with Class III outcome (worthwhile improvement, >90% reduction in seizure frequency), and 16 with Class IV outcome (no worthwhile improvement, <90% reduction in seizure frequency).

Due to the small number of patients in Classes II and III, we grouped patients into two consolidated outcome groups for classification purposes. Two approaches were used. For the first approach, outcome was defined as experiencing worthwhile improvement in terms of seizure frequency (Engel's Classes I, II, and III, n=65), or not (Engel's Class IV, n=16). This grouping was chosen in order to consider the largest possible number of patients who would attain at least some benefit from surgery. For the second approach, outcome was defined as being free from seizures following surgery (Engel's Class I, n=52), or not (Engel's Classes II, III, and IV, n=29). This grouping was used because freedom from seizures is the optimal outcome and therefore the one sought by many patients.

MRI acquisition and volumetric analysis

MRI studies were performed using a Philips ACS II or III combined imaging and spectroscopy system (1.5 T, Philips Medical Systems, Best, The Netherlands). Because of

changes in clinical practice at our institute, two MRI volumetry protocols were used over the course of this study. Initially, we used 3-mm thick, contiguous coronal slices perpendicular to the plane of the Sylvian fissure acquired with a three-dimensional fast-field echo or inversion recovery sequence (n=20). Subsequently, we used global MR images obtained with an interpulse delay (TR) of 18 ms, a gradient-echo refocusing time (TE) of 10 ms, a 30° angle, and 1 mm isotropic voxels (n=61). The MRI data were exported to a SunSparc workstation and the volumes of the left and right amygdaloid and

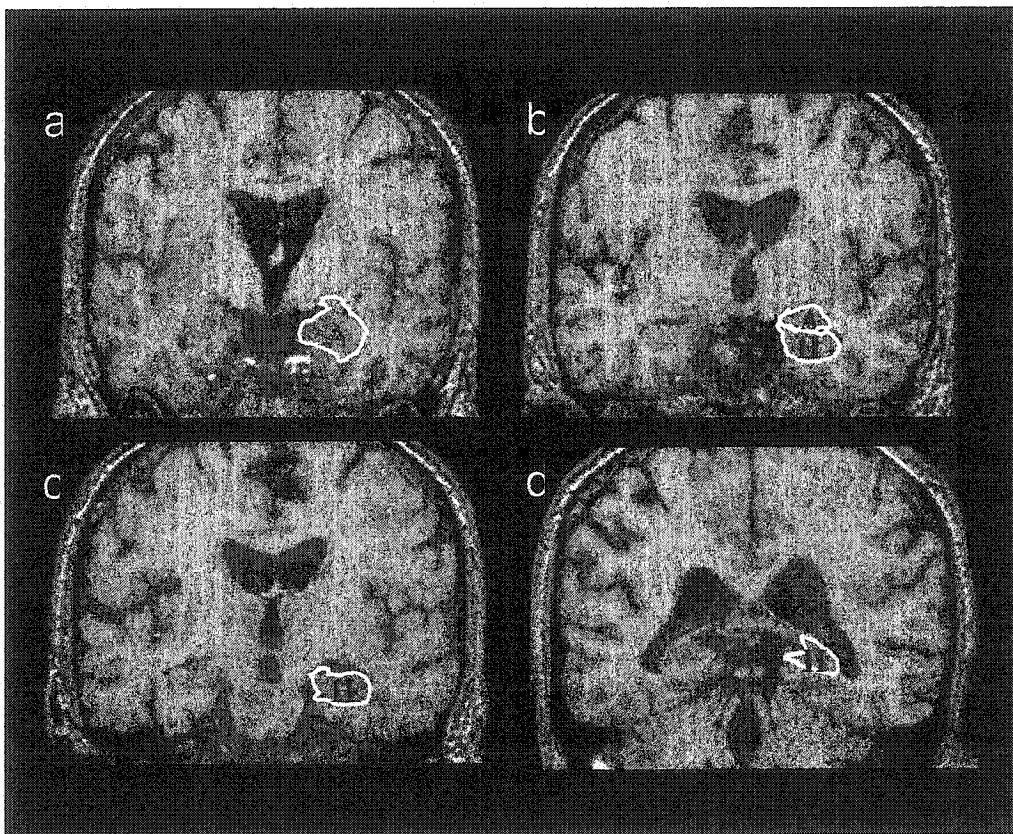


Figure 1. MRI volumetry protocol. Angled coronal MRIs of the cerebral hemispheres with mesial structures outlined on the left side. a) amygdala (A). b) Posterior portion of the amygdala (top) and head of hippocampus (H) (bottom). c) body of hippocampus. d) tail of hippocampus.

anatomical protocol (figure 1) described elsewhere.²² All volumetric analyses were done blind as to the side of the seizure focus.

As described previously⁴, the volumes of the left and right amygdalae and hippocampi were obtained. Asymmetry scores for the amygdaloid and hippocampal volumes were calculated as $(\text{left volume} - \text{right volume}) / [(\text{left volume} + \text{right volume}) / 2]$. These six values were transformed into Z-scores by comparison to measurements made on a group of healthy control subjects using the same two protocols (n=30 and n=22, respectively). Z-scores were subsequently categorized as contralateral or ipsilateral relative to side of surgery, rather than left or right.

MRSI acquisition and data analysis

MRSI studies were performed using the same scanner. Scout images were obtained in the axial and sagittal planes. These were followed by acquisition of a multi-slice transverse spin-echo MRI using a TR of 2000 ms and a TE of 30 ms. The temporal lobe MRSI volume of interest (VOI) included part of the head, the whole body and the whole tail of the left and right hippocampi, as well as portions of gray and white matter in the mid and posterior parts of the temporal lobes (figure 2). The size of this VOI was approximately 85-100 mm in the left-right axis, 75-95 mm in the antero-posterior axis, and 20 mm in thickness. After post-processing, individual voxels within the VOI measured approximately 12 mm x 12 mm x 20 mm.

A water-suppressed MRSI was acquired from the VOI (TR = 2000 ms, TE = 272 ms, 250 x 250 mm field of view (FOV), and 32 x 32 phase-encoding steps), followed by a MRSI without water suppression (TR = 850 ms, TE = 272 ms, 250 x 250 mm FOV, and

16 x 16 phase-encoding steps). Post-processing included zero-filling the non-water-suppressed MRSI to obtain 32 x 32 profiles, followed by application of a mild Gaussian k -space filter and an inverse 2D Fourier transformation to both water-suppressed and non-suppressed MRSI scans. The resulting time domain signal was left-shifted and subtracted from itself to improve water suppression.²³

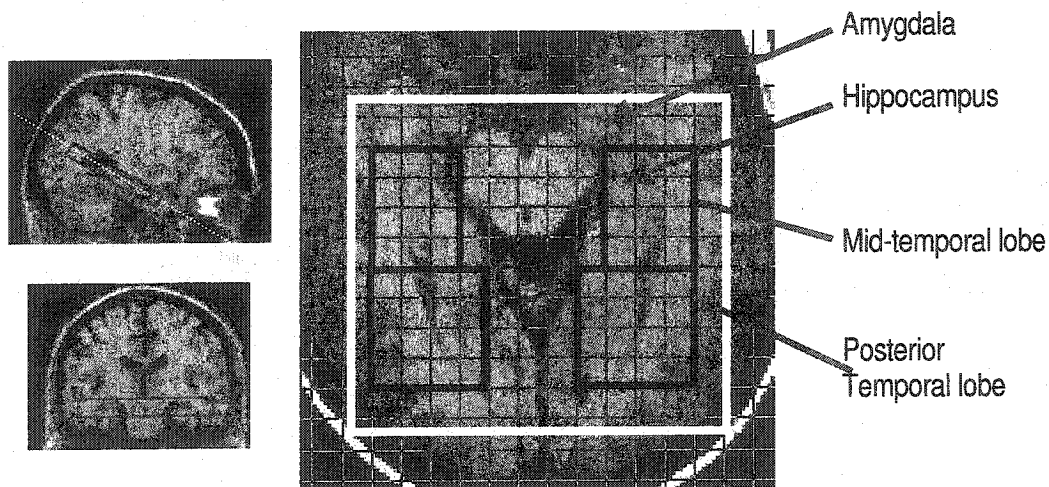


Figure 2. Proton magnetic resonance spectroscopic imaging (MRSI) volume of interest (VOI). Positioning of VOI (outer rectangle) was angled along the hippocampal axis (dotted line on sagittal slice). The size of VOI was ~85-100 mm in the left-right axis, 75-95 mm in the antero-posterior axis, and 20 mm in thickness. After post-processing, individual voxels within the VOI were ~ 12mm x 12mm in plane. The medial temporal lobe included the head and part of the body of the hippocampus. The posterior temporal lobe included the tail and part of the body of the hippocampus, as well as axonal projections.

MRSI spectra were excluded from the analyses if they were artifactually broadened (*i.e.* full width at half maximum >10 Hz). For each subject, locally developed

software was used to calculate the average NAA/Cr values for the mid and posterior regions of interest (ROI) in left and right medial temporal lobes, as previously described⁴. The mid temporal ROI included tissue from the head and body of the hippocampus, whereas the posterior temporal ROI included tissue from the tail of the hippocampus. Both ROIs also included surrounding portions of gray and white matter. Asymmetry scores for mid-temporal NAA/Cr and posterior temporal NAA/Cr were calculated as $(\text{left value} - \text{right value}) / [(\text{left value} + \text{right value}) / 2]$. The regional NAA/Cr levels and asymmetry values were transformed into Z-scores by comparison to measurements made on a group of 30 healthy control subjects. Z-scores were subsequently categorized as contralateral or ipsilateral relative to side of surgery, rather than left or right. All MRSI analyses were done blind as to the side of the seizure focus.

Design of Bayesian classifiers and statistical analysis

The Bayesian classifiers were implemented in MATLAB 4.2 (The MathWorks Inc., Natick, MA) running on a Red Hat Linux 5.2 platform. A Bayesian classifier predicts outcome based on how closely a pattern of data for an individual matches those of the outcome groups based on conditional probability distributions. The major steps involved in constructing our Bayesian classifiers were to i) estimate the probability of a patient from each outcome group having a particular pattern of results (class conditional probability); ii) calculate class-conditional covariance matrices for the variables used as inputs to the classifier; iii) use the results of steps i and ii to calculate the distance (in feature space) from a particular patient's pattern to that of each of the target classes; iv) use the results from steps i-iii to determine the probability of a patient belonging to each

outcome group; v) assign the patient to the outcome group associated with the highest probability. Detailed treatment of Bayesian classification methods can be found elsewhere.^{19, 20} Due to the limited sample size, we were unable to use separate training and testing sets. Rather, we used the leave-one-out cross-validation technique²⁴, wherein each individual case is withheld and subsequently classified using the remaining N-1 cases as the training set.

The volumetric MRI and MRSI investigations yielded 12 features which could be used as inputs to the classifier. These were ipsilateral, contralateral, and asymmetry Z-scores for each of the following: hippocampal volume, amygdaloid volume, NAA/Cr in the mid-temporal lobe, and NAA/Cr in the posterior temporal lobe. The choice of which combination of MR features to feed into the classifier was based on an automated, exhaustive feature-space search over these twelve available features.²⁵ For each of the twelve attributes, we performed two-tailed t-tests across the two outcome groups.

RESULTS

Worthwhile improvement vs. no worthwhile improvement.

After an exhaustive feature-space search, it was found that the highest classification accuracy for predicting whether a patient would experience worthwhile improvement following surgery was achieved using the following combination of input variables (in no particular order): NAA/Cr in the ipsilateral mid-temporal region, NAA/Cr in the ipsilateral posterior temporal region, amygdaloid asymmetry, and hippocampal asymmetry. Using this combination of features, 60 out of 65 (92%, 95% confidence interval = {89.3%-95.3%}) patients who had worthwhile improvement and 10 out of 16

(63%, 95% confidence interval = {50.4% - 74.6%}) of patients who did not have worthwhile improvement were correctly classified, as shown in table 1. Predictive value was 91% for patients who had worthwhile improvement, and 67% for patients who did not have worthwhile improvement.

	Predicted WI	Predicted NWI	Accuracy
True WI (n=65)	60	5	92%
True NWI (n=16)	6	10	63%
Predictive Value	91%	67%	Overall: 86%

Table 1. Confusion matrix for Bayesian classifier: predicting worthwhile improvement. WI=patients with worthwhile improvement in seizure frequency following surgery (Engel's class I,II, & III). NWI=patients with no worthwhile improvement in seizure frequency following surgery (Engel's class IV).

Seizure-free vs. not seizure-free

After a separate exhaustive feature-space search, it was found that the highest classification accuracy for predicting patients to be seizure free following surgery was achieved using the following combination of input variables (in no particular order): asymmetry of NAA/Cr in the mid-temporal region, NAA/Cr in the contralateral posterior temporal region, asymmetry of NAA/Cr in the posterior temporal region, and hippocampal asymmetry. Using this combination of features, 39 out of 52 (75%, 95% confidence interval = {64%-86%}) patients who were seizure-free, and 21 out of 29 (72%, 95% confidence interval = {56% - 88%}) of patients who were not seizure-free

were correctly classified, as shown in table 2. Predictive value was 83% for seizure-free patients, and 62% for patients who did not become seizure-free.

Figure 3 shows box-and-whisker plots representing the distribution of all twelve features for the two outcome groups. Asymmetry values were significantly more accentuated ipsilaterally for NAA/Cr in both the mid and posterior temporal lobes, and for hippocampal and amygdaloid volumes in patients who had worthwhile improvement compared to patients who did not have worthwhile improvement. NAA/Cr in the contralateral posterior temporal region and contralateral hippocampal volume were significantly lower in patients who did not have worthwhile improvement as compared to patients who had worthwhile improvement.

	Predicted SF	Predicted NSF	Accuracy
True SF (n=52)	39	13	75%
True NSF (n=29)	8	21	72%
Predictive Value	83%	62%	Overall: 74%

Table 2. Confusion matrix for Bayesian classifier: predicting freedom from seizures. SF=patients who became seizure-free following surgery (Engel's Class I). NSF=patients who did not become seizure-free following surgery (Engel's Class II, III, & IV).

Figure 4 shows box-and-whisker plots representing the distribution of all twelve features for seizure-free vs. non-seizure-free patients. NAA/Cr in the contralateral posterior temporal lobe was significantly higher, and asymmetry of NAA/Cr in the posterior temporal lobe was significantly more accentuated ipsilaterally for seizure-free patients.

DISCUSSION

The Bayesian classifiers developed in this study provide a simple method of utilizing MR results to predict surgical outcome in TLE patients. For both classification problems, there was considerable overlap between the two outcome groups for all twelve MR attributes (figures 3 and 4), demonstrating the robustness of the classifiers to such data.

The worthwhile improvement classifier correctly predicted poor outcome for more than half of the patients who experienced no worthwhile improvement following surgery. This is an important result because the conventional pre-surgical evaluation process identified all patients in this study as viable surgical candidates (indicated by the very fact that they underwent an operation).

For the patients included in this study, the overall accuracy of the worthwhile improvement classifier (defined as the number of correct predictions across outcome group divided by the total number of patients; see table 1) was higher (70/81, or 86%) than conventional pre-surgical evaluation (65/81, or 80%; all 81 patients in the study were operated upon, indicating an expectation of worthwhile improvement in all cases. This expectation was correct for the 65 patients who experienced worthwhile improvement following surgery). Unfortunately, a full comparison of the predictions made by this classifier to the predictions based on conventional pre-surgical evaluation is impossible. Predictions of no worthwhile improvement generated by the classifier can be checked against actual surgical outcome because surgery was performed on all patients in this study. However, predictions of no worthwhile improvement made by conventional

pre-surgical evaluation (i.e., a decision to not operate) cannot be tested against actual surgical outcome, since surgery was not performed in these cases. For the seizure-free classifier, comparison to the results of conventional pre-surgical evaluation is not possible, as predictions regarding freedom from seizures were not recorded as part of the standard pre-surgical evaluation, and are not necessarily the basis for a decision to operate.

For both classifiers, it is difficult to draw conclusions from the combination of features that produced the highest classification accuracy, since our relatively small sample size precludes finding significant differences in classification accuracy across various feature combinations. A more important point is that MR features can be used to predict an individual patient's surgical outcome with reasonable accuracy. These features directly address the neurodegenerative aspects of TLE. Atrophy of the mesial temporal structures results from neuronal loss. Decreases in NAA/Cr levels can indicate either neuronal loss or dysfunction.³¹ Thus, the pattern of MRI and MRSI markers over the various regions and structures of interest can indicate the distribution of structural or metabolic changes within the mesial temporal lobes and therefore help define the area(s) involved in seizure generation.

Methods for lateralizing seizure foci in TLE patients using only MRSI and volumetric MRI have been previously established.^{4, 5, 15} An MR-based classifier for outcome prediction that is not dependent on *extensive* EEG results could eventually lead to faster and less invasive techniques for pre-surgical evaluation. This is not to say that conventional depth-EEG evaluation is unnecessary. Our classifiers were developed and

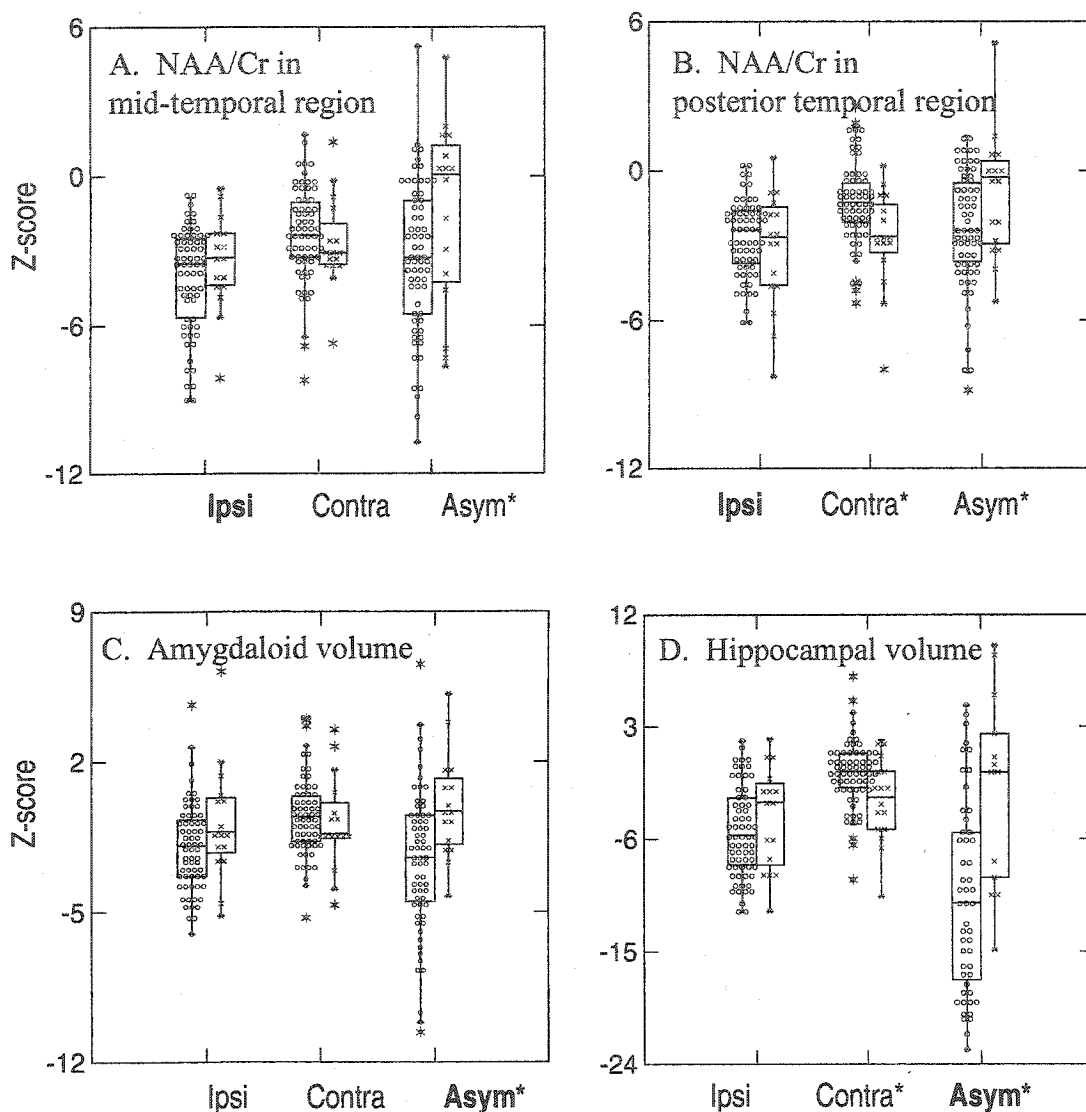


Figure 3. Box-and-whisker plots showing the distribution of the twelve MR features (in Z-scores) for patients with worthwhile improvement in seizure frequency following surgery (Engel's Classes I-III) compared to patients with no worthwhile improvement in seizure frequency following surgery (Engel's Class IV). The height of each box describes the range within which the central 50% of values fall. The top and bottom edges of the box indicate the 75th and 25th percentiles, respectively. The whiskers indicate the range of observed values that fall within 1.5*(75th percentile – 25th percentile). The overlaid symmetrical dot density plot displays the density of the data points; o = worthwhile improvement (n=65), x = no worthwhile improvement (n=16). A) NAA/Cr in the mid-temporal region; B) NAA/Cr in the posterior temporal region; C) amygdaloid volume; D) hippocampal volume. Ipsi=ipsilateral value; Contra=contralateral value; Asym=asymmetry score. Asterisks (*) indicate a significant difference between the two outcome groups; **bold type** indicates features used as inputs to the classifier..

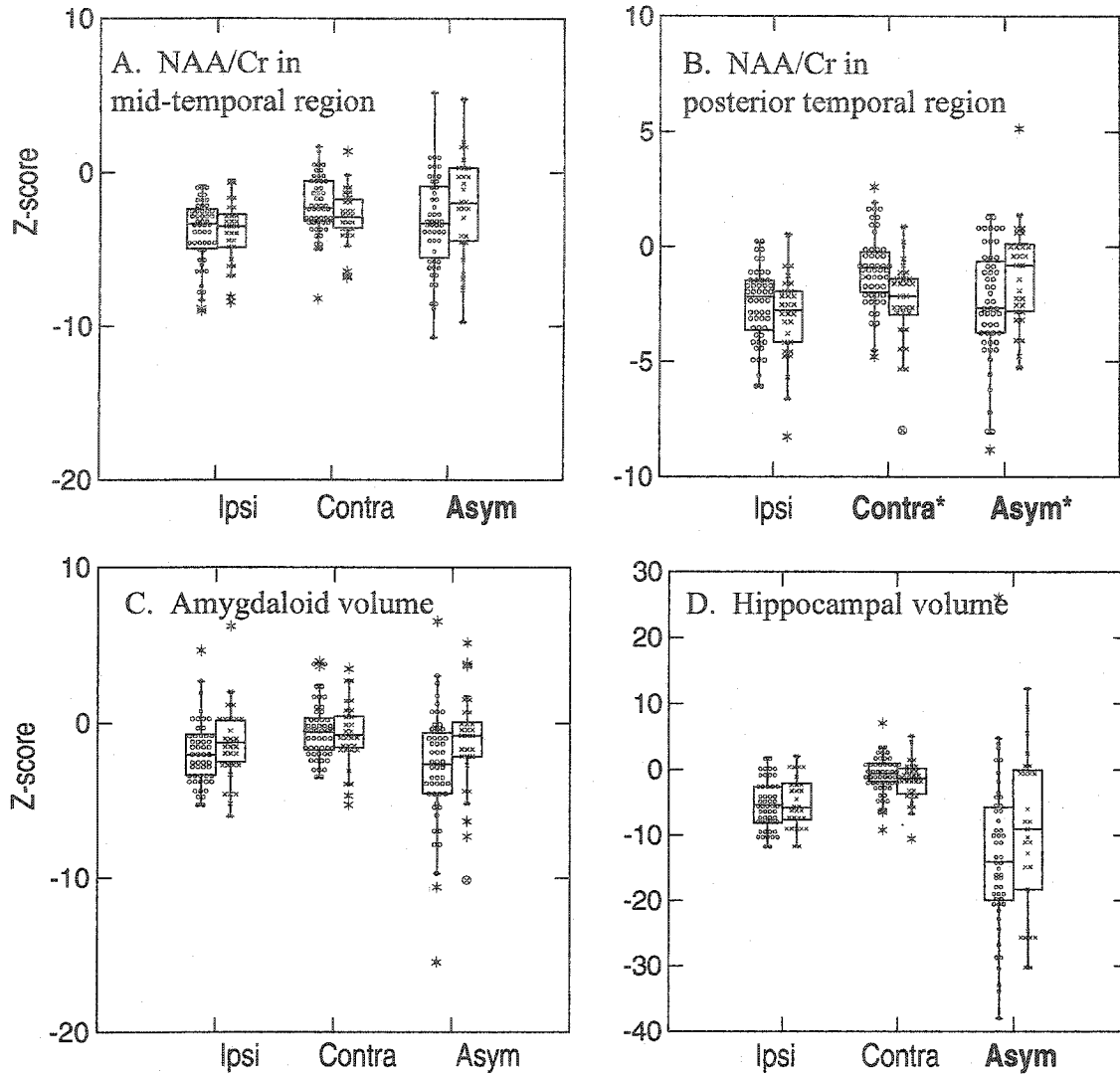


Figure 4. Box-and-whisker plots showing the distribution of the twelve MR features (in Z-scores) for patients who became seizure free following surgery (Engel's Class I) compared to those who did not (Engel's Classes II-IV). The height of each box describes the range within which the central 50% of values fall. The top and bottom edges of the box indicate the 75th and 25th percentiles, respectively. The whiskers indicate the range of observed values that fall within 1.5*(75th percentile – 25th percentile). The overlaid symmetrical dot density plot displays the density of the data points; o = worthwhile improvement (n=65), x = no worthwhile improvement (n=16). A) NAA/Cr in the mid-temporal region; B) NAA/Cr in the posterior temporal region; C) amygdaloid volume; D) hippocampal volume. Ipsi=ipsilateral value; Contra=contralateral value; Asym=asymmetry score. Asterisks (*) indicate a significant difference between the two outcome groups; **bold type** indicates features used as inputs to the classifier..

tested only on patients already diagnosed with TLE. However, the classifiers do offer the potential of more efficient pre-surgical evaluation.

Comparing patients who experienced worthwhile improvement to those who did not, all four asymmetry indices differed significantly across outcome group, with patients who had worthwhile improvement having more negative values, indicating a more ipsilaterally-weighted abnormality. These results support previous studies of the relationship of amygdaloid²⁶ and hippocampal^{9, 11} asymmetry, and mid and posterior temporal lobe NAA/Cr asymmetry^{15, 27} to surgical outcome. The value of asymmetry scores was highlighted by the finding that while neither ipsilateral nor contralateral amygdaloid volumes differed significantly across outcome group, asymmetry of amygdaloid volume was significantly different for patients who had worthwhile improvement compared to patients who did not have worthwhile improvement.

NAA/Cr in the *contralateral* posterior temporal lobe was found to be significantly lower for patients with no worthwhile improvement compared to patients with worthwhile improvement. These findings support previous work in which NAA reduction in the contralateral posterior temporal lobe significantly increased the chances of poor surgical outcome in patients with bilateral hippocampal atrophy¹⁵ and in patients with normal-appearing hippocampi.¹⁶ The results of the present study suggest this holds regardless of a patient's volumetric results and indicate that NAA/Cr in the posterior temporal region is an important prognostic marker.

Contralateral hippocampal atrophy was significantly more pronounced in patients who did not have worthwhile improvement. We consider this to be a novel finding; previous studies have not examined the prognostic value of the contralateral

hippocampus independently of the ipsilateral hippocampus, focusing instead on the role of bilateral hippocampal atrophy.^{11,28} Nevertheless, our results are in keeping with findings reported in groups with bilateral hippocampal atrophy.¹¹

Comparing seizure-free to non-seizure-free patients, NAA/Cr in the contralateral posterior temporal lobe was significantly higher, and appropriately lateralized asymmetry of NAA/Cr in the posterior temporal lobe was greater for seizure-free patients. These results mirror the pattern of the comparison between patients who experienced worthwhile improvement and those who did not, in that contralateral involvement was more pronounced in the poorer outcome group, while abnormalities were more ipsilaterally accentuated in the favorable outcome group.

A limitation of this study is the relatively small patient sample size. With a larger database than is currently available, one single classifier could be constructed to consider the four main outcome classes in Engel's system separately. While we used the leave-one-out cross-validation technique to minimize over-fitting of our data in the current study, a larger database would further improve the generalization of the classifiers by allowing the use of separate training and test sets.

Including other MR data such as T2-relaxometry in the classifier may also help improve the classification accuracy. This would be a worthwhile avenue to pursue in future work. Resection size may also influence outcome.^{29,30} The decision to perform a temporal lobectomy or a selective amygdalohippocampectomy is made pre-operatively, although the choice of procedure does not appear to affect outcome.¹¹ However, resection size is not determined pre-surgically, and therefore cannot be included as part of a pre-surgical attribute set used to predict outcome. Hypothetically, this obstacle could

be overcome, with a much larger patient database, by matching the outcome class with the resection size. This approach would create "complex" outcome classes of worthwhile improvement with large resection, worthwhile improvement with small resection, no worthwhile improvement with large resection, and no worthwhile improvement with small resection, or similar outcome complexes using the seizure-free and not seizure free outcome groups.

We are not suggesting that classifiers such as the one developed in this study can make the ultimate decision to operate on a particular patient. The classifier does not make the diagnosis of TLE, and reduction in seizure frequency is only one aspect of surgical outcome. For example, the possibility of cognitive deficits after surgery is also an important consideration when deciding whether to operate on a patient. The individual circumstances of patients involved also need to be considered when evaluating the surgical option. Nevertheless, our results suggest that the classifier developed in this study can provide valuable guidance in identifying surgical candidates, and that MR markers should be used more widely for this purpose.

REFERENCES

1. Engel JJ. Update on surgical treatment of the epilepsies. *Neurology* 1993;43(8):1612-1617.
2. Scott CA, Fish DR, Smith SJ, et al. Presurgical evaluation of patients with epilepsy and normal MRI: role of scalp video-EEG telemetry. *J Neurol Neurosurg Psychiatry* 1999;66(1):69-71.

3. ILAE. A global survey on epilepsy surgery, 1980-1990: a report by the Commission on Neurosurgery of Epilepsy, the International League Against Epilepsy. *Epilepsia* 1997;38(2):249-255.
4. Cendes F, Caramanos Z, Andermann F, Dubeau F, Arnold DL. Proton magnetic resonance spectroscopic imaging and magnetic resonance imaging volumetry in the lateralization of temporal lobe epilepsy: a series of 100 patients. *Annals of Neurology* 1997;42:737-746.
5. Kuzniecky R, Hugg JW, Hetherington H, et al. Relative utility of 1H spectroscopic imaging and hippocampal volumetry in the lateralization of mesial temporal lobe epilepsy. *Neurology* 1998;51(1):66-71.
6. Hetherington H, Kuzniecky R, Pan J, et al. Proton nuclear magnetic resonance spectroscopic imaging of human temporal lobe epilepsy at 4.1 T. *Annals of Neurology* 1995;38(3):396-404.
7. Connelly A, Jackson GD, Duncan JS, King MD, Gadian DG. Magnetic resonance spectroscopy in temporal lobe epilepsy. *Neurology* 1994;44(8):1411-1417.
8. Li LM, Caramanos Z, Cendes F, et al. Lateralization of temporal lobe epilepsy (TLE) and discrimination of TLE from extra-TLE using pattern analysis of MR spectroscopic and volumetric data. *Epilepsia* 2000;In Press.
9. Jack CR, Sharbrough FW, Cascino GD, Hirschorn KA, O'Brien PC, Marsh WR. Magnetic resonance image-based hippocampal volumetry: correlation with outcome after temporal lobectomy. *Annals of Neurology* 1992;31:138-146.

10. Gilliam F, Bowling S, Bilir E, et al. Association of combined MRI, interictal EEG, and ictal EEG results with outcome and pathology after temporal lobectomy. *Epilepsia* 1997;38(12):1315-1320.
11. Arruda F, Cendes F, Andermann F, et al. Mesial atrophy and outcome after amygdalohippocampectomy or temporal lobe removal. *Annals of Neurology* 1996;40:446-450.
12. Knowlton RC, Laxer KD, Ende G, et al. Presurgical multimodality neuroimaging in electroencephalographic lateralized temporal lobe epilepsy. *Annals of Neurology* 1997;42:829-837.
13. Radhakrishnan K, Silbert PL, Jack CR, Cascino GD, Sharbrough FW, O'Brien PC. Predictors of outcome of anterior temporal lobectomy for intractable epilepsy. *Neurology* 1998;51:465-471.
14. Ho SS, Consalvo D, Gilliam F, et al. Amygdala atrophy and seizure outcome after temporal lobe epilepsy surgery. *Neurology* 1998;51:1502-1504.
15. Li LM, Cendes F, Antel SB, et al. Prognostic value of proton magnetic resonance spectroscopic imaging for surgical outcome in patients with intractable temporal lobe epilepsy and bilateral hippocampal atrophy. *Annals of Neurology* 2000;47(2):195-200.
16. Ende GR, Laxer KD, Knowlton RC, et al. Temporal lobe epilepsy: bilateral hippocampal metabolite changes revealed at proton MR spectroscopic imaging. *Radiology* 1997;202:809-817.

17. Grigsby J, Kramer RE, Schneiders JL, Gates JR, Smith WB. Predicting outcome of anterior temporal lobectomy using simulated neural networks. *Epilepsia* 1998;39(1):61-66.
18. Arle JE, Perrine K, Devinsky O, Doyle WK. Neural network analysis of preoperative variables and outcome in epilepsy surgery. *Journal of Neurosurgery* 1999;90:998-1004.
19. Duda RO, Hart PE. *Pattern classification and scene analysis*. New York: Wiley & Sons; 1973.
20. Mitchell TM. *Machine Learning*. Boston: WCB McGraw-Hill; 1997.
21. Engel JJ, Van Ness PC, Rasmussen TB, Ojemann LM. Outcome with respect to epileptic seizures. In: Engel JJ, editor. *Surgical treatment of the epilepsies*. 2nd ed. New York: Raven Press, Ltd.; 1993. p. 609-621.
22. Watson C, Andermann F, Gloor P, et al. Anatomic basis of amygdaloid and hippocampal volume measurement by magnetic resonance imaging. *Neurology* 1992;42(9):1743-1750.
23. Roth K, B.J. K, Feeney J. Data shift accumulation and alternate delay accumulation techniques for overcoming the dynamic range problem. *Journal of Magnetic Resonance* 1980;41:302-309.
24. Hand DJ. *Discrimination and classification*. Chichester: Wiley; 1981.
25. Webb A. *Statistical Pattern Recognition*. London: Oxford University Press; 1999.
26. Kuzniecky R, Ho SS, Martin R, et al. Temporal lobe developmental malformations and hippocampal sclerosis: epilepsy surgical outcome. *Neurology* 1999;52(3):479-484.

27. Kuzniecky R, Hugg J, Hetherington H, et al. Predictive value of 1H MRSI for outcome in temporal lobectomy. *Neurology* 1999;53(4):694-698.
28. Jack CR, Jr., Trenerry MR, Cascino GD, Sharbrough FW, So EL, O'Brien PC. Bilaterally symmetric hippocampi and surgical outcome. *Neurology* 1995;45(7):1353-1358.
29. Siegel AM, Wieser HG, Wichmann W, Yasargil GM. Relationships between MR-imaged total amount of tissue removed, resection scores of specific mediobasal limbic subcompartments and clinical outcome following selective amygdalohippocampectomy. *Epilepsy Research* 1990;6:56-65.
30. Wyler AR, Hermann BP, Somes G. Extent of medial temporal resection on outcome from anterior temporal lobectomy: a randomized prospective study. *Neurosurgery* 1995;37(5):982-991.
31. Cendes F, Andermann F, Dubeau F, Matthews PM, Arnold DL. Normalization of neuronal metabolic dysfunction after surgery for temporal lobe epilepsy. Evidence from proton MR spectroscopic imaging. *Neurology* 1997;49(6):1525-1533.

4. ■ Assisting visual detection of FCD lesions

4.1 Preface

The results in the previous chapter demonstrated the utility of machine learning methods applied to MR data regarding the pre-surgical evaluation of patients with TLE. Another common form of epilepsy is extra-temporal lobe epilepsy (ETLE). Malformation of cortical development (MCD) is a common underlying cause of ETLE. Focal cortical dysplasia (FCD) is in turn a common form of MCD. For patients with FCD, lesion detection is a critical component of pre-surgical evaluation. Several MRI characteristics of FCD lesions have been identified¹⁴³. However, in many patients, lesions of FCD are characterized by minor structural abnormalities that go unrecognized or are too subtle to be detected by standard radiological analysis. Thus we hypothesized that improved lesion detection could be achieved through the use of mathematical models of the MRI characteristics of FCD.

The papers in this chapter trace the development of a method for assisting the visual detection of FCD lesions based on this idea. Our initial approach was to implement first-order statistical and morphological operators to measure visually discernable MRI characteristics of FCD lesions. We built upon our initial results by including results from second-order texture analysis, a technique which can quantify

information regarding tissue structure or organization not readily accessible through visual analysis, and by employing machine learning techniques to perform automated lesion detection.

4.2 Manuscript 2

Presented in part at the:

American Epilepsy Society annual meeting, 2000.

and

9th Annual Meeting of the International Society for Magnetic Resonance in Medicine, 2001

Published in Annals of Neurology 2001;49(6), 770-775.

Texture analysis and morphological processing of MRI assist detection of focal cortical dysplasia in extra-temporal partial epilepsy.

A. Bernasconi, MD; S.B. Antel, MSc; L.D. Collins, PhD; N. Bernasconi, MD; A. Olivier, MD, PhD (FRCSC); F. Dubeau, MD (FRCPC); B. Pike, PhD; F. Andermann, MD (FRCPC); D.L. Arnold, MD (FRCPC)

Department of Neurology and Neurosurgery and Brain Imaging Center, Montreal Neurological Hospital and Institute, McGill University, Montreal, Quebec, Canada

Correspondence to:

**D.L. Arnold, M.D. F.R.C.P.(C.)
Magnetic Resonance Spectroscopy Unit
Montreal Neurological Institute
3801 University Street
Montreal, Quebec, Canada H3A 2B4
telephone: (514) 398-8185; fax: (514) 398-2975**

ABSTRACT

In many patients, focal cortical dysplasia (FCD) is characterized by minor structural changes that may go unrecognized by standard radiological analysis. To increase the sensitivity of MRI for the detection of subtle lesions of FCD, we developed voxel-based image post-processing methods, including first-order texture analysis and morphological processing modeled on known MRI features of FCD. We selected 16 patients with histologically proven FCD. Image processing features were calculated over a neighborhood for each voxel in the 3D T1-weighted MRI. Three feature maps were generated: (i) gray matter thickness map to model cortical thickening (ii) gradient map to model blurring of the GM-WM junction, and (iii) relative intensity map to model hyperintense signal within the lesion. These feature maps were combined into a single “ratio map” to facilitate visual analysis. Two observers detected lesions on conventional MRI in 8/16 and on ratio maps in 14/16 patients. Sensitivity was 87.5% (14/16) for the ratio maps compared to 50% (8/16) for MRI ($p < 0.003$). Specificity was 95% (19/20) for ratio maps and 100% (20/20) for MRIs. Cohen’s Kappa was 0.53 for MRIs indicating moderate agreement and 0.83 for ratio maps indicating strong agreement beyond chance between the two observers. The image processing methods developed in this study improve visual detection of FCD, even in cases where no lesion is obvious on MRI. These techniques could increase the number of patients with partial epilepsy who could benefit from surgery.

INTRODUCTION

Focal cortical dysplasia (FCD), a neuronal migration disorder, was originally reported by Taylor¹. It corresponds to a localized disruption of the normal cortical lamination associated with an excess of large, aberrant neurons, an increase in cortical thickness, and often, abnormal neuroglial elements in the underlying white matter (WM). The dysplastic tissue retains sufficient connectivity to produce seizures^{2,3}. Indeed, FCD is the most common form of developmental disorder in patients with pharmacologically intractable partial epilepsy referred for presurgical evaluation⁴.

On magnetic resonance imaging (MRI), FCD is mainly characterized by variable degrees of cortical thickening, a poorly defined transition between gray matter (GM) and white matter (WM), and hyperintense signal within the dysplastic lesion with respect to normal cortex⁵. High-resolution MRI of the brain has been proven to be clinically useful in the evaluation of patients with partial epilepsy of neocortical origin and has made it possible to identify FCD in an increasing number of patients^{6,7}. However, in many patients, lesions of FCD are characterized by minor structural abnormalities that go unrecognized or are too subtle to be detected by standard radiological analysis.

Morphology and texture are important features for visual assessment of an image. The texture of an image can be described by the distribution of brightness and darkness within that image. Computer-based texture analysis of digital images provides quantitative information about spatial gray level variations in pixel neighborhoods^{8,9}. Mathematical texture analytic techniques are objective and more sensitive than the human eye. Statistical, or first-order, texture analysis involves the extraction of various mathematically defined image texture features, often measured via a histogram, which characterizes the gray level distribution within local pixel neighborhoods¹⁰.

To improve our ability to detect dysplastic lesions in patients with intractable partial epilepsy, we developed straightforward voxel-based image processing techniques, including gray matter thickness, local gradient and pixel intensities with regard to gray matter and white matter. These features were chosen to model *in vivo* the pathological characteristics of FCD. We hypothesized that such image post-processing could increase the sensitivity of MRI for the detection of subtle lesions of FCD.

METHODS

Subjects

We selected 16 patients who had histologically proven FCD at operation. All patients had focal corticectomies. In eight patients, FCD had been recognized on MRI prior to the surgery. In the remaining eight patients, MRI had been reported as normal. For patients in whom no lesion was visible on MRI, surgery was based on strong clinical and EEG co-localizing data. Resections were performed in the parietal lobe in 7 patients and the frontal lobe in 9 patients. Fourteen patients became seizure free and two had a significant reduction in attack frequency and severity (mean follow up 26 months).

MRI acquisition

Preoperative MRI volumetric images were acquired on a 1.5 T Gyroscan (Philips Medical System, Best, The Netherlands) using a T1-fast field echo, TR=18, TE=10, 1 acquisition average pulse sequence, flip angle=30°, matrix size=256x256, FOV=256, thickness=1mm. Approximately 170 slices with an isotropic voxel size of 1 mm³ were acquired. Proton-density and T₂-weighted images (thickness 3.0 – 5.0 mm, gap 0.3, TR

2100 ms, TE 20, 78 ms) were obtained in all patients and showed an increase in signal within the lesion in 9 of them. Fluid attenuation inversion recovery images (FLAIR, slice thickness 3.0 mm, inter-slice gap 0.3 mm, TR 6000 ms, TE 150 ms, TI 1900 ms, FOV 230 mm) were obtained in 12 patients and showed signal abnormality in 5 of them. T1-weighted MRIs were examined by a neuroradiologist on a workstation. Standard T2-weighted images and FLAIR images were examined on film.

Image preparation

Images were analyzed on a Silicon Graphics workstation (Mountain View, California, USA, 200 MHz, MIPS R 5000, 56 Mb RAM) using locally developed software. All MRIs were free of visible motion artifacts. Images were automatically registered into stereotaxic space to adjust for differences in total brain volume and brain orientation¹¹. Each image underwent automated correction for intensity non-uniformity and intensity standardization¹². This correction produces consistent relative gray matter, white matter and CSF intensities. Classification of brain tissue in GM and WM was done using a histogram-based method with automated threshold.

Image processing

Image processing features were calculated for each individual voxel within the T1-weighted 3D MRI, resulting in a three-dimensional map for each feature.

To model cortical thickening, a morphological operator was used wherein each individual voxel was used as the starting point for gray matter run-length coding¹³, performed in each possible point-to-point direction (Figure 1A). On the gray matter

thickness map, regions of increased intensities correspond to increased gray matter thickness.

To model blurring of the transition between GM and WM, we calculated the absolute gradient¹⁰ of gray level intensities. This first-order texture feature was calculated over a 5x5x5 cube centered on each voxel. In regions of normal transition between GM and WM, the gradient was expected to be steep. In regions of GM-WM blurring, the gradient was expected to be less steep (Figure 1 B). On the gradient map, low intensity corresponds to blurring of the GM-WM transition.

To model the hyperintense signal within the lesions of focal cortical dysplasia on T1-weighted images, we developed a feature that calculated the absolute difference between the intensity of a given voxel and the intensity at the boundary between GM and WM (B_g), defined using a histogram, given by the function

$$f(i,j,k) = 100*[B_g - |B_g - g(i,j,k)|] / B_g ,$$

where $g(i,j,k)$ represents the intensity of a given voxel and $f(i,j,k)$ is the value of the feature for the given voxel (Figure 1 C). Using the relative difference enables the analysis of voxels located within cortical GM in which the intensity is higher than normal and overlaps that of the WM. GM at higher intensity is close to the GM-WM boundary. On the relative intensity map, higher intensity corresponds to hyperintense signal within the lesion.

On T1-weighted MRI, lesions of focal cortical dysplasia are characterized by an increase in gray matter thickness and an increase in relative intensity, and a reduction in the gradient. Therefore, to maximize visibility of FCD lesions, a ratio map (GM thickness x relative intensity/gray level intensity gradient) was generated.

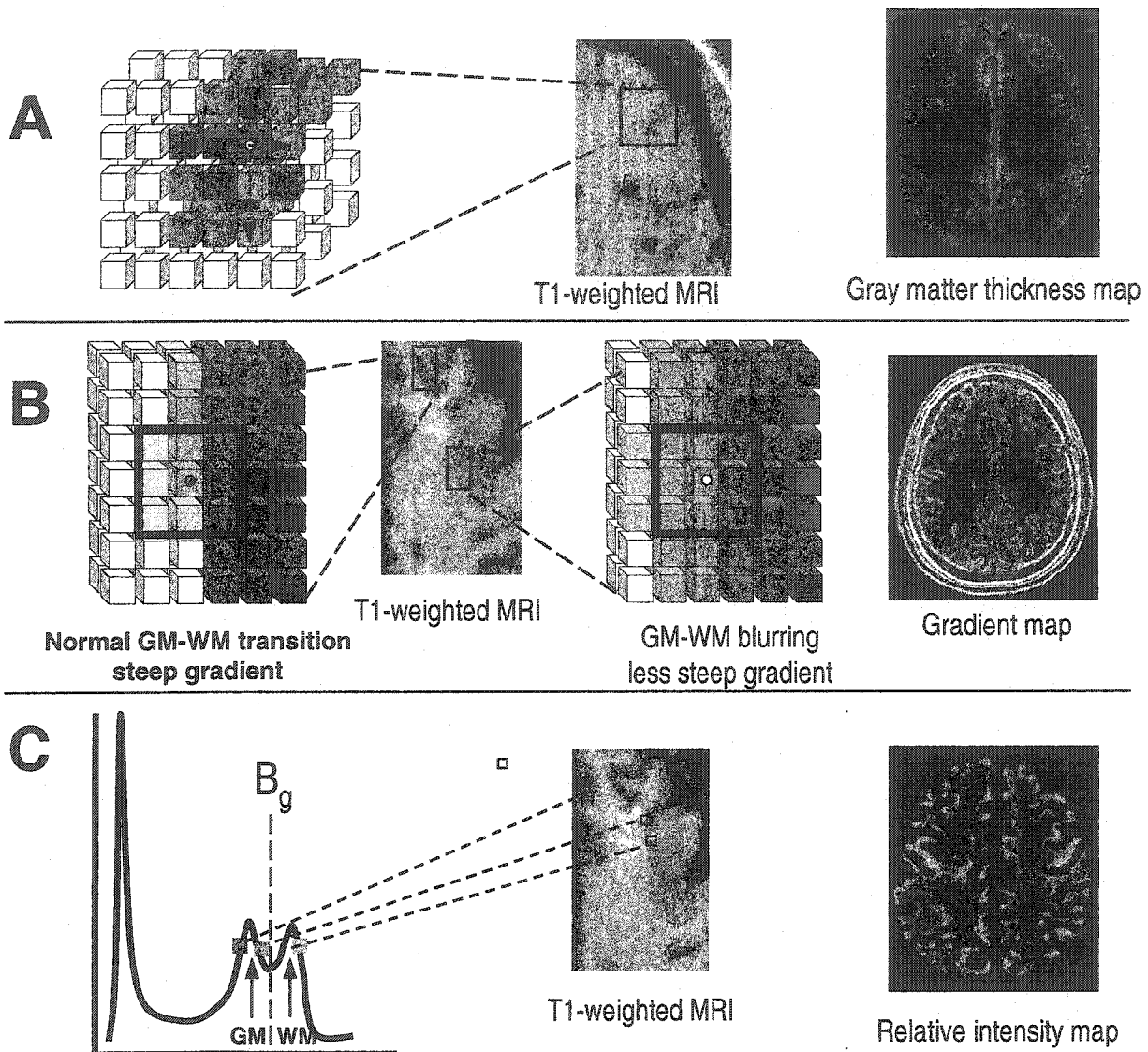


Figure 1. (A) The figure in the center shows a portion of a T1-weighted MRI. On the left, a small region of cortex and adjacent white matter (box) are schematically represented in three dimensions and magnified. Each cube represents a voxel. To model cortical thickening, each individual voxel in the T1-weighted MRI was used as the starting point for gray matter run-length coding, performed in each possible discrete direction (schematically represented by the arrows in the magnified brain region). A gray matter thickness map of a healthy control is shown on the right. (B) To model the blurring between gray matter (GM) and white matter (WM), the absolute gradient of gray level intensities was calculated in a cube centered on each voxel (dot) in the T1-weighted MRI. In regions of normal transition (magnified region on the left) between GM and WM (magnified region on the left), the gradient was expected to be steep. In regions of GM-WM blurring (magnified region on the right), the gradient was less steep. A gradient map of a healthy control is shown on the right. (C) To model the hyperintense signal within the lesions of focal cortical dysplasia on T1-weighted MRI, the absolute difference between the intensity of a given voxel $g(i,j,k)$ and the intensity at the GM-WM boundary (B_g), as defined by a histogram was calculated. This feature is represented mathematically as the function $f(i,j,k) = 100 \cdot [B_g - |B_g - g(i,j,k)|] / B_g$. A relative intensity map of a healthy control is shown on the right.

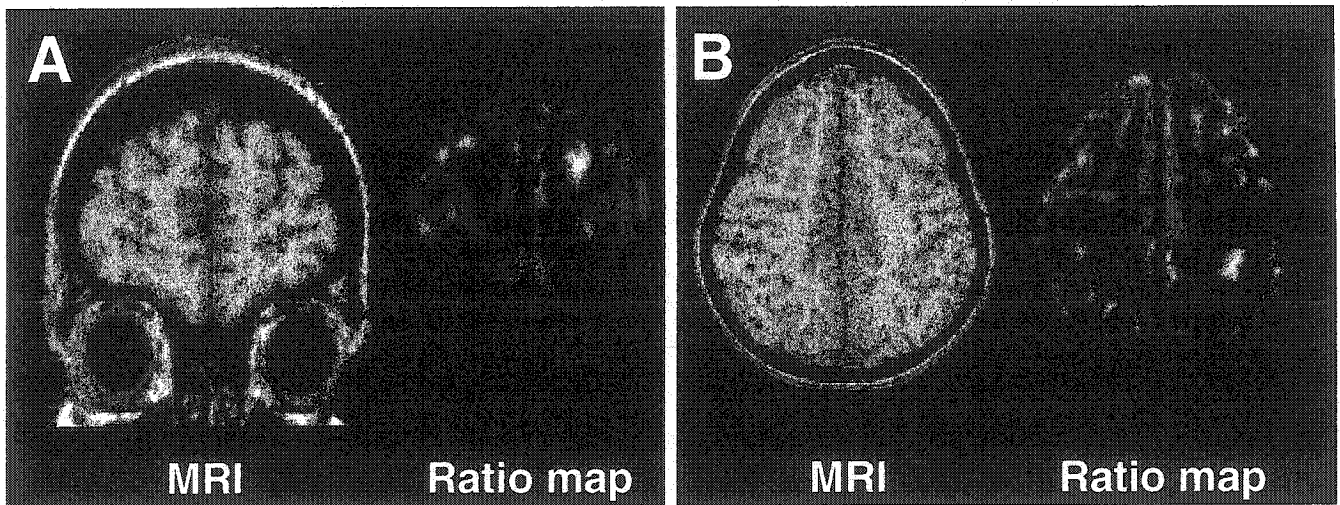
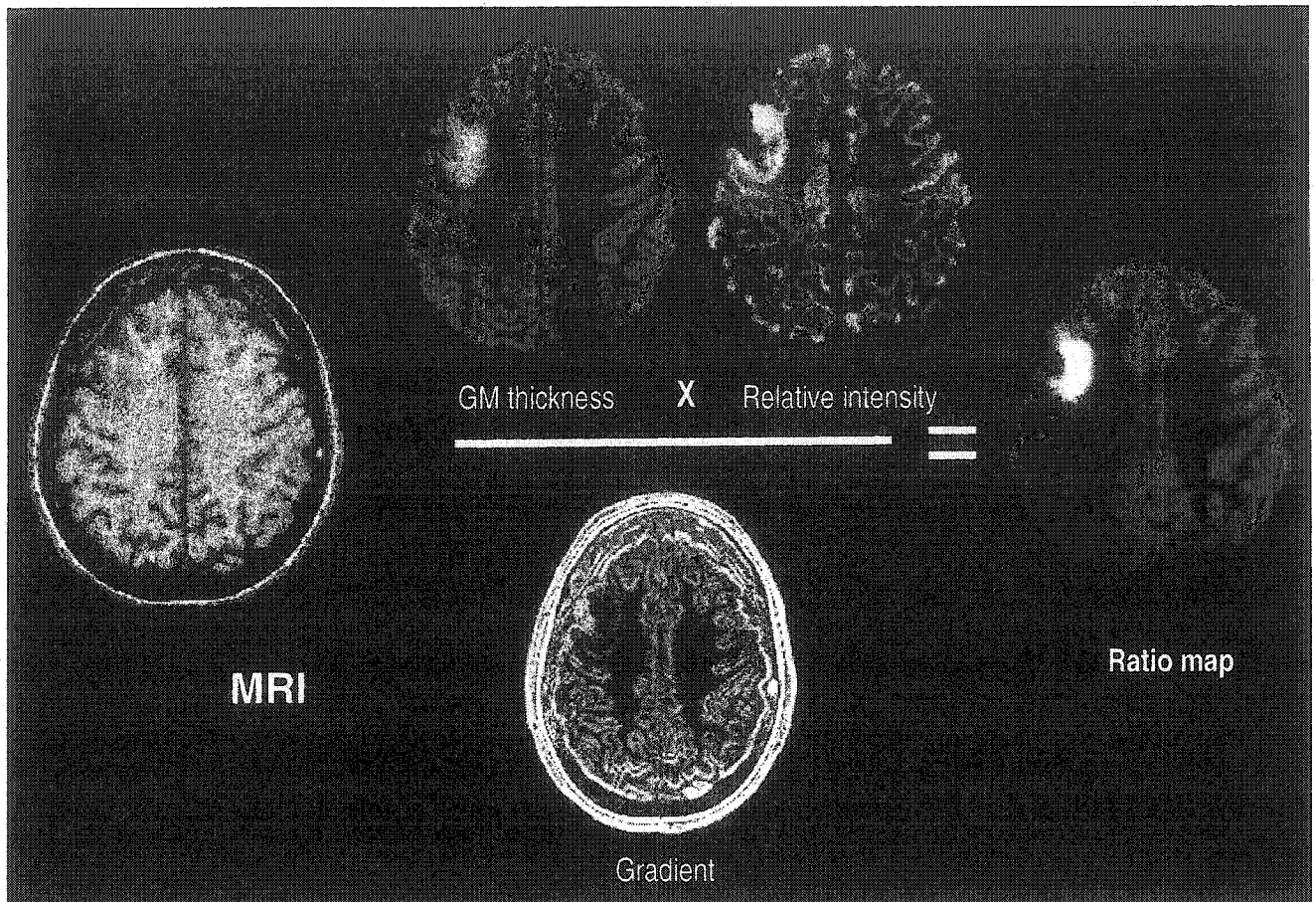


Figure 2. Top panel shows a representative patient with intractable frontal lobe epilepsy, in whom the MRI showed a lesion of focal cortical dysplasia in the left frontal lobe. The maps show increased gray matter thickness and intensity of the lesion, and a reduction in the gradient. The ratio map (GM thickness \times relative intensity/gray level intensity gradient) clearly shows the lesion. Bottom panels show MRI and ratio map of (A) a patient with intractable frontal lobe epilepsy and (B) a patient with parietal lobe epilepsy. In both patients, the lesions of focal cortical dysplasia demonstrated by the ratio maps were not seen on pre-operative MRI.

The generation of the different texture maps (gray matter thickness, gradient, relative intensity, and ratio maps) for the entire brain volume takes about 20 minutes. Images were reviewed using the software package *Display* developed at the Brain Imaging Center of the Montreal Neurological Institute. This software allows simultaneous displaying of an MRI volume in the transverse, sagittal, and coronal planes. The user can move throughout the volumes.

Assessment of the performance of diagnostic tests and inter-rater agreement

A series of images consisting of MRIs and ratio maps for 16 patients and 20 healthy control subjects were presented on a Silicon Graphics workstation (Mountain View, California, USA) in random order to two trained observers who were unaware of the final diagnosis. The evaluations were made independently; i.e., one physician did not know the results of the other physician's determination. A lesion was considered to have been detected only if found independently by both observers. All other cases were considered to be non-lesional. Mean duration for the examination of the ratio maps was 8 minutes.

To assess the performance of MRI and ratio maps as diagnostic tests, we calculated: accuracy (percentage of correctly classified cases = $[\text{true positives} + \text{true negatives}] / \text{all cases}$), sensitivity (the percentage of positives correctly identified = $\text{true positives} / [\text{true positives} + \text{false negatives}]$), specificity (the percentage of negatives correctly identified = $\text{true negatives} / [\text{true negatives} + \text{false positives}]$), reliability of positive predictions (reliability in the prediction of positives = $\text{true positives} / [\text{true}$

positives + false positives]), and reliability of negative predictions (reliability in the prediction of negatives = true negatives/[true negatives + false negatives]).

Inter-rater agreement between the two observers was assessed using Cohen's kappa coefficient. Values of kappa greater than 0.75 were considered to indicate strong agreement, beyond chance, values between 0.4 and 0.79 to indicate fair to good, and values below 0.40 to indicate poor agreement.

Statistical analysis was performed using a spreadsheet for calculation of comprehensive statistics for the assessment of diagnostic tests and inter-rater agreement ¹⁴.

RESULTS

Table 1 presents the classification results. Overall accuracy (correctly classified/ total cases) was 91.7% (33/36) for the ratio maps and 77.8% (28/36) for the MRIs. Sensitivity (predicted positives/ total positives) was 87.5% (14/16) for the ratio maps compared to 50% (8/16) for MRI. This increase in sensitivity was found to be statistically significant ($p < 0.003$) using a Pearson's chi-square analysis for frequency tables.

Specificity (predicted negatives/total negatives) was 95% (19/20) for ratio maps and 100% (20/20) for MRIs. Positive predictive value was 93% (14/15) for ratio maps and 100% (8/8) for MRIs in this group. Negative predictive value was 90.5% (19/21) for ratio maps, compared to 71.4% (20/28) for MRIs.

Cohen's Kappa was 0.53 for MRIs indicating moderate agreement and 0.83 for ratio maps indicating strong agreement beyond chance between the two observers.

Figure 2 shows a representative example of a patient with an obvious lesion of FCD on preoperative MRI, and two examples of a patient in whom the MRI was reported as normal, but ratio maps showed a lesion.

MRI	Predicted positive FCD	Predicted negative FCD	
Actual positive	8	8	Sensitivity=8/16
Actual negative	0	20	Specificity=20/20
	PPV=8/8	NPV=8/28	

Ratio Maps	Predicted positive FCD	Predicted negative FCD	
Actual positive	14	2	Sensitivity=14/16
Actual negative	1	19	Specificity=19/20
	PPV=14/15	NPV=19/21	

Table 1. Confusion matrix for performance evaluation of MRI (top) and ratio maps (bottom) for the predicted and actual classification of control subjects (n=20) and patients with focal cortical dysplasia (n=16). FCD: focal cortical dysplasia; PPV: positive predictive value; NPV: negative predictive value

DISCUSSION

Using voxel-based image post-processing methods adapted to the pathology of FCD, we were able to detect lesions on MRI that were unrecognized by standard visual radiological analysis. By using ratio maps based on GM thickness, blurring of the GM-WM junction and the hyperintense signal of the lesion, we increased sensitivity of lesion detection by 37.5% over conventional MRI analysis while maintaining a high degree of reliability. In all cases the identified lesion overlapped with the surgically resected area.

Subtle cortical lesions are being increasingly recognized in patients with epilepsy with the aid of high-resolution MRI and the ability to analyze the brain volume by multiplanar ^{7,15} and curvilinear ¹⁶ reformatting. However, our results indicate that detection of subtle dysplastic lesions may be further improved by performing computerized quantitative analysis of the structural changes that characterize FCD pathologically and *in vivo* on MR images. This approach makes use of the large amount of data available in volumetric MRI scans, much of which may be too subtle to be appreciated by visual analysis alone.

To our knowledge, this is the first study specifically dedicated to the quantitative lesion detection of FCD in patients with intractable partial epilepsy. Previous quantitative MRI studies dealt with the regional distribution of gray and white matter volumes ^{17,18} in patients with various types of malformations of cortical development, mainly heterotopias, and in idiopathic generalized and juvenile myoclonic epilepsy ^{19,20}. Furthermore, unlike previously published data, we were able to confirm histologically the identified lesions of FCD in all patients.

First order texture analysis

The calculation of the absolute gradient was one of the voxel-based image post-processing methods used in this study. Usefulness of texture analysis has been proven for many types of images, ranging from satellite data to biomedical images. In medical imaging, this technique has been shown to increase the level of diagnostic information extracted from many modalities such as MRI and ultrasound and to characterize differences in appearances unrecognizable by visual observation. Reported applications

include classification of pathological tissue in liver, thyroid, breast, kidney, prostate and the heart, and characterization of brain tumors and human trabecular bone^{8,21,22}.

The first-order texture analysis that we used involved the extraction of image texture features that characterizes the gray level intensity distribution within local pixel neighborhoods. We did not calculate second-order texture features, which result from operations performed on co-occurrence matrices and represent the joint gray level distributions for pairs of spatially related pixels¹⁰. We did not extend our methods to second-order texture analysis as the calculation of co-occurrence matrices on a voxel-by-voxel basis is computationally intensive and not feasible for whole brain volume at present. Furthermore, physiological rationales for the discriminatory ability of features are more easily generated for simple image processing techniques and first-order features compared to second order features.

Morphological processing

We used run-length coding to measure gray-matter thickness because of its simplicity. This feature resulted in a consistent high intensity along the midline cortical gray matter, particularly the cingulate gyrus, in the GM thickness map. This is an artifact in that it represents gray matter continuity in the plane of the cortex as opposed to orthogonal to it. This type of artifact was largely responsible for the one misclassified normal control ratio map. This effect could be overcome by normalizing the feature maps of each patient to a set of maps from healthy controls or by a more sophisticated implementation that takes orientation of the cortex into account when determining thickness.

In conclusion, the simple MR image processing methods used in this study, including first-order texture and morphological analysis, improves visual detection of FCD even in patients where no lesion is obvious on pre-operative MRI. These techniques could considerably increase the number of patients with so-called “non-lesional” partial epilepsy who could benefit from surgery.

REFERENCES

1. Taylor DC, Falconer MA, Bruton CJ, Corsellis JAN. Focal dysplasia of the cerebral cortex in epilepsy. *J Neurol Neurosurg Psychiatry* 1971;34:369-387.
2. Gambardella A, Palmieri A, Andermann F, et al. Usefulness of focal rhythmic discharges on scalp EEG of patients with focal cortical dysplasia and intractable epilepsy. *Electroencephalogr Clin Neurophysiol* 1996;98:243-249.
3. Avoli M, Bernasconi A, Mattia D, et al. Epileptiform discharges in the human dysplastic neocortex: in vitro physiology and pharmacology. *Ann Neurol* 1999;46:816-826.
4. Sisodiya SM. Surgery for malformations of cortical development causing epilepsy. *Brain* 2000;123:1075-1091.
5. Barkovich AJ, Kuzniecky RI. Neuroimaging of focal malformations of cortical development. *J Clin Neurophysiol* 1996;13:481-494.

6. Grant PE, Vingneron DB, Barkovich AJ. High-resolution imaging of the brain. *Magn Reson Imaging Clin N Am* 1998;1:139-154.
7. Barkovich AJ, Rowley HA, Andermann F. MR in partial epilepsy: value of high-resolution volumetric techniques. *AJNR Am J Neuroradiol* 1995;16:339-343.
8. Lerski RA, Straughan K, Schad LR, et al. MR image texture analysis-an approach to tissue characterization. *Magn Reson Imaging* 1993;11:873-887.
9. Kjaer L, Ring P, Thomsen C, Henriksen O. Texture analysis in quantitative MR imaging. Tissue characterization of normal brain and intracranial tumors at 1.5 T. *Acta Radiol* 1995;36:127-135.
10. Haralick RM, Shanmugam K, Dinstein I. Textural features for image classification. *IEEE Trans Sys Man Cyber* 1973;SMC-3:610-621.
11. Collins DL, Neelin P, Peters TM, Evans AC. Automatic 3D intersubject registration of MR volumetric data in standardized Talairach space. *J Comput Assist Tomogr* 1994;18:192-205.
12. Sled JG, Zijdenbos AP, Evans AC. A nonparametric method for automatic correction of intensity nonuniformity in MRI data. *IEEE Trans Med Imaging* 1998;17:87-97.

13. Galloway MM. Texture analysis using grey level run lengths. *Comp Vision Graph Im Proc* 1975;4:172-179.

14. Mackinnon A. A spreadsheet for the calculation of comprehensive statistics for the assessment of diagnostic tests and inter-rater agreement. *Comput Biol Med* 2000;30:127-134.

15. Grant PE, Barkovich AJ, Wald LL, et al. High-resolution surface-coil MR of cortical lesions in medically refractory epilepsy: a prospective study. *AJNR Am J Neuroradiol* 1997;18:291-301.

16. Bastos AC, Comeau RM, Andermann F, et al. Diagnosis of subtle focal dysplastic lesions: curvilinear reformatting from three-dimensional magnetic resonance imaging. *Ann Neurol* 1999;46:88-94.

17. Sisodiya SM, Free S, Stevens JM, et al. Widespread cerebral structural changes in patients with cortical dysgenesis and epilepsy. *Brain* 1995;118:1039-1050.

18. Free S, Sisodiya SM, Cook MJ, et al. Three-dimensional fractal analysis of the white matter surface from magnetic resonance images of the human brain. *Cereb Cortex* 1996;6:830-836.

19. Woermann FG, Sisodiya SM, Free S, Duncan JS. Quantitative MRI in patients with idiopathic generalized epilepsy: evidence of widespread cerebral structural changes. *Brain* 1998;121:1661-1667.

20. Woermann FG, Free SL, Koepp MJ, et al. Abnormal cerebral structure in juvenile myoclonic epilepsy demonstrated with voxel-based analysis of MRI. *Brain* 1999;122:2101-2108.

21. Garra BS, Krasner BH, Horii SC, et al. Improving the distinction between benign and malignant breast lesions: the value of sonographic texture analysis. *Ultrason Imaging* 1993;15:267-285.

22. Sinha S, Lucas-Quesada FA, DeBruhl ND, et al. Multifeature analysis of Gd-enhanced MR images of breast lesions. *JMRI* 1997;7:1016-1026.

4.3 Manuscript 3

Published in NeuroImage 2002;17, 1755-1760.

Computational models of MRI characteristics of focal cortical dysplasia improve lesion detection.

Samson B. Antel*, MSc; Andrea Bernasconi†, MD; Neda Bernasconi†, MD; D. Louis Collins*†, PhD; Robert.E. Kearney*, PhD; Rajjan Shinghal‡, PhD; Douglas L. Arnold†, MD, FRCP(C)

*Departments of Biomedical Engineering and †Neurology and Neurosurgery, Montreal Neurological Hospital and Institute, McGill University, Montreal, Quebec, Canada

‡Department of Computer Science, Concordia University, Montreal, Quebec, Canada

Correspondence to:
Andrea Bernasconi, M.D.
Montreal Neurological Institute
3801 University Street
Montreal, Quebec, Canada H3A 2B4
telephone: (514) 398-8524; fax: (514) 398-2975
andrea@bic.mni.mcgill.ca

ABSTRACT

In many patients, focal cortical dysplasia (FCD) is characterized by minor structural changes that may go unrecognized by standard radiological analysis. We previously demonstrated that visual analysis of a composite map based on three simple models of MRI features of FCD increased the sensitivity of FCD lesion detection, compared to visual analysis of conventional MRI. Here we report on the use of improved methods for characterizing FCD which improve contrast in the composite maps: a Laplacian-based metric for measuring cortical thickness, a convolutional kernel to model blurring of the GM/WM interface, and an operator to measure hyperintense T1 signal. To validate these methods, we processed the MRIs of 14 FCD patients with our original set of image processing operators and an improved set of image processing operators. Comparison of the composite maps associated with the two sets of operators revealed that contrast between lesional tissue and non-lesional cortex was significantly increased in the composite maps associated with the set of improved operators. Increasing this contrast is an important step towards the goal of automated FCD lesion detection.

INTRODUCTION

Focal cortical dysplasia (FCD) is a neuronal migration disorder corresponding to a localized disruption of the normal cortical lamination associated with an excess of large, aberrant neurons, an increase in cortical thickness, and often, abnormal neuroglial elements in the underlying white matter (WM). FCD is the most common developmental disorder in patients with medically refractory partial epilepsy referred for presurgical evaluation¹.

On T1-weighted magnetic resonance imaging (MRI), FCD is generally characterized by variable degrees of cortical thickening, a poorly defined transition between gray matter (GM) and white matter (WM), and hyperintense signal within the dysplastic lesion relative to normal cortex². High-resolution MRI of the brain has made it possible to identify FCD in an increasing number of patients^{3,4}. However, in many patients, FCD lesions are characterized by minor structural abnormalities that go unrecognized or are too subtle to be detected by standard radiological analysis.

In a previous preliminary study⁵, we demonstrated that simple image-processing operators modeled on the characteristics of FCD as seen on T1-weighted MRI volumes significantly improved the sensitivity of FCD lesion detection relative to standard evaluation of the original MRI itself (95% vs. 50%). In that study, three FCD features were each modeled with voxelwise image-processing operators, producing a three-dimensional map for each feature. To overcome the difficulty (for a human observer) of reconciling visual information from three separate maps, the feature maps were combined into a single composite map for each patient, in which FCD lesions appeared hyperintense relative to normal cortex. Lesion detection was performed through visual analysis of the composite maps by an expert observer. The task was complicated by the presence of hyperintense regions in presumably non-lesional cortex, associated with shortcomings in the selected models. These hyperintense regions served to reduce the contrast between lesion and presumably non-lesional cortex. In almost all cases, the expert observer could discriminate FCD lesions on the composite map, based on their experience at analyzing composite maps and their sense of the respective spatial distributions of lesions and other hyperintense regions within the maps. However, to

facilitate and eventually automate FCD lesion detection, it is necessary to obtain greater contrast between lesions and non-lesional cortex. In this paper, we incorporate more sophisticated methods to model MRI features useful for detecting FCD and compare them with the methods used in our previous study. Specifically, we examine whether the improved methods increase contrast between lesions and non-lesional cortex.

METHODS

Patients and MRI acquisition

Fourteen FCD patients were studied. All patients underwent focal corticectomy, and FCD was subsequently proven based on histological examination of the resected tissue. Preoperative MRI images were acquired on a 1.5 T Gyroscan (Philips Medical System, Best, The Netherlands) using a T1-fast field echo, TR=18, TE=10, 1 acquisition average pulse sequence, flip angle=30°, matrix size=256x256, FOV=256, thickness=1mm. Approximately 170 slices with an isotropic voxel size of 1 mm³ were acquired. All MRIs were free of visible motion artifacts. To ensure image quality, the signal to noise ratio (SNR) was calculated for each patient (mean=27.86, sd=2.01).

Image preparation

Images were analyzed on a Silicon Graphics workstation (Mountain View, California, USA) using locally developed software. All preparatory steps were fully automated. Each image underwent automated correction for intensity non-uniformity⁶. This correction produces consistent relative GM, WM, and cerebrospinal fluid (CSF) intensities. An effect on pathologically reduced GM/WM contrast resulting from this

technique is highly unlikely as it uses a spline-based model of the intensity artifact field. The spline has a support of approximately 100 mm, thus it is very unlikely that image contrast will be significantly changed over the space of 1 cm. Images were then registered into stereotaxic space to adjust for differences in total brain volume and brain orientation⁷. Next, images were intensity normalized using a subject-specific linear multiplier based on the median voxelwise intensity ratio of the image to an average control brain. Finally, the skull and lipid layers were stripped from each image using the Brain Extraction Tool⁸.

Image processing

Image processing operators were chosen to model three commonly noted attributes of FCD lesions on T1-weighted MRI: increased cortical thickness, blurring of the gray matter-white matter interface, and hyperintense signal relative to normal cortex. Each MRI was processed with the set of operators used in the original study and with the set of improved operators described in this work. All operators were voxel-based and therefore produced three-dimensional feature maps. For each set of operators, the resulting feature maps were combined into a composite map (figure 1). The calculation of feature maps and composite maps was fully automated. Total processing time was approximately 15 minutes per patient on an SGI workstation running IRIX 6.5.

Cortical thickness model

In the set of improved operators, cortical thickness was measured using a recently developed procedure⁹ in which the cortex is modeled as an electrostatic field. Borrowing

a tool from mathematical physics, Laplace's equation is solved over the cortical volume with boundary conditions specified at the gray-white and gray-CSF interfaces, creating a series of streamlines corresponding to "equipotential surfaces". In this sense, the method parallels the anatomical structure of the cortex as a series of sublayers. The cortical thickness at a given voxel is defined as the length of the path that connects the voxel to both the GM-WM and GM-CSF interfaces and is orthogonal to all intermediary streamlines.

The technique requires segmentation of the MRI into GM, WM, and CSF. To perform this segmentation, a gaussian curve was fit to each of the gray and white matter peaks in the histogram. The intensity threshold between gray and white matter was then automatically determined by the intersection of the two gaussian curves, eliminating the reliance on the local minimum between the gray and white matter peaks, which can be influenced by noise¹⁰.

This cortical thickness measurement technique overcomes the primary disadvantage of the method used in our preliminary work. In that study, cortical thickness was estimated by gray-matter run-length coding. Such a method is prone to artifacts which arise when portions of the cortex happen to be aligned along a particular search direction. In our preliminary study, this type of artifact was often visible along the midline of the brain, particularly within the cingulate gyrus.

Blurred GM-WM interface model

In the current study, blurring of the GM/WM interface was modeled with a gradient magnitude map. This was calculated through convolution of the MRI volume,

(accomplished by multiplication in the Fourier domain) with a three-dimensional gaussian kernel calculated explicitly over the whole field. The final result was obtained by inverse Fourier transform. In the preliminary study blurring of the GM/WM interface was modeled with the gradient magnitude calculated in the spatial domain over a cubic neighborhood.

Hyperintense GM model

The same model of hyperintense GM signal within lesional tissue was incorporated in both the original and improved feature sets. We developed a feature that calculated the difference between the intensity of a given voxel and the boundary intensity B_g between gray matter and white matter (defined using the automated histogram-based method previously described). Letting g represent the intensity of a given voxel, we defined the relative intensity feature at that voxel as $1 - |B_g - g| / B_g$.

Composite maps and contrast measurement

On T1-weighted MRI, lesions of FCD are characterized by an increase in GM thickness and an increase in relative intensity, and a reduction in the gradient. Therefore, as was done for the original feature set, a composite feature map was calculated as [cortical thickness X relative intensity]/[gradient magnitude]. Because we calculated the gradient magnitude, the value of the composite feature map at any voxel was non-negative. For the small number of voxels with a gradient magnitude of zero, the corresponding value within the composite feature map was defined as zero. In order to standardize the composite maps, the mean and standard deviation of each composite map were computed

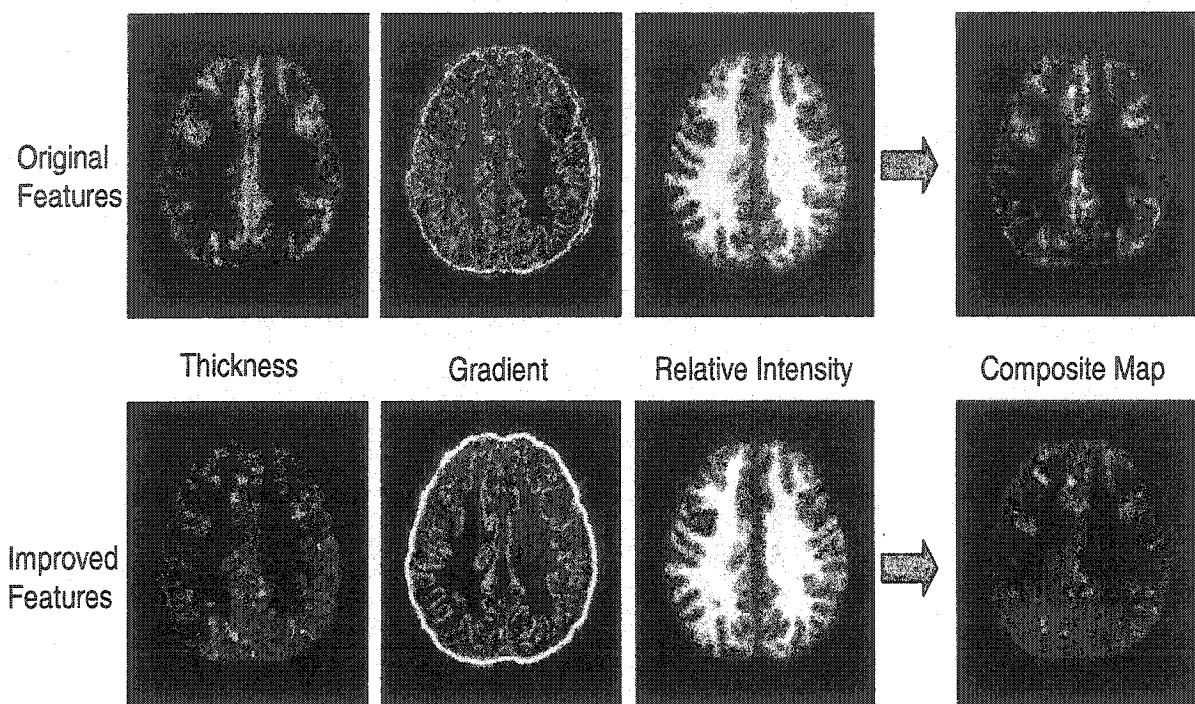


Figure 1. Original and improved feature maps and their associated composite maps.

Axial slices taken from 3D feature maps generated by the three operators used to model commonly noted attributes of FCD lesions on T1-weighted MRI (increased cortical thickness, blurring of gray-matter-white matter interface, and hyperintense signal relative to normal cortex). The associated composite map, defined as thickness times gradient divided by relative intensity, is also shown. Subject is a normal control.

Top row: Original feature maps and composite map. Cortical thickness modeled with gray matter run-length coding. Blurring of GM-WM interface modeled with the gradient magnitude calculated over a moving cubic window. Hyperintense T1 signal modeled as $1 - |B_g - g| / B_g$ where g is the gray level intensity at a given voxel and B_g is the boundary intensity between GM and WM as determined from histogram analysis.

Bottom row: Improved feature maps and composite map. Cortical thickness modeled with a metric based on the solution of Laplace's equation over the cortical GM. Blurring of GM-WM interface modeled with magnitude gradient calculated using a 3mm gaussian kernel calculated explicitly over the whole field in the fourier domain. Hyperintense T1 signal modeled as in the original feature set. The improved composite map exhibits a reduction of hyperintense regions within the cortex.

over all voxels with non-zero intensities. Since the cortical thickness metric is computed only over cortical GM and the portion of the lesion within the GM, WM and CSF were zero-valued within the composite maps. This process was performed for both the original and new composite maps for each patient. Thus the units of the composite maps were Z-scores, representing the number of standard deviations away from the mean. Contrast, defined as the mean Z-score within lesional tissue, was calculated in both the original and the new composite map for each patient. Lesional tissue was identified using lesion labels that had been previously manually segmented on the MRI by an expert observer. Percent change in contrast from the original to the new composite map was then calculated.

Statistical Analysis

To assess whether contrast between lesional tissue and non-lesional cortex was increased in the new set of composite maps, a one-sample t-test was performed to test whether any increase in contrast over the patients was significantly different from zero.

RESULTS

Contrast between lesional tissue and non-lesional cortex was higher in the improved composite maps for 11/14 patients and unchanged for 3/14. The mean percent change of contrast was $59.3\% \pm 61.6\%$. A one-sample t-test demonstrated that this increase in contrast was significant ($p=.002$). In a qualitative sense, most hyperintense regions within non-lesional cortex were eliminated, resulting in easier visual discrimination of lesions. Representative examples are shown in figure 2. In one patient,

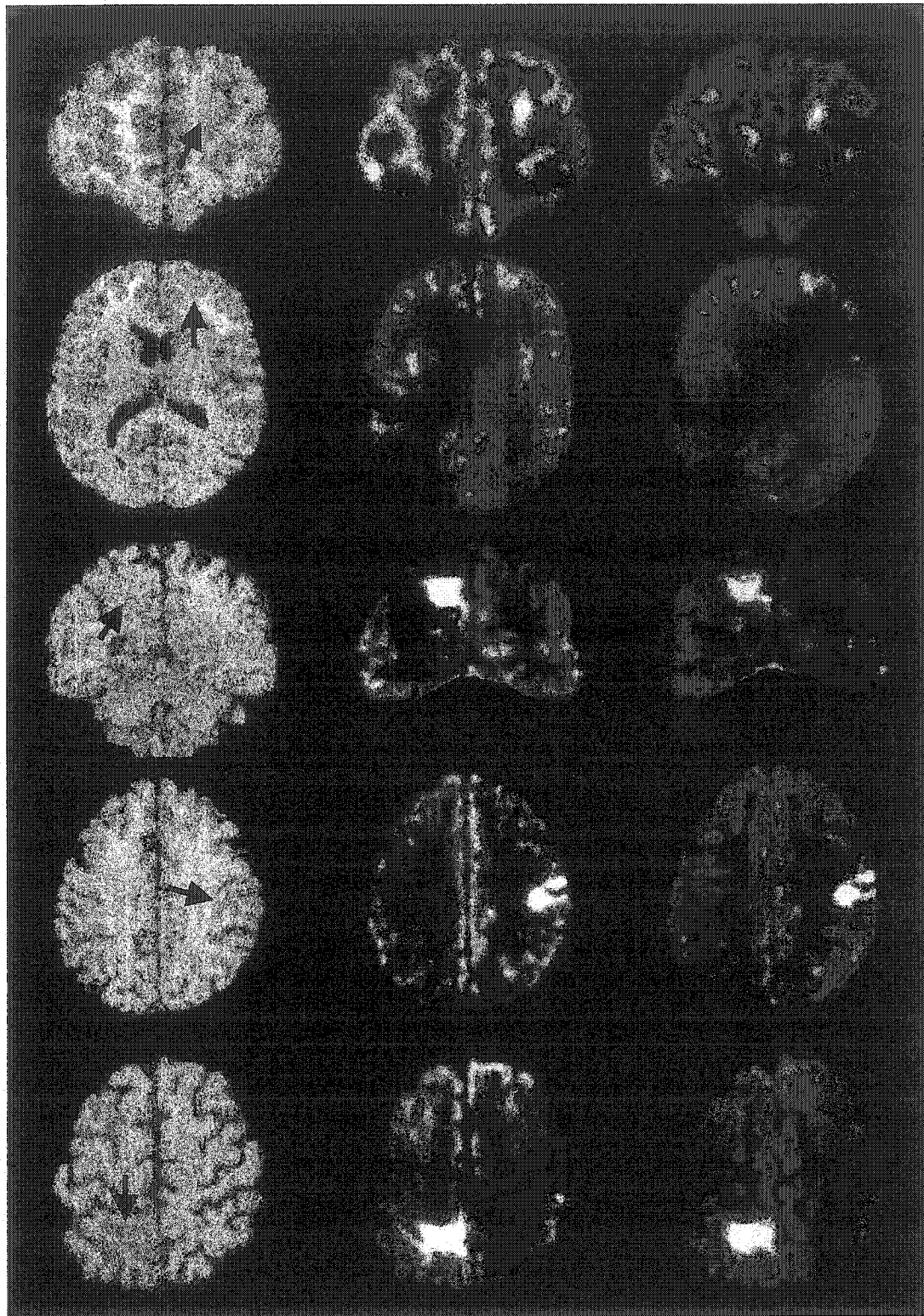


Figure 2. Five examples of improved contrast. Within each panel, the conventional T1-weighted MRI is in the leftmost column, the original composite map set is in the middle column, and the improved composite map is in the right column. Lesion locations are indicated on the conventional MRI by arrows. Intensity within non-lesional cortex is reduced in the improved composite map relative to the original composite map for all five examples.

a lesion which was not visible at all on the original composite map was clearly visible on the improved composite map (figure 3).

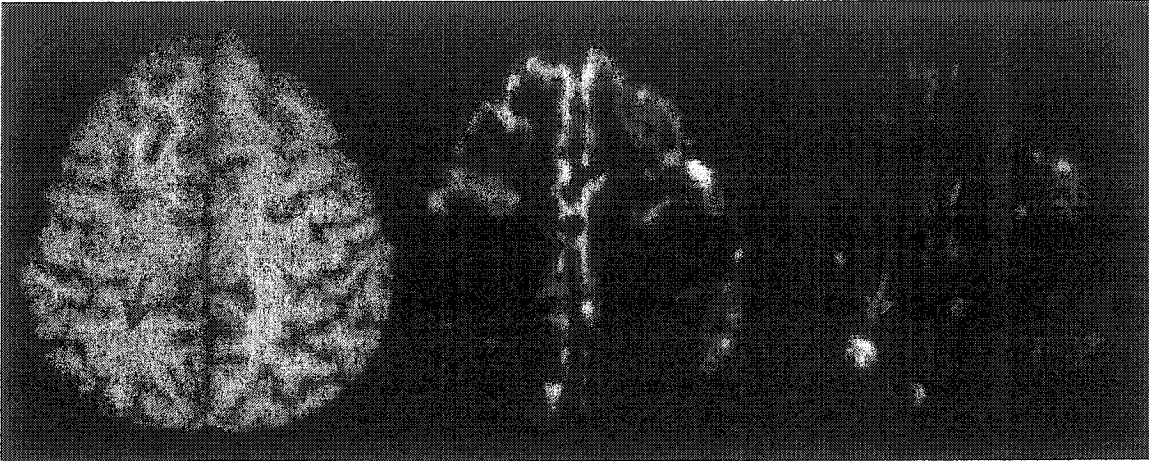


Figure 3. MRI and composite maps for a patient whose lesion was not visible on the original composite map but was evident on the improved composite map. Lesion is indicated by a red arrow on the conventional T1-weighted MRI (left). The lesion is not visible in the original composite map (center). However, generalized hyperintensities are seen along the midline and within the frontal cortex, and in a localized region in the right pre-central area. The improved composite map (right) clearly shows the lesion in the left parietal area and a reduction of the intensity elsewhere in the cortex.

DISCUSSION

We previously used simple image processing models of the pathology of FCD to demonstrate that we could enhance lesion detection through qualitative visual analysis of composite feature maps. The present study builds upon our previous work by incorporating more sophisticated image processing methods that enabled us to increase the contrast of lesions from non-lesional cortex, and thereby enhance lesion visibility. Importantly, in one patient, the FCD lesion was visible only on the improved composite map. The primary cause of the lower contrast in the original composite maps was greater

incidence of hyperintense regions in presumably non-lesional cortex. Most artifacts in the original composite map co-localized with artifacts on the original cortical thickness map, associated with weaknesses in the original model which was based on multidirectional GM run-length coding. The reduction of potential false positives seen in the new composite maps was driven by the use of more sophisticated models of the MRI characteristics of FCD, in particular, the cortical thickness model⁹. The results of our study provide, for the first time, a clinical validation of this cortical thickness metric, which is based upon solving Laplace's equation over the cortical GM. Identification of some FCD lesions on visual inspection of conventional MRI is difficult due to their subtlety and the complexity of the brain's convolution. A primary advantage of the method of Jones et al. is that the thickness metric is based upon the calculation of the equivalent of isopotential surfaces, which follow the convolution of the cortex.

While new techniques are being developed to measure cortical thickness¹¹ and perform tissue segmentation^{10,12,13} and much research has been done on integrating information from multiple attributes, the results of our paper demonstrate that by combining stable, simple mathematical models with high quality imaging data, we have improved upon our previous methods and developed a clinically useful technique.

For use in the measurement of contrast between lesions and non-lesional cortex, manually segmented lesion labels retrospectively painted on pre-operative MRI by an expert observer were used to determine lesion extent. This technique was used because a fully objective or automated technique for lesion segmentation has not yet been developed. To maximize accuracy, the observer relied upon experience as well as

knowledge of the extent and location of surgical resection. The latter information was of particular assistance in the demarcation of smaller lesions.

Although potential false positives were significantly reduced in the improved composite maps, they were not completely eliminated. Undoubtedly, most of these instances can be attributed to overlap of feature values between lesional and non-lesional tissue. Yet it is important to consider the possibility that some potential false positives may in fact be true lesions of FCD. Histopathological analysis of surgical specimens in patients who underwent surgery for medically intractable seizures have shown that FCD may be disseminated rather than confined to a single patch¹⁴ or even be multifocal¹⁵. However, given the very limited availability of autopsy studies in these patients, the degree to which the brain as a whole may be affected remains uncertain. Furthermore, scalp EEG studies and intraoperative recordings in patients with FCD have demonstrated that in many patients epileptic abnormalities emanate not only from the visible lesion, but also from normal-appearing brain regions, which were subsequently proven histologically to harbor FCD¹⁶. It has become clear that the areas of the brain generating these abnormalities have to be surgically resected in addition to the visible lesion in order to obtain a good result. Therefore, our quantitative MRI method, which makes use of the large amount of data that may be too subtle to be appreciated by visual analysis, has an obvious potential in identifying the true extent of malformations of cortical development. The challenge is to identify areas of lesser but still significant pathological abnormality and to determine if their resection may influence surgical outcome.

In conclusion, the use of the improved models of FCD pathology presented in this paper produce feature maps with fewer potential false positives. This improvement is an important step towards the eventual goal of automated FCD lesion detection.

REFERENCES

1. Sisodiya SM. Surgery for malformations of cortical development causing epilepsy. *Brain* 2000; 123:1075-1091.
2. Barkovich AJ, Kuzniecky RI. Neuroimaging of focal malformations of cortical development. *J Clin Neurophysiol* 1996; 13(6):481-494.
3. Grant PE, Vingneron DB, Barkovich AJ. High-resolution imaging of the brain. *Magn Reson Imaging Clin N Am* 1998; 1:139-154.
4. Barkovich AJ, Rowley HA, Andermann F. MR in partial epilepsy: value of high-resolution volumetric techniques. *AJNR Am J Neuroradiol* 1995; 16(2):339-343.
5. Bernasconi A, Antel SB, Collins DL, Bernasconi N, Olivier A, Dubeau F et al. Texture analysis and morphological processing of magnetic resonance imaging assist detection of focal cortical dysplasia in extra-temporal partial epilepsy. *Ann Neurol* 2001; 49(6):770-775.
6. Sled JG, Zijdenbos AP, Evans AC. A nonparametric method for automatic correction of intensity nonuniformity in MRI data. *IEEE Trans Med Imaging* 1998; 17:87-97.

7. Collins DL, Neelin P, Peters TM, Evans AC. Automatic 3D intersubject registration of MR volumetric data in standardized Talairach space. *J Comput Assist Tomogr* 1994; 18(2):192-205.
8. Smith S. Robust automated brain extraction. *Sixth International Conference on Functional Mapping of the Human Brain* 2000;625.
9. Jones SE, Buchbinder BR, Aharon I. Three-dimensional mapping of cortical thickness using Laplace's equation. *Hum Brain Mapp* 2000; 11(1):12-32.
10. Schnack HG, Hulshoff Pol HE, Baare WF, Staal WG, Viergever MA, Kahn RS. Automated separation of gray and white matter from MR images of the human brain. *Neuroimage* 2001; 13(1):230-237.
11. Yezzi A, Prince JL. A PDE approach for measuring tissue thickness. *Proc 2001 CVPR*.
12. Ruan S, Jaggi C, Xue J, Fadili J, Bloyet D. Brain tissue classification of magnetic resonance images using partial volume modeling. *IEEE Trans Med Imaging* 2000; 19(12):1179-1187.
13. Shattuck DW, Sandor-Leahy SR, Schaper KA, Rottenberg DA, Leahy RM. Magnetic resonance image tissue classification using a partial volume model. *Neuroimage* 2001; 13(5):856-876.
14. Taylor DC, Falconer MA, Bruton CJ, Corsellis JA. Focal dysplasia of the cerebral cortex in epilepsy. *J Neurol Neurosurg Psychiatry* 1971; 34(4):369-387.

15. Prayson RA, Spreafico R, Vinters HV. Pathologic characteristics of the cortical dysplasias. *Neurosurg Clin N Am* 2002; 13(1):17-25.

16. Palmini A, Gambardella A, Andermann F, Dubeau F, da Costa JC, Olivier A et al. Intrinsic epileptogenicity of human dysplastic cortex as suggested by corticography and surgical results. *Ann Neurol* 1995; 37(4):476-487.

4.4 Manuscript 4

Manuscript is revision for publication in NeuroImage.

Automated Detection of Focal Cortical Dysplasia Lesions using Computational Models of Their MRI Characteristics and Texture Analysis.

Samson B. Antel, MSc¹; D. Louis Collins, PhD^{1,2}; Neda Bernasconi, MD²; Rajjan Shinghal, PhD³; Robert E. Kearney, PhD¹; Douglas L. Arnold, MD²; Andrea Bernasconi, MD²

¹Departments of Biomedical Engineering and ²Neurology & Neurosurgery, Montreal Neurological Institute, McGill University, and ³Department of Computer Science, Concordia University, Montreal, Quebec, Canada

Correspondance to:

Andrea Bernasconi, MD
Montreal Neurological Institute
3801 University St.
Montreal, PQ H3A 2B4
Phone: (514)-398-8524
Fax: (514)-398-2975
E-mail: andrea@bic.mni.mcgill.ca

ABSTRACT

Focal cortical dysplasia (FCD), a malformation of cortical development, is a frequent cause of pharmacologically intractable epilepsy. FCD is characterized on T1-weighted MRI by cortical thickening, blurring of the gray-matter/white-matter interface, and gray-level hyperintensity. We have previously used computational models of these characteristics to enhance visual lesion detection. In the present study we seek to improve our methods by combining these models with features derived from texture analysis of MRI, which allows measurement of image properties not readily accessible by visual analysis. These computational models and texture features were used to develop a two-stage Bayesian classifier to perform automated FCD lesion detection. Eighteen patients with histologically confirmed FCD and 14 normal controls were studied. On the MRI volumes of the 18 patients, 20 FCD lesions were manually labeled by an expert observer. 3D maps of the computational models and texture features were constructed for all subjects. A Bayesian classifier was trained on the computational models to classify voxels as cerebrospinal fluid, gray-matter, white-matter, transitional, or lesional. Voxels classified as lesional were subsequently re-classified based on the texture features. This process produced a 3D lesion map, which was compared to the manual lesion labels. The automated classifier identified 17/20 manually labeled lesions. No lesions were identified in controls. Thus, combining models of the T1-weighted MRI characteristics of FCD with texture analysis enabled successful construction of a classifier. This computer-based, automated method may be useful in the pre-surgical evaluation of patients with severe epilepsy related to FCD.

INTRODUCTION

Focal cortical dysplasia (FCD) is a malformation of cortical development corresponding to a localized disruption of the normal cortical lamination associated with an excess of large, aberrant neurons, an increase in cortical thickness, and often, abnormal neuroglial elements in the underlying white matter (WM). The dysplastic tissue retains sufficient connectivity to produce seizures (Palmini et al. 1995; Gambardella et al. 1996; Avoli et al. 1999). FCD is the most common form of developmental disorder in patients with pharmacologically intractable partial epilepsy referred for pre-surgical evaluation (Sisodiya 2000).

On T1-weighted MRI, FCD is mainly characterized by variable degrees of cortical thickening, a poorly defined transition between gray matter (GM) and WM, and hyperintense signal within the dysplastic lesion relative to normal cortex (Barkovich & Kuzniecky 1996; Lee et al. 1998). High-resolution MRI of the brain has made it possible to identify FCD in an increasing number of patients (Barkovich & Kuzniecky 1996; Grant et al. 1998). However, in many patients, lesions of FCD are characterized by minor structural abnormalities that go unrecognized or are too subtle to be detected by standard radiological analysis. Previous attempts in assisting lesion detection included different contrast imaging (Chan et al. 1998), multiplanar curvilinear reformatting of 3D MRI (Bastos et al. 1999), and statistical parametric mapping (Woermann et al. 1999; Kassubek et al. 2002).

We previously implemented and used for the first time computational models of MRI characteristics of FCD for the purposes of lesion enhancement (Bernasconi et al. 2001).(Antel et al. 2002) Models were applied on a voxelwise basis, creating 3D maps of

cortical thickness, gradient magnitude (modeling the transition between GM and WM), and a relative intensity operator (designed to emphasize areas with hyperintense T1 signal). Visual analysis of a composite map of these features yielded significantly higher sensitivity for lesion detection compared to visual analysis of conventional T1-weighted MRI (Bernasconi et al. 2001).

While this technique facilitated visual lesion detection, two shortcomings of the method were: i) subjectivity, requiring the expertise of a highly trained observer with particular regard to differentiating between FCD lesions and localized hyperintense regions in presumably non-lesional cortex; and ii) reliance on a composite of feature maps, potentially losing information regarding the pattern of feature values within lesions and non-lesional tissue.

An automated, computer-based classifier addresses both issues by performing a quantitative analysis of the pattern of feature values. The first issue can also be partially addressed through the use of gray-level co-occurrence matrix (GLCM) based texture analysis (Haralick et al. 1973), which quantifies the spatial distribution of gray-level intensity pairs. This information may not be readily accessible through visual analysis, and thus this technique can provide an additional basis for decision making. GLCM-based texture analysis has been applied to MRI of the brain in several contexts: characterization of brain tumors (Schad et al. 1993; Lerski et al. 1993), differentiating the brains of patients with Alzheimer's disease from those of normal controls (Freeborough & Fox 1998), revealing hippocampal abnormalities related to hippocampal sclerosis (Yu et al. 2001), and characterization of brain and spinal cord pathology in multiple sclerosis (Yu et al. 1999; Mathias et al. 1999). The usefulness of applying GLCM-based texture

analysis to brain MRI may in part arise from an intuitive parallel between changes in spatial distributions of gray level intensity patterns and abnormal tissue organization (Schad et al. 1993), such as those thought to give rise to FCD.

Thus, the purpose of this study is to use computational models of MRI characteristics of FCD as well as features derived from GLCM-based texture analysis as a basis for a computer-based classifier to perform automated FCD lesion detection.

METHODS

Subjects

Eighteen patients with FCD (mean age = 34 +/- 2.5 yrs; 9 females, 9 males) and 14 healthy controls (mean age = 32 +/- 4.1 yrs; 8 females, 5 males) were studied. All 18 FCD patients underwent surgical resection of the FCD lesion due to pharmacologically intractable epilepsy. As part of a standard pre-surgical radiological investigation, FCD had been prospectively recognized on MRI prior to surgery in 11 of the 18 patients. For the seven patients in whom no lesion was visible, surgery was based on strong clinical and EEG co-localizing information. In all 18 patients, FCD was subsequently proven based on histological examination of the resected tissue. Lesions were categorized according to a recent classification scheme (Barkovich et al. 2001). All patients had malformations of cortical development due to abnormal glial proliferation or apoptosis, namely non-neoplastic abnormal proliferation (cortical dysplasia with balloon cells) (N=16), or malformations due to abnormal cortical organization, namely cortical dysplasia without balloon cells (N=2).

MRI acquisition

Preoperative MRI images were acquired on a 1.5 T Gyroscan (Philips Medical System, Best, The Netherlands) using a T1-fast field echo sequence (TR=18, TE=10, 1 acquisition average pulse sequence, flip angle=30°, matrix size=256x256, FOV=256, thickness=1mm). Approximately 170 slices with an isotropic voxel size of 1 mm³ were acquired. Signal to noise ratio was calculated for each subject to ensure image quality (mean=27.86, sd=2.01).

Image Preparation

Images were analyzed on a Silicon Graphics workstation (Mountain View, California, USA). All MRIs were free of visible motion artifacts. Images were automatically registered into stereotaxic space to adjust for differences in total brain volume and brain orientation (Collins et al. 1994). Each image underwent automated correction for intensity non-uniformity and intensity standardization (Sled et al. 1998). This correction produces consistent relative GM, WM, and cerebrospinal fluid (CSF) intensities. Manual lesion segmentation was performed retrospectively on the corrected images by an experienced observer who was aware of findings from EEG data as well as the area of surgical resection. Hence this observer was able to identify lesions in all 18 patients. Note that this retrospective manual lesion segmentation represents a different analysis than the standard pre-surgical MRI evaluation that identified lesions in 11/18 patients and overlooked lesions in the remaining seven patients. As will be described later, these manual lesion labels were used in the training and validation of the classifier.

Brain extraction was then performed on the MRI using the Brain Extraction Tool (Smith 2000).

Tissue Segmentation

Segmentation of MRI volumes into GM, WM, and CSF was performed by fitting gaussian curves to the peaks within the histogram corresponding to GM and WM (figure 1A). The intersection of these gaussian peaks was taken as the boundary intensity between GM and WM. Voxels with intensities of more than 2 SDs below the mean GM intensity were segmented as CSF. The resulting segmented map was used as a basis for calculating cortical thickness.

Further segmentation was performed for eventual use in training the classifier by defining three additional classes. A GM/WM transition class was defined as follows, based on the construction of a 3x3x3 neighborhood around each voxel. A voxel was identified as belonging to the GM/WM transition class if at least 30% of neighboring voxels were GM and at least 30% of neighboring voxels were WM. An analogous procedure was performed to define a GM/CSF transition class. For patients, a lesional class was created by incorporating the manual lesion labels. The derivation and a typical example of a 6-class segmented map are shown in figures 1B and 1C.

Calculation of computational models of MRI characteristics of FCD

Three common *in vivo* characteristics of FCD lesions as seen on T1-weighted MRI were modeled: cortical thickening, blurring of the GM/WM interface, and hyperintense T1 signal. The following sections describe these models.

Cortical Thickness Measurement

An approach developed by Jones et al. (Jones et al. 2000) was used to measure cortical thickness. This method considers the cortical volume as an electrostatic field, Ψ , with the inner and outer cortical surfaces set to arbitrary (but non-equal) constants. The solution of Laplace's equation:

$$\nabla^2\Psi = \partial^2\Psi/\partial x^2 + \partial^2\Psi/\partial y^2 + \partial^2\Psi/\partial z^2 = 0$$

over the cortical volume yields a series of smoothly varying intermediate "isopotential" surfaces between the two boundaries. Upon solving for Ψ , a unit vector field can be computed over the cortex as

$$N = -\nabla\Psi/||-\nabla\Psi||$$

such that the field is defined everywhere between the inner and outer cortical surfaces, and is always perpendicular to the adjacent isopotential surface. To determine cortical thickness, then, so-called streamlines are computed by starting at any point on one of the surfaces, and integrating N . The length of the streamline that passes through a particular voxel is the cortical thickness at that voxel.

Gradient magnitude

Gradient magnitude is a standard first-order statistical operator that measures the rate of intensity change over a given domain. To model the blurring of the GM-WM interface, gradient magnitude was calculated through convolution of the MRI volume, (accomplished by multiplication in the Fourier domain) with a three-dimensional gaussian kernel (FWHM = 3mm) calculated explicitly over the whole field. The final result was obtained by inverse Fourier transform.

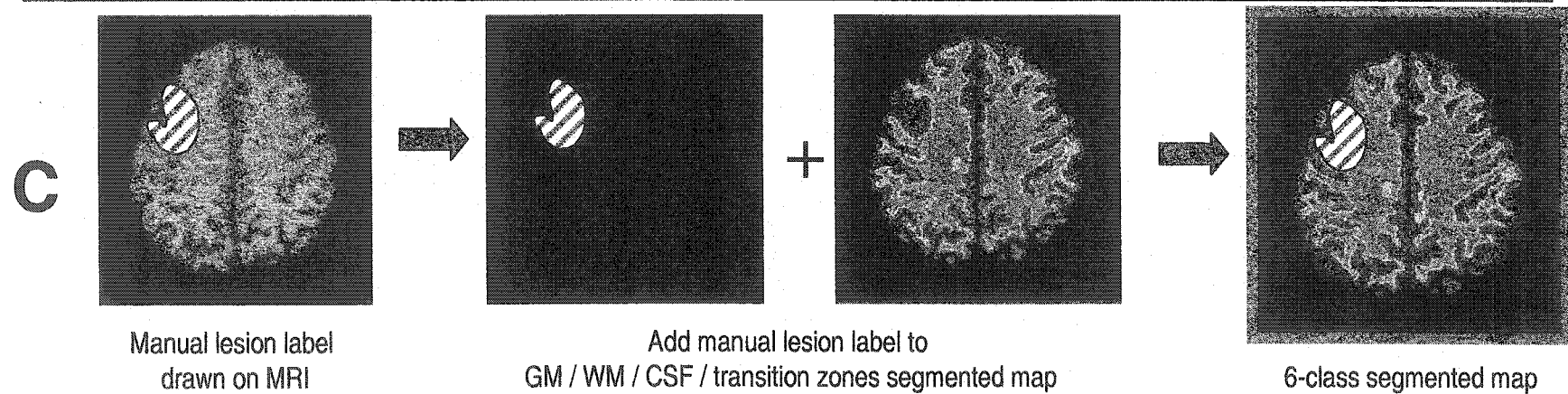
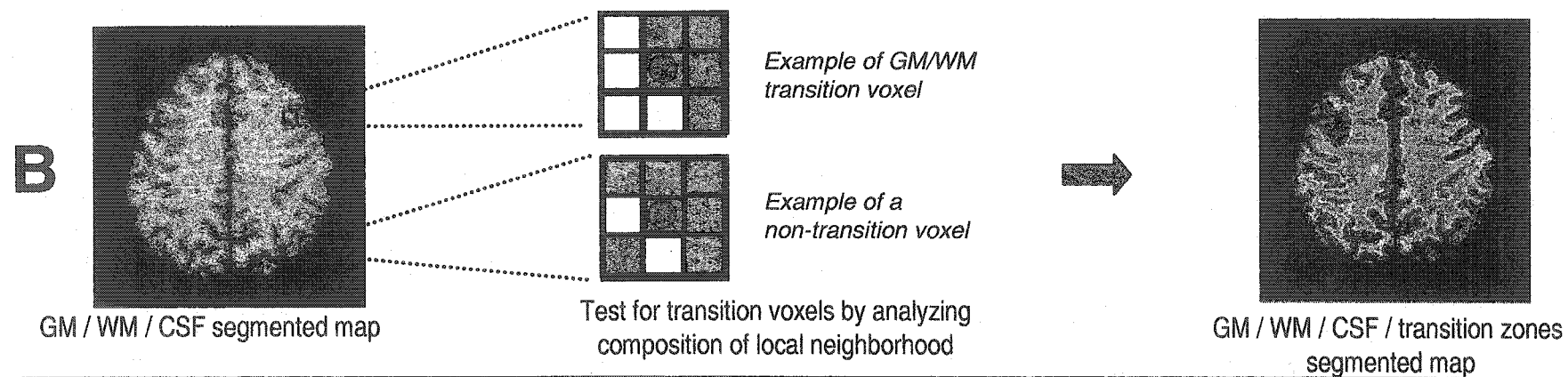
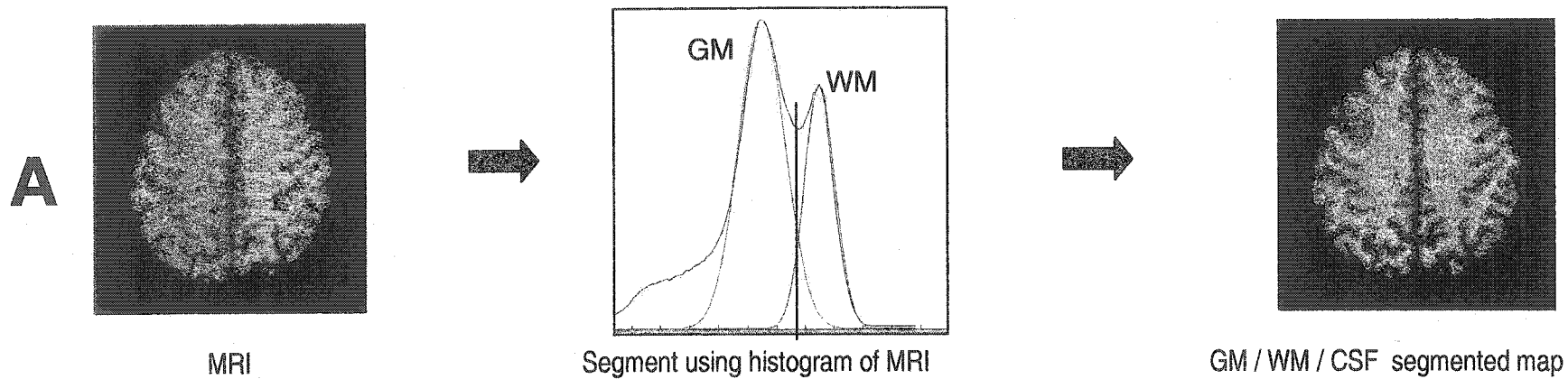


Figure 1. Segmentation of MR volumes.

(A). T1-weighted MRI volumes were segmented into gray matter (GM), white matter (WM), and cerebro-spinal fluid (CSF) by fitting Gaussian curves to the gray-level histogram (middle), resulting in a GM/WM/CSF segmented map (right), used as a basis for measuring cortical thickness.

(B). The GM/WM/CSF segmented maps were further segmented into more classes for use in training the classifiers. GM/WM and GM/CSF transition classes were defined by analyzing the local neighborhood surrounding each voxel within the GM/WM/CSF map (schematically represented by red box). A voxel (indicated by the red dot) was determined to belong to the GM/WM transition class if at least 30% of neighboring voxels were GM and at least 30% of neighboring voxels were WM. A similar algorithm was used for the GM/CSF transition class. The result is a segmented map exhibiting the following classes: CSF, GM, WM, GM/WM transition, and GM/CSF transition.

(C) As an additional step performed for patients, lesions were manually segmented by an expert observer (left). Adding these lesion labels to the segmented map generated by the previous step (middle) resulted in the 6-class segmented map (right).

Relative Intensity

The relative intensity operator is designed to emphasize hyperintense T1 signal within GM. It is defined as

$$1 - |g - Bg| / Bg$$

where g is the intensity at a given voxel, and Bg is the threshold intensity between the GM and WM peaks as determined from the grey level histogram of the MRI volume.

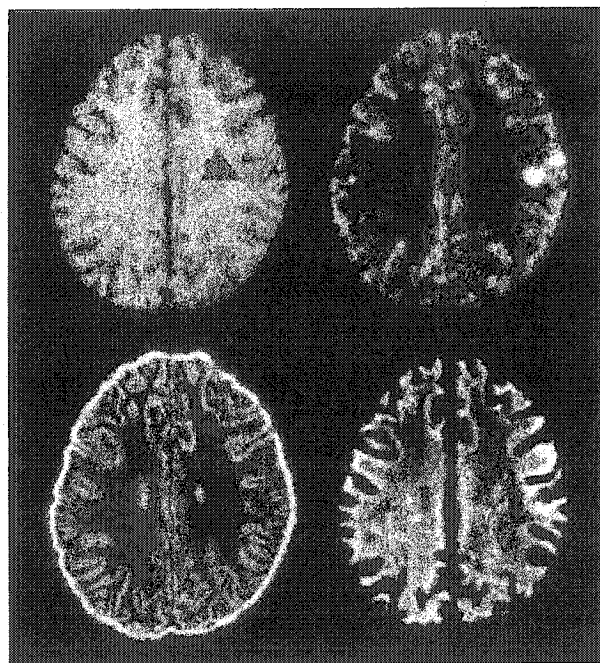


Figure 2. Representative axial slices from maps of the three computational models of MRI characteristics of FCD pathology in a patient. Clockwise from top left: T1-weighted MRI; cortical thickness; gradient magnitude; relative intensity. Lesion can be seen in the right central area (indicated by red arrow on T1-weighted MRI).

Texture Analysis

The basic procedure of texture analysis is to compute a set of gray-level co-occurrence matrices (GLCMs) and then run a set of mathematical texture operators on the co-occurrence matrices to produce a corresponding set of texture feature values (Haralick

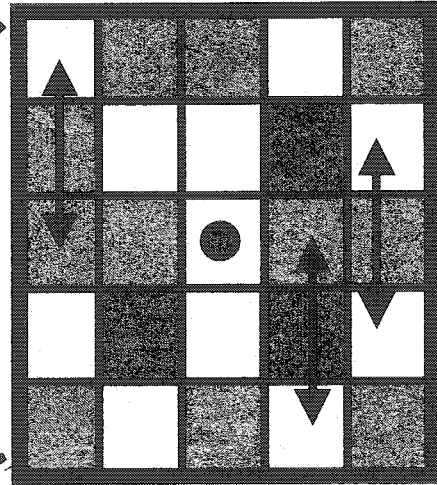
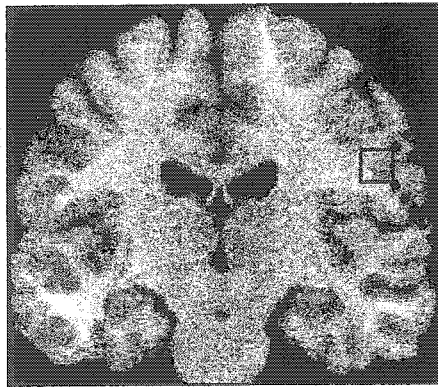
et al. 1973). A co-occurrence matrix is calculated over a region of interest by tallying the occurrences of all voxel intensity pairs separated by a given distance in a given direction (Figure 3). The matrix is then normalized by the total number of voxel intensity pairs within the region to yield the probability of observing each pair. In order to produce three-dimensional texture maps, we calculated co-occurrence matrices over a neighborhood centered on each voxel within the volume, with the resulting texture feature values being mapped to the location of the center voxel.

There are several parameters that can be manipulated in the calculation of co-occurrence matrices. Primary among these are neighborhood size, distance (d), and direction (θ). The number of possible permutations of these parameters necessitates that only a subset be chosen for use in analysis.

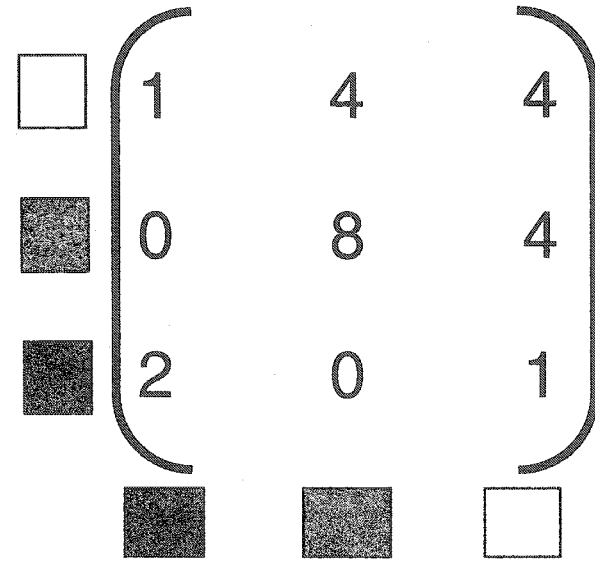
In the context of our aim of detecting FCD lesions of variable size, neighborhood size must be chosen to be large enough to capture meaningful information, but small enough that smaller lesions are not lost within a large ROI. We chose to use a 3D neighborhood, 7 voxels in each dimension.

Varying the distance parameter allows texture to be measured at different scales. Care must be taken not to overstep the size of the lesions. Neighborhood size is also a limiting factor in the choice of the distance parameter so as to avoid sparse co-occurrence matrices. We set the distance parameter to 3 voxels. As a further precaution against sparse co-occurrence matrices and to reduce processing time, the intensity range of the MRI volumes was reduced to 32 gray levels.

When constructing a co-occurrence matrix over a 2D neighborhood, there are eight possible discretized values of θ ($0^\circ, \pm 45^\circ, \pm 90^\circ, \pm 135^\circ, 180^\circ$). A common approach

A

MRI voxels



Gray-level co-occurrence matrix

B

T1-weighted MRI

Angular second momentum

Contrast

Difference entropy

Figure 3. Construction of second-order texture maps.

(A) To obtain a second-order texture map, a small ROI (schematically represented by the red square) was constructed around each voxel in an MR volume. Within this ROI, the number of occurrences of the various voxel-intensity pairs, separated by a given distance in a given direction (sample pairs are indicated by arrows), are tallied to produce a co-occurrence matrix. Second-order texture feature operators are then run on the matrix, with the resulting value being mapped back to the position of the voxel at the center of the ROI.

(B) Representative axial slices from the three second-order texture maps used to construct a Bayesian classifier, with the associated T1-weighted MRI. Lesion is visible in the right central area, indicated by the red arrow on the T1-weighted MRI.

is to create symmetric co-occurrence matrices by considering θ and $-\theta$ together. We used the same approach in the 3D case, collapsing the 26 possible discretized directions into 13.

Thus, at each voxel we calculated 13 co-occurrence matrices, one for each value of θ . The value of d was set to 3 for all matrices. Texture feature operators were then run on each co-occurrence matrix at each voxel to create a three-dimensional texture feature map. As there is no expectation of a particular orientation to the texture of FCD lesions within T1 volumes, the texture feature value assigned to a voxel was the average of the texture feature value calculated over each of the 13 co-occurrence matrices.

Haralick (Haralick et al. 1973) proposed 14 second order features; we chose to calculate those that are among the most commonly used in the literature: angular second momentum, contrast, correlation, difference entropy, dissimilarity, entropy, inverse difference moment, sum entropy, and variance. Appendix A details the mathematical operations necessary to derive these second order texture features from a co-occurrence matrix.

Classifier Design

Automated lesion identification was performed using a sequence of two Bayesian classifiers. As a first step, lesion identification was performed using a classifier trained on the three computational models (the “computational-model classifier”). Voxels classified as lesional were then re-classified by a classifier trained on the second-order texture features (the “texture feature classifier”). For the construction of the texture feature classifier, Fisher’s discriminant ratio (Duda et al. 2001) was calculated to select

three texture features (angular second momentum, difference entropy, contrast) from among the 9 that were calculated. The two-classifier approach is justified since the computational models of MRI characteristics of FCD and the texture features extract different types of information from the MRI volume. The computational models measure first-order statistical or morphometric properties of individual voxels, while the texture features measure second-order properties of the volume by examining spatial relationships between voxels of varying intensities. Thus, two classifiers are appropriate as they would be highly trained in different regions of feature space (Duda et al. 2001).

Due to the limited number of patients in the study, both the computational model classifier and the texture feature classifier were constructed using the leave-one-out cross-validation technique, in which each member of a set N members is classified based on a classifier trained on the remaining N-1 members. In this study, we implemented a leave-one-out classifier on a subject-wise basis, such that all voxels in a particular subject's brain were classified based on voxels within the brains of the other subjects. Each classifier was trained on the appropriate data (i.e., the computational models or texture features) for a subset of voxels that had been automatically sampled from each subject within the training set. To sample the voxels, the following tissue-specific (based on the 6-class segmented map) sampling frequencies were used: every 45th background/CSF voxel, every 10th GM voxel, every 10th WM voxel, every 5th GM/WM transition voxel, every 5th GM/CSF transition voxel, and every 2nd lesional voxel. These sampling frequencies were chosen to achieve roughly equal numbers of voxels in each class, and resulted in approximately 3000 sampled voxels per subject. A target label was determined for each sampled voxel from the 6-class segmented map.

The two classifiers were combined as follows. First, all voxels within a test subject's brain were classified with the computational model classifier. Prior probabilities were set so as to bias the computational model classifier toward increasing sensitivity regarding lesional voxels at the expense of mis-classifying some GM voxels as lesional. Next, voxels classified as lesional by the computational model classifier were re-classified using the texture feature classifier. Primarily due to the use of the cortical thickness metric, almost all voxels classified as lesional by the computational model classifier belonged to either the true lesional or GM classes. Thus, the texture feature classifier was restricted to classifying voxels as either lesional or GM. A 3D lesion map was constructed from the voxels classified as lesional by the texture feature classifier.

Voxels within several anatomical structures (thalamus, basal ganglia, caudate nucleus, and cerebellum) were not included when assessing the performance of the classifier. Most voxels within these structures (consisting mainly of GM) were classified as lesional in both patients and normal controls, primarily due to their high thickness relative to the cortex. Further, no biological evidence exists that these structures are involved in FCD.

An additional artifact was the random scattering of small clusters of voxels classified as lesional across the classified volumes. Thus, to establish a baseline noise level in the classified volumes, a noise threshold was defined as two standard deviations above the mean size of the largest lesional cluster in each control subject, such that lesional clusters smaller than this threshold were considered to be due to random noise and excluded from the lesion map produced by the classifier. This threshold was applied to all subjects, both patients and controls. This technique assumes that lesional clusters in

the controls are not due to FCD. Even if the clusters in control subjects were due to something physiologically meaningful, from the point of view of FCD lesion detection they would still be considered noise, as FCD lesions are unlikely to occur in control subjects.

The Bayesian classifier code was implemented in C running on an SGI platform, incorporating a library of MRI volume handling routines developed at the McConnell Brain Imaging Center of the Montreal Neurological Institute.

Analysis

The performance of the classifier was compared to standard neuroradiological pre-surgical evaluation of MRI by calculating subject-wise sensitivity and specificity for both methods. Subject-wise sensitivity was defined as the number of patients in whom a lesion was identified divided by the total number of patients. Subject-wise specificity was defined as the number of control subjects in whom no lesions were identified divided by the total number of control subjects. For the classifier, a lesion was considered to be identified in a patient if a lesional cluster wholly or partially co-localized with a manual lesion label, and in a control subject if any lesional cluster was found. Pearson's chi-squared test for 2 way tables was used to test for significant differences.

Lesional sensitivity of the classifier was measured by calculating the number of lesional clusters identified by the classifier which wholly or partially co-localized with a manually-drawn lesion label divided by the total number of manually drawn lesion labels. This differs from subject-wise sensitivity due to the presence of multiple manually-drawn lesion labels in some patients. Lesion specificity was not calculated since the absence of

a lesion cluster generated by the classifier in non-lesional regions of the brain (a “true negative”) is not a quantifiable concept. Therefore, to measure the degree of false positives with respect to lesional clusters, the number of lesional clusters not co-localizing with a manual lesion label was determined for each subject.

To measure the ability of the classifier to identify the full extent and boundaries of lesions, voxelwise sensitivity on a patient-wise basis was calculated as the total number of voxels correctly classified as lesional within a patient divided by the total number of voxels within the manual lesion labels for the same subject. An aggregate voxel sensitivity was calculated as the total number of voxels correctly classified as lesional across all patients divided by the total number of voxels within the manual lesion labels across all patients.

As a further measure of agreement between the lesional clusters identified by the classifier and the manual lesion labels, an agreement index was calculated. Letting L_c represent the lesional cluster identified by the classifier and L_m representing the corresponding manual lesion label, the agreement index was defined as:

$$\frac{L_c \cap L_m}{(L_c \cup L_m) - (L_c \cap L_m)}$$

Differences in texture feature values within lesions compared to non-lesional cortex was assessed as follows. For each texture feature used in the classifier (angular second momentum, contrast, difference entropy), the average value over the manual lesion label and the average value over non-lesional GM (as defined in the 6-class

segmented map) were calculated for each patient. These results were then averaged across patients and two-tailed t-tests were used to check for significant differences.

RESULTS

The classifier identified lesions in 15/18 patients, resulting in a subject-wise sensitivity of 83%. FCD was detected on conventional MRI during standard pre-surgical evaluation in 11 of the 18, resulting in a subject-wise sensitivity of 61%. The increased sensitivity provided by the classifier was shown to be significant ($p < .03$). Neither standard pre-surgical evaluation nor the classifier identified lesions in any control subjects; thus subject-wise specificity was 100% for both techniques.

Within the 18 patients, 20 lesions were manually labeled. The classifier identified wholly or partially co-localizing lesional clusters corresponding to 17 of these manual labels, for a lesion sensitivity of 85%. A comparison of manual lesion labels and lesional clusters determined by the classifier for seven typical subjects are shown in Figures 4 and 5.

While no lesional clusters were identified by the classifier in the control subjects, the classifier identified small lesional clusters not co-localizing with a manual lesion label in 5 out of 18 patients. Retrospective visual review of conventional MRI for these cases did not definitively reveal lesional tissue in these areas.

Average voxelwise sensitivity across all patients was $13.4\% \pm 13.3\%$ (range=0% to 42.4%). Voxelwise sensitivity collapsed across patients was 18.1% (26300/145632). When considering only patients in whom a lesion was identified by the classifier, these results increase to $16.0\% \pm 13.0\%$ and 20.0% (26300/131217), respectively. The average

of the individual patients' agreement index between lesional clusters identified by the classifier and the manual lesion labels was 18% with a standard deviation of 20%.

Within control subjects, the average size of the largest lesional cluster created by the classifier was 16.2 +/- 18.9 (minimum = 0, maximum = 31), and thus the noise threshold was set to 54.0. For patients, the average size of the lesions identified by the classifier which co-localized with the manual lesion labels was 1364.2, +/- 3352.83 (minimum = 12, maximum = 14435).

Angular second momentum was significantly higher in lesions compared to non-lesional cortex, while contrast and difference entropy were significantly lower in lesions compared to non-lesional cortex. These results are summarized in Table 1.

DISCUSSION

The classifier presented in this paper is an extension of our previous work, which introduced (Bernasconi et al. 2001) and refined (Antel et al. 2002) the use of computational models of FCD to enhance visual lesion detection. The classifier improved upon these earlier techniques by providing an automated, objective approach to lesion detection, based on information from two sets of features.

The first set of features, modeled on visually discernable MRI characteristics of FCD lesions, enabled prior knowledge of an expert observer to be built into the classifier. In lesions, relative to non-lesional cortex, cortical thickness and relative intensity are increased, while gradient magnitude is decreased. Increased cortical thickness is due to an abnormal accumulation of neurons in the affected cortical layers. A decrease in gradient magnitude suggests a more gradual transition between GM and WM, reflective

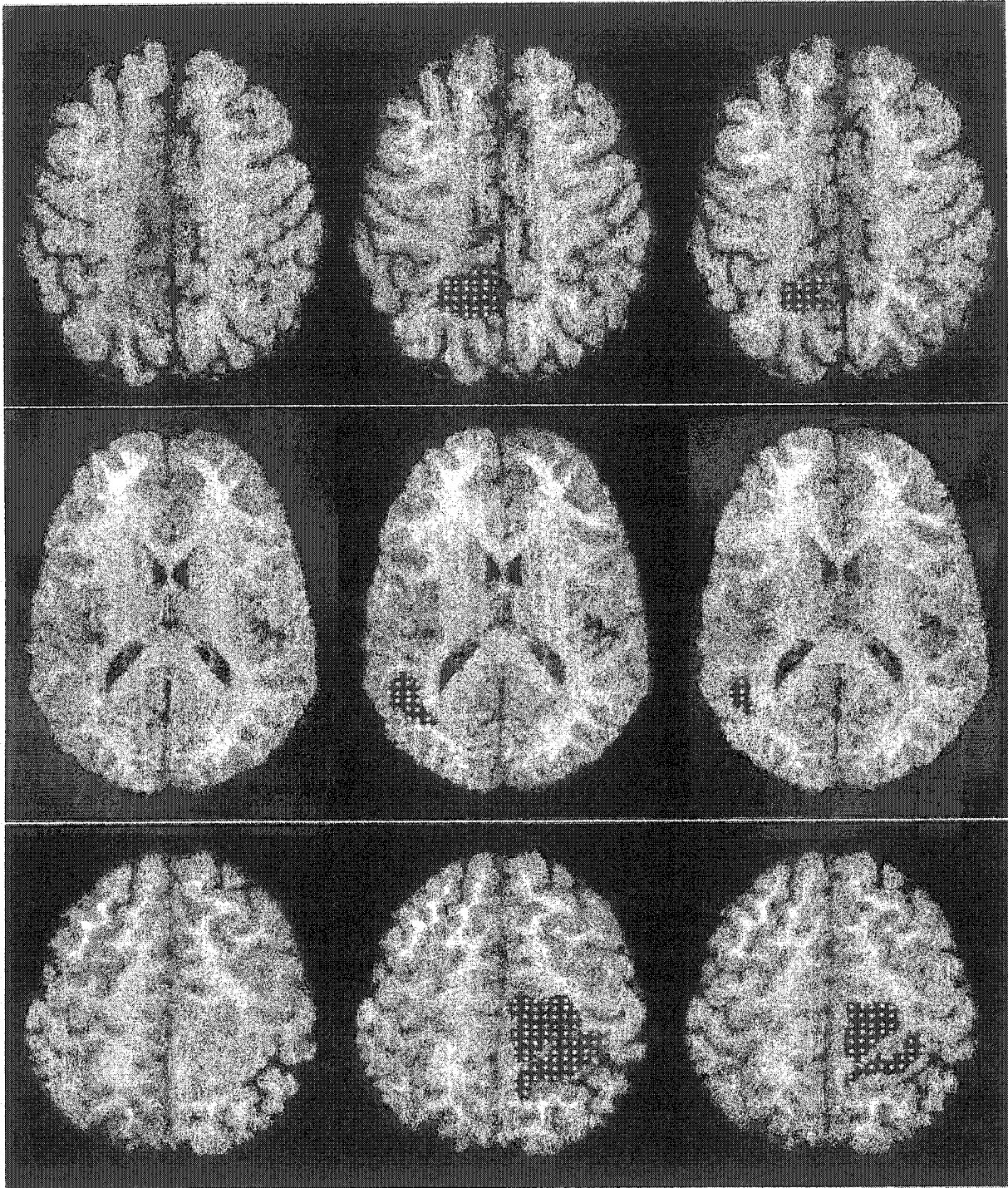


Figure 4a. Three examples of automated lesion identification. Left: T1-weighted MRI. Center: MRI with manual lesion label. Right: MRI with lesion identified by classifier. Both manual and classifier-generated labels are shown as white dots on a black background.

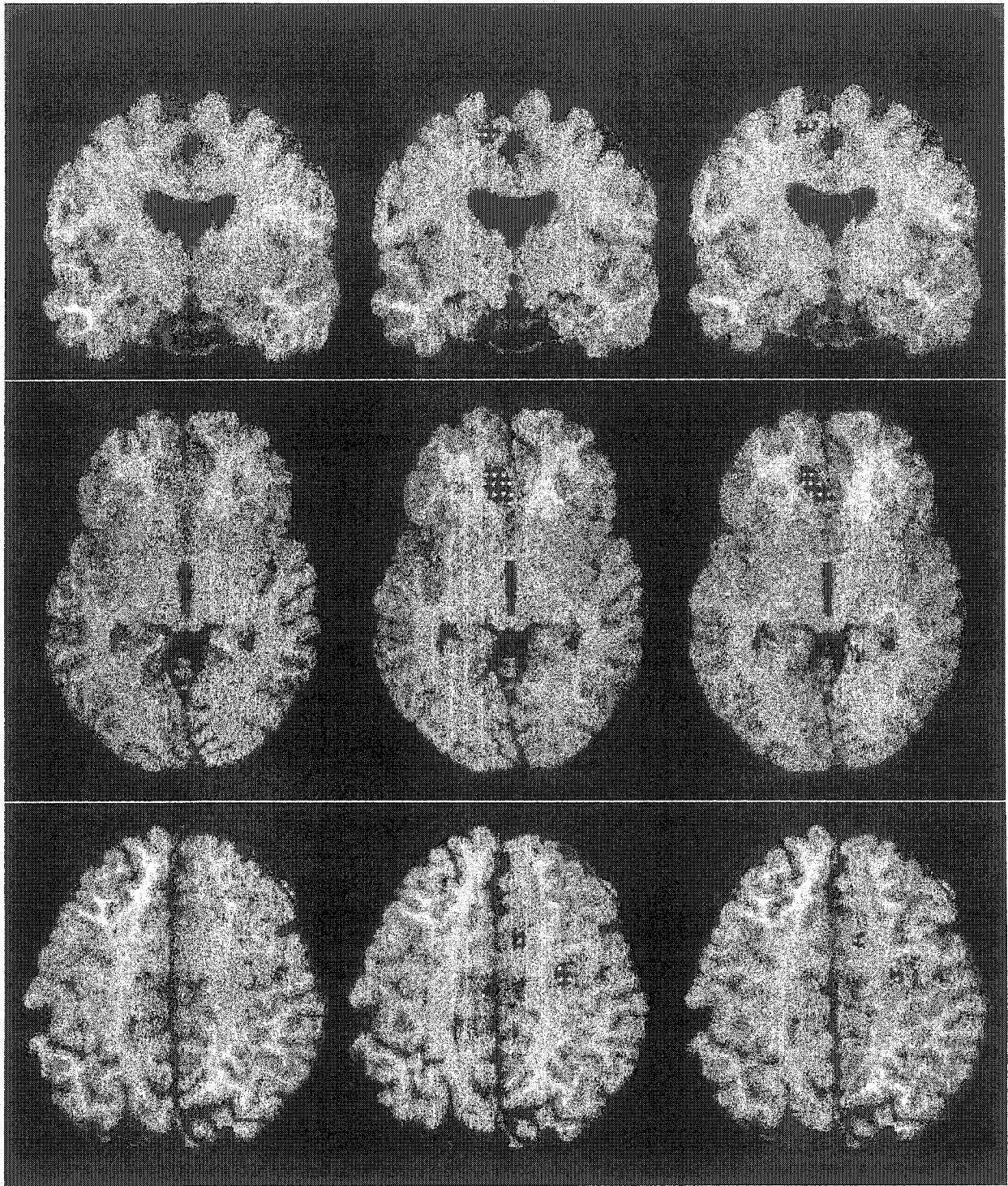


Figure 4b. Three more examples of automated lesion identification. Left: T1-weighted MRI. Center: MRI with manual lesion label. Right: MRI with lesion identified by classifier. Both manual and classifier-generated labels are shown as white dots on a black background. The bottom case shows an example of proper localization but poor coverage.

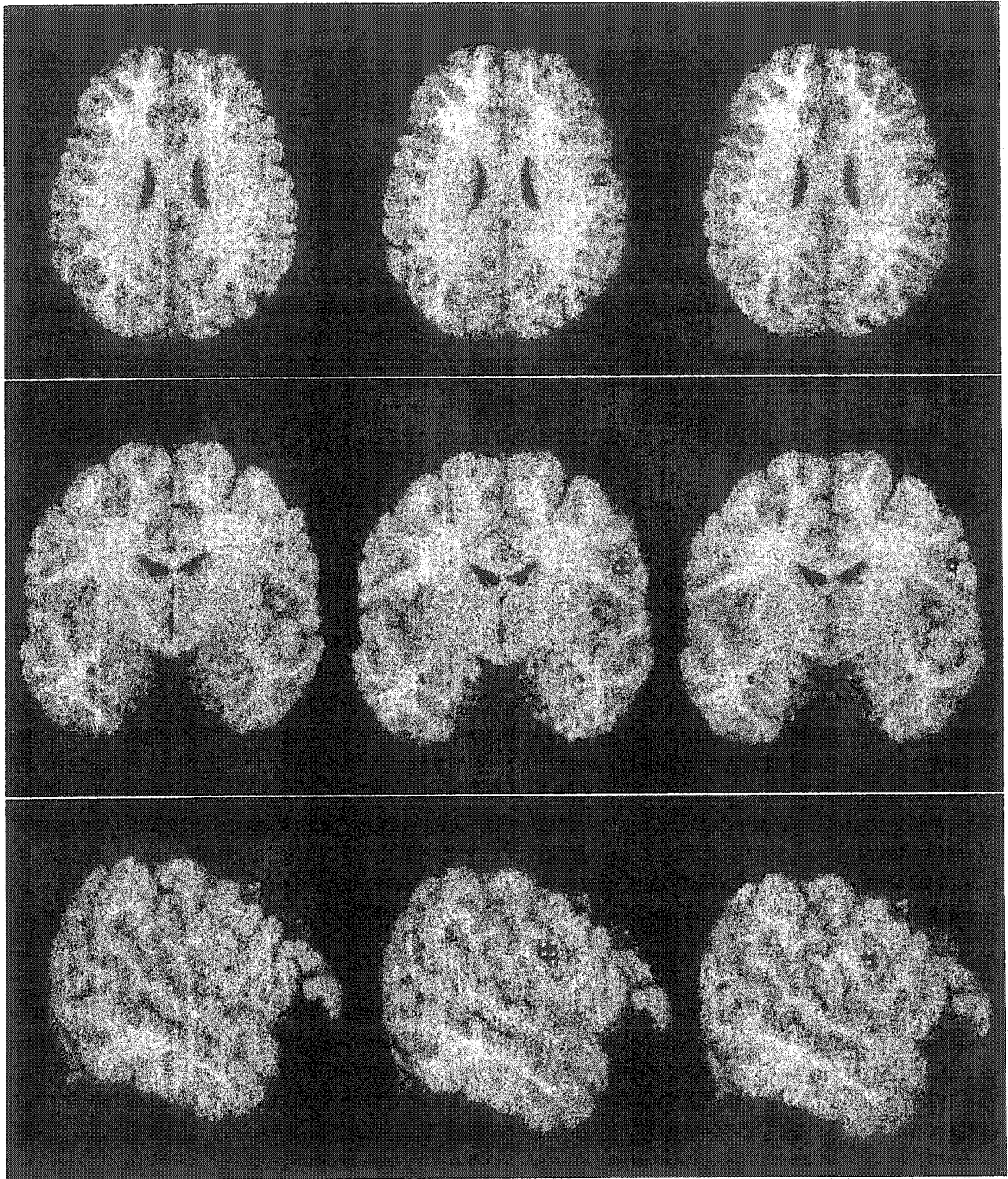


Figure 5. Classification results for a single patient, displayed in the axial, coronal, and sagittal planes. Top row: axial view. Middle row: coronal view. Bottom row: sagittal view. Left column: T1-weighted MRI. Center column: MRI with manual lesion label. Right column: MRI with lesion identified by classifier. Both manual and classifier-generated labels are shown as white dots on a black background.

of abnormal neuronal accumulation and positioning in this area. Increased relative intensity may reflect demyelination and gliosis.

The second set of features, based on texture analysis, incorporated information regarding tissue structure or organization not readily accessible through visual analysis. Our results demonstrated increased angular second momentum in lesions relative to non-lesional cortex, while contrast and difference entropy were decreased. This pattern is consistent with results reported in studies of multiple sclerosis lesions relative to normal appearing white matter (Mathias et al. 1999). From a mathematical standpoint, angular second momentum increases with image homogeneity, contrast increases with local variation of pixel intensity and is largest for local gray level differences, and difference entropy is a measure of general image complexity (Haralick et al. 1973; Lerski et al. 1993). Thus, physiological and mathematical findings indicate that the pattern in texture feature values seen in FCD lesions may reflect changes in image complexity, suggestive of a breakdown of structural integrity due to the disease process.

The potential of our approach to FCD lesion detection is demonstrated by the fact that the classifier found lesions in 15 out of 18 FCD patients (83%), while the standard pre-surgical investigation found lesions in 11 (61%). An advantage of three-dimensional texture analysis, as well as the cortical thickness and gradient models among the first order features, is that they operate in three dimensions. This allows the simultaneous consideration of information from consecutive slices of the brain, whereas a human observer performing standard visual analysis examines the brain volume a slice at a time, and therefore must mentally synthesize information from consecutive slices. Furthermore, second-order texture analysis allows the quantification of the spatial

relationships between gray level intensity pairs. This information may not always be easily appreciated through visual analysis.

In addition to the high sensitivity of lesion detection, another equally important result is that no lesional voxels were identified in any control subject. This finding is especially relevant in light of the fact that in five patients the classifier identified a lesional cluster that did not co-localize with a manual lesion label. Retrospective visual analysis of the individual feature maps input revealed that these lesional clusters exhibited a pattern of features similar to the known FCD lesions; no individual feature unduly influenced the classifier in these cases. However, EEG data from these regions did not exhibit patterns found to be associated with FCD (Gambardella et al. 1996), and retrospective visual analysis of these regions on conventional MRI was also not suggestive of FCD pathology. No clinical or histopathological characteristics that would differentiate these five patients from the remaining 13 were found. Yet the absence of any false positives in control subjects combined with reports of diffuse (Taylor et al. 1971) or non-focal (Prayson et al. 2002) cortical involvement in FCD suggests that these clusters may indeed indicate abnormal regions that are otherwise undetectable via conventional means.

While the classifier successfully located most of the FCD lesions, it tended to partially sample their extent. The definition of the true boundaries of FCD lesions is a difficult task. In particular, there is the possibility that over-estimation of lesion boundaries by the expert observer may account for some of the discrepancy in size between the classifier and manual lesion labels. The use of cortical thickness as an input feature might also have been a contributing factor. Since cortical thickness within WM is

necessarily equal to 0, it is unlikely that a WM voxel will be classified as lesional.

Hence, portions of the lesions within WM go unrecognized by the classifier.

An important issue to be addressed in future research is etiological and diagnostic specificity. All subjects in this study were known to be either normal controls or patients with FCD and no other apparent pathology. However, differential diagnosis between FCD and benign tumors (such as dysembryoplastic neuroepithelial tumors), which may present similarly both clinically and on MRI, is sometimes required. Specificity of the classifier when dealing with a possible differential diagnosis will need to be examined in future studies.

In conclusion, we considered two sources of information regarding FCD lesions. Visually discernable information was provided by computational models of MRI characteristics of FCD, while texture analysis was used to quantify less-available information regarding tissue organization through the quantification of spatial relationships of gray-level intensity pairs. The resulting classifier succeeded in locating most FCD lesions.

REFERENCES

- Antel,S.B., Bernasconi,A., Bernasconi,N., Collins,D.L., Kearney,R.E., Shinghal,R. & Arnold,D.L. 2002. Computational models of MRI characteristics of focal cortical dysplasia improve lesion detection. *Neuroimage In Press*.
- Avoli,M., Bernasconi,A., Mattia,D., Olivier,A. & Hwa,G.G. 1999. Epileptiform discharges in the human dysplastic neocortex: in vitro physiology and pharmacology. *Ann. Neurol.* **46**, 816-826.
- Barkovich,A.J. & Kuzniecky,R.I. 1996. Neuroimaging of focal malformations of cortical development. *J. Clin. Neurophysiol.* **13**, 481-494.
- Barkovich,A.J., Kuzniecky R.I., Jackson G.D., Guerrini R., & Dobyns W.B. 2001. Classification system for malformations of cortical development: update 2001. *Neurology* **57**, 2168-78.

Bastos,A.C., Comeau,R.M., Andermann,F., Melanson,D., Cendes,F., Dubeau,F., Fontaine,S., Tampieri,D. & Olivier,A. 1999. Diagnosis of subtle focal dysplastic lesions: curvilinear reformatting from three-dimensional magnetic resonance imaging. *Ann. Neurol.* **46**, 88-94.

Bernasconi,A., Antel,S.B., Collins,D.L., Bernasconi,N., Olivier,A., Dubeau,F., Pike,G.B., Andermann,F. & Arnold,D.L. 2001. Texture analysis and morphological processing of magnetic resonance imaging assist detection of focal cortical dysplasia in extra-temporal partial epilepsy. *Ann. Neurol.* **49**, 770-775.

Chan,S., Chin,S.S., Nordli,D.R., Goodman,R.R., DeLaPaz,R.L. & Pedley,T.A. 1998. Prospective magnetic resonance imaging identification of focal cortical dysplasia, including the non-balloon cell subtype. *Ann. Neurol.* **44**, 749-757.

Collins,D.L., Neelin,P., Peters,T.M. & Evans,A.C. 1994. Automatic 3D intersubject registration of MR volumetric data in standardized Talairach space. *Journal of Computer Assisted Tomography* **18**, 192-205.

Duda,R.O., Hart,P.E. & Stork,D.G. 2001. *Pattern Classification*. 2nd edn. New York: John Wiley & Sons.

Freeborough,P.A. & Fox,N.C. 1998. MR image texture analysis applied to the diagnosis and tracking of Alzheimer's disease. *IEEE Trans. Med. Imaging* **17**, 475-479.

Gambardella,A., Palmmini,A., Andermann,F., Dubeau,F., da Costa,J.C., Quesney,L.F., Andermann,E. & Olivier,A. 1996. Usefulness of focal rhythmic discharges on scalp EEG of patients with focal cortical dysplasia and intractable epilepsy. *Electroencephalogr. Clin. Neurophysiol.* **98**, 243-249.

Grant,P.E., Vigneron,D.B. & Barkovich,A.J. 1998. High-resolution imaging of the brain. *Magn Reson. Imaging Clin. N. Am.* **6**, 139-154.

Haralick,R.M., Shanmugam,K. & Dinstein,I. 1973. Textural features for image classification. *IEEE Transactions on Systems, Man, and Cybernetics* **SMC-3**, 610-621.

Jones,S.E., Buchbinder,B.R. & Aharon,I. 2000. Three-dimensional mapping of cortical thickness using Laplace's equation. *Hum. Brain Mapp.* **11**, 12-32.

Kassubek,J., Huppertz,H.J., Spreer,J. & Schulze-Bonhage,A. 2002. Detection and localization of focal cortical dysplasia by voxel-based 3-D MRI analysis. *Epilepsia* **43**, 596-602.

Lee,B.C., Schmidt,R.E., Hatfield,G.A., Bourgeois,B. & Park,T.S. 1998. MRI of focal cortical dysplasia. *Neuroradiology* **40**, 675-683.

Lerski,R.A., Straughan,K., Schad,L.R., Boyce,D., Bluml,S. & Zuna,I. 1993. MR image texture analysis--an approach to tissue characterization. *Magn Reson. Imaging* **11**, 873-887.

Mathias,J.M., Tofts,P.S. & Losseff,N.A. 1999. Texture analysis of spinal cord pathology in multiple sclerosis. *Magn Reson. Med.* **42**, 929-935.

Palmini,A., Gambardella,A., Andermann,F., Dubeau,F., da Costa,J.C., Olivier,A., Tampieri,D., Gloor,P., Quesney,F., Andermann,E. & . 1995. Intrinsic epileptogenicity of human dysplastic cortex as suggested by corticography and surgical results. *Ann. Neurol.* **37**, 476-487.

Prayson,R.A., Spreafico,R. & Vinters,H.V. 2002. Pathologic characteristics of the cortical dysplasias. *Neurosurg. Clin. N. Am.* **13**, 17-25.

Schad,L.R., Bluml,S. & Zuna,I. 1993. MR tissue characterization of intracranial tumors by means of texture analysis. *Magn Reson. Imaging* **11**, 889-896.

Sisodiya,S.M. 2000. Surgery for malformations of cortical development causing epilepsy. *Brain* **123**, 1075-1091.

Sled,J.G., Zijdenbos,A.P. & Evans,A.C. 1998. A nonparametric method for automatic correction of intensity nonuniformity in MRI data. *IEEE Transactions on Medical Imaging* **17**, 87-97.

Smith,S. 2000. Robust automated brain extraction. *Sixth International Conference on Functional Mapping of the Human Brain* 625.

Taylor,D.C., Falconer,M.A., Bruton,C.J. & Corsellis,J.A. 1971. Focal dysplasia of the cerebral cortex in epilepsy. *J. Neurol. Neurosurg. Psychiatry* **34**, 369-387.

Woermann,F.G., Free,S.L., Koepp,M.J., Ashburner,J. & Duncan,J.S. 1999. Voxel-by-voxel comparison of automatically segmented cerebral gray matter--A rater-independent comparison of structural MRI in patients with epilepsy. *Neuroimage.* **10**, 373-384.

Yu,O., Mauss,Y., Namer,I.J. & Chambron,J. 2001. Existence of contralateral abnormalities revealed by texture analysis in unilateral intractable hippocampal epilepsy. *Magn Reson. Imaging* **19**, 1305-1310.

Yu,O., Mauss,Y., Zollner,G., Namer,I.J. & Chambron,J. 1999. Distinct patterns of active and non-active plaques using texture analysis on brain NMR images in multiple sclerosis patients: preliminary results. *Magn Reson. Imaging* **17**, 1261-1267.

APPENDIX A. Calculation of texture features from the co-occurrence matrix

$$C_x(i) = \sum_{j=1}^N C(i,j) \quad C_y(i) = \sum_{i=1}^N C(i,j) \quad \begin{array}{l} \mu_x, \sigma_x = \text{mean, standard deviation of } C_x \\ \mu_y, \sigma_y = \text{mean, standard deviation of } C_y \end{array}$$

$$C_{x+y}(k) = \sum_{\substack{i=1 \\ i+j=k}}^N \sum_{j=1}^N C(i,j), \quad k=2,3,\dots,2N$$

$$C_{x-y}(k) = \sum_{\substack{i=1 \\ |i-j|=k}}^N \sum_{j=1}^N C(i,j) \quad k=0,1,\dots,N-1$$

$$\text{Angular second momentum} \quad \sum_{i=1}^N \sum_{j=1}^N \{C(i,j)\}^2$$

$$\text{Contrast} \quad \sum_{n=0}^{N-1} n^2 \left\{ \sum_{\substack{i=1 \\ |i-j|=n}}^N \sum_{j=1}^N C(i,j) \right\}$$

$$\text{Correlation} \quad \sum_{i=1}^N \sum_{j=1}^N \frac{ij C(i,j) - \mu_x \mu_y}{\sigma_x \sigma_y}$$

$$\text{Difference entropy} \quad - \sum_{i=0}^{N-1} C_{x-y}(i) \log \{C_{x-y}(i)\}$$

$$\text{Dissimilarity} \quad \sum_{i=1}^N \sum_{j=1}^N |i-j| C(i,j)$$

$$\text{Entropy} \quad - \sum_{i=1}^N \sum_{j=1}^N C(i,j) \log \{C(i,j)\}$$

$$\text{Inverse difference moment} \quad \sum_{i=1}^N \sum_{j=1}^N \{1+(i-j)^2\}^{-1} C(i,j)$$

$$\text{Sumentropy} \quad \sum_{i=2}^{2N} C_{x+y}(i) \log \{C_{x+y}(i)\}$$

$$\text{Variance} \quad \sum_{i=1}^N \sum_{j=1}^N (i - \mu)^2 C(i,j)$$

5 ■ Summary and Conclusions

5.1 Predicting surgical outcome in TLE patients based on MR data

Our first study applied a Bayesian classifier to MRI and MRSI data of TLE patients to predict surgical outcome. By making predictions of surgical outcome for individual patients, we expanded on previous studies which demonstrated correlations between one or more MR markers and surgical outcome^{9,12,20,31-36}. The few previous studies that have utilized automated classifiers to make individual outcome predictions³⁷⁻³⁹ have focused on classifying patients into seizure free or non seizure free groups following surgery. While seizure free vs. non seizure free is a clinically important distinction to consider, it does not fully address the question of whether surgery is an appropriate option for a patient; surgical resection which fails to completely eliminate seizures yet achieves a near-complete or partial reduction in seizure frequency may still be an appropriate and beneficial course of action for certain patients. Our study addressed this issue by developing two classifiers, one to separate seizure free from non seizure free patients, and one to separate patients achieving a worthwhile reduction in seizure frequency from patients not achieving a worthwhile reduction in seizure frequency. The latter approach makes it possible to identify patients who may not be good surgical candidates. Indeed, this classifier correctly identified 10/16 patients who

did not achieve a worthwhile reduction in seizure frequency. This is an important result given that all 16 of these patients were operated upon, implying that conventional pre-surgical evaluation had identified them as viable surgical candidates.

Future studies should address classification of patients into the individual outcome classes, rather than aggregate groups of seizure free vs. not seizure free, or worthwhile improvement vs. no worthwhile improvement. The key to addressing these issues will be the construction of a considerably larger patient database, providing sufficient sample sizes for each individual outcome class. Training the classifier on additional MR-based information, such as results from texture methods such as those described in other sections of this thesis, may also prove useful for further improving classification accuracy.

5.2 Assisting lesion detection in FCD

Localizing lesions is an important pre-cursor to surgical resection for FCD patient. Papers 2, 3, and 4 traced the development of an automated method for locating FCD lesions on T1-weighted MRI. Paper 2 originated the idea of using of simple image processing techniques to model three common characteristics of FCD as seen on T1 weighted MRI. These techniques were used to create a series of feature maps for each patient, which were then combined and presented for visual analysis. The results of this study represented a significant improvement in the sensitivity of lesion detection compared to the standard expert visual analysis of conventional MRI.

Paper 3 further developed the ideas outlined in paper 2. In paper 3, we selected more sophisticated techniques for modeling two of the three MRI characteristics of FCD.

This was done in order to improve the visibility of FCD lesions by reducing the presence of so-called “potential false positives”, small regions within the cortex that appeared hyperintense and therefore similar to lesional areas on the composite feature map.

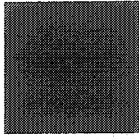
Our results demonstrated improved contrast between lesions and non-lesional cortex, thereby reducing the subjectivity involved in visual lesion detection. Using the techniques outlined in these papers, we increased the sensitivity of lesion detection by 50% relative to conventional MRI. This compares favorably to increases in sensitivity reported in studies employing different approaches, such as curvilinear reconstruction^{57,58}, voxel-based morphometry⁶⁰ and FLAIR images⁵⁶, to aide in lesion detection on MRI.

Papers 2 and 3 were preliminary steps towards the ultimate goal of this project, automated lesion detection. Advantages of an automated method include i) elimination of subjectivity regarding the differentiation of lesions from similar regions in the non-lesional cortex, and ii) it can be applied equally over the whole brain, potentially identifying lesions in regions where human observers may not be inclined to search. Paper 4 approached this task by supplementing the models presented in our previous studies with texture analysis applied to conventional MRI. A Bayesian classifier trained on this data located 17/20 lesions, a sensitivity increase of 35% over visual analysis of conventional MRI. The classifier did not identify any abnormalities in a set of control subjects. This is an important point that differentiates our method from a recently described technique employing voxel-based morphometry to perform automated lesion detection.⁶⁰

Further studies should address ways to increase the extent of the lesion that is identified by the classifier. One approach would be to train the classifier on additional MR results, such as T2 relaxometry, or voxel-based morphometry. An interesting future avenue of exploration would be to perform texture analysis within the curvilinear framework, rather than in the standard 3D orthogonal axes. Application of the statistical, morphological, and texture operators described here to the study of other types of epilepsy or even other neurological disorders would also be interesting to explore in the future.

5.3 Conclusion

In conclusion, the papers constituting this thesis present clinically useful techniques for applying machine learning methods to MR data to assist in the pre-surgical evaluation of epilepsy patients. These methods are intended to be used in conjunction with conventional approaches to improve the identification of lesions and patients who will benefit from surgery.



Bibliography

1. Jones SE, Buchbinder BR, Aharon I. Three-dimensional mapping of cortical thickness using Laplace's equation. *Hum Brain Mapp* 2000; 11(1):12-32.
2. Hauser WA. Epidemiology of epilepsy. *Adv Neurol* 1978; 19:313-39.:313-339.
3. Sander JW, Shorvon SD. Epidemiology of the epilepsies. *J Neurol Neurosurg Psychiatry* 1996; 61(5):433-443.
4. Semah F, Picot MC, Adam C, Broglin D, Arzimanoglou A, Bazin B et al. Is the underlying cause of epilepsy a major prognostic factor for recurrence? *Neurology* 1998; 51(5):1256-1262.
5. Spencer SS, Katz A. Arriving at the surgical options for intractable seizures. *Semin Neurol* 1990; 10(4):422-430.
6. Wiebe S, Blume WT, Girvin JP, Eliasziw M. A randomized, controlled trial of surgery for temporal-lobe epilepsy. *N Engl J Med* 2001; 345(5):311-318.
7. Dam M. Epilepsy surgery. *Acta Neurol Scand* 1996; 94(2):81-87.
8. Engel JJ. Update on surgical treatment of the epilepsies. *Neurology* 1993; 43(8):1612-1617.
9. Arruda F, Cendes F, Andermann F, Dubeau F, Villemure JG, Jones-Gotman M et al. Mesial atrophy and outcome after amygdalohippocampectomy or temporal lobe removal. *Ann Neurol* 1996; 40(3):446-450.
10. Falconer MA, Serafetinides EA, Corsellis JAN. Etiology and pathogenesis of temporal lobe epilepsy. *Archives of Neurology* 1964; 10:233-248.
11. Babb T, Brown WJ. Pathological findings in epilepsy. In: Engel J, Jr., editor. *Surgical treatment of the epilepsies*. New York: Raven Press, 1987: 511-540.
12. Cascino GD, Trenerry MR, Sharbrough FW, So EL, Marsh WR, Strelow DC. Depth electrode studies in temporal lobe epilepsy: relation to quantitative magnetic resonance imaging and operative outcome. *Epilepsia* 1995; 36(3):230-235.
13. Cook MJ, Fish DR, Shorvon SD, Straughan K, Stevens JM. Hippocampal volumetric and morphometric studies in frontal and temporal lobe epilepsy. *Brain* 1992; 115(Pt 4):1001-1015.

14. Lencz T, McCarthy G, Bronen RA, Scott TM, Inserni JA, Sass KJ et al. Quantitative magnetic resonance imaging in temporal lobe epilepsy: relationship to neuropathology and neuropsychological function. *Ann Neurol* 1992; 31(6):629-637.
15. Cendes F, Andermann F, Gloor P, Evans A, Jones-Gotman M, Watson C et al. MRI volumetric measurement of amygdala and hippocampus in temporal lobe epilepsy. *Neurology* 1993; 43(4):719-725.
16. Jack CR, Jr., Trenerry MR, Cascino GD, Sharbrough FW, So EL, O'Brien PC. Bilaterally symmetric hippocampi and surgical outcome. *Neurology* 1995; 45(7):1353-1358.
17. Kuzniecky RI, Burgard S, Bilir E, Morawetz R, Gilliam F, Faught E et al. Qualitative MRI segmentation in mesial temporal sclerosis: clinical correlations. *Epilepsia* 1996; 37(5):433-439.
18. Bernasconi N, Bernasconi A, Andermann F, Dubeau F, Feindel W, Reutens DC. Entorhinal cortex in temporal lobe epilepsy: a quantitative MRI study. *Neurology* 1999; 52(9):1870-1876.
19. Cendes F, Caramanos Z, Andermann F, Dubeau F, Arnold DL. Proton magnetic resonance spectroscopic imaging and magnetic resonance imaging volumetry in the lateralization of temporal lobe epilepsy: a series of 100 patients. *Annals of Neurology* 1997; 42:737-746.
20. Ende GR, Laxer KD, Knowlton RC, Matson GB, Schuff N, Fein G et al. Temporal lobe epilepsy: bilateral hippocampal metabolite changes revealed at proton MR spectroscopic imaging. *Radiology* 1997; 202(3):809-817.
21. Cross JH, Connelly A, Jackson GD, Johnson CL, Neville BG, Gadian DG. Proton magnetic resonance spectroscopy in children with temporal lobe epilepsy. *Ann Neurol* 1996; 39(1):107-113.
22. Hugg JW, Laxer KD, Matson GB, Maudsley AA, Weiner MW. Neuron loss localizes human temporal lobe epilepsy by in vivo proton magnetic resonance spectroscopic imaging. *Ann Neurol* 1993; 34(6):788-794.
23. Laxer KD. Clinical applications of magnetic resonance spectroscopy. *Epilepsia* 1997; 38(Suppl. 4):S13-S17.
24. Vermathen P, Ende G, Laxer KD, Knowlton RC, Matson GB, Weiner MW. Hippocampal N-acetylaspartate in neocortical epilepsy and mesial temporal lobe epilepsy. *Annals of Neurology* 1997; 42:194-199.

25. Cendes F, Andermann F, Preul MC, Arnold DL. Lateralization of temporal lobe epilepsy based on regional metabolic abnormalities in proton magnetic resonance spectroscopic images. *Annals of Neurology* 1994; 35:211-216.
26. Connelly A, Jackson GD, Duncan JS, King MD, Gadian DG. Magnetic resonance spectroscopy in temporal lobe epilepsy. *Neurology* 1994; 44(8):1411-1417.
27. Hetherington H, Kuzniecky R, Pan J, Mason G, Morawetz R, Harris C et al. Proton nuclear magnetic resonance spectroscopic imaging of human temporal lobe epilepsy at 4.1 T. *Annals of Neurology* 1995; 38(3):396-404.
28. Connelly A, Van Paesschen W, Porter DA, Johnson CL, Duncan JS, Gadian DG. Proton magnetic resonance spectroscopy in MRI-negative temporal lobe epilepsy. *Neurology* 1998; 51:61-66.
29. Moffett JR, Namboodiri MA, Cangro CB, Neale JH. Immunohistochemical localization of N-acetylaspartate in rat brain. *Neuroreport* 1991; 2(3):131-134.
30. Simmons ML, Frondoza CG, Coyle JT. Immunocytochemical localization of N-acetyl-aspartate with monoclonal antibodies. *Neuroscience* 1991; 45(1):37-45.
31. Knowlton RC, Laxer KD, Ende G, Hawkins RA, Wong ST, Matson GB et al. Presurgical multimodality neuroimaging in electroencephalographic lateralized temporal lobe epilepsy. *Ann Neurol* 1997; 42(6):829-837.
32. Jack CR, Sharbrough FW, Cascino GD, Hirschorn KA, O'Brien PC, Marsh WR. Magnetic resonance image-based hippocampal volumetry: correlation with outcome after temporal lobectomy. *Annals of Neurology* 1992; 31:138-146.
33. Radhakrishnan K, So EL, Silbert PL, Jack CR, Jr., Cascino GD, Sharbrough FW et al. Predictors of outcome of anterior temporal lobectomy for intractable epilepsy: a multivariate study. *Neurology* 1998; 51(2):465-471.
34. Ho SS, Consalvo D, Gilliam F, Faught E, Bilir E, Morawetz R et al. Amygdala atrophy and seizure outcome after temporal lobe epilepsy surgery. *Neurology* 1998; 51(5):1502-1504.
35. Kuzniecky R, Hugg J, Hetherington H, Martin R, Faught E, Morawetz R et al. Predictive value of 1H MRSI for outcome in temporal lobectomy. *Neurology* 1999; 53(4):694-698.
36. Li LM, Cendes F, Antel SB, Andermann F, Serles W, Dubeau F et al. Prognostic value of proton magnetic resonance spectroscopic imaging for surgical

outcome in patients with intractable temporal lobe epilepsy and bilateral hippocampal atrophy. *Ann Neurol* 2000; 47(2):195-200.

37. Arle JE, Perrine K, Devinsky O, Doyle WK. Neural network analysis of preoperative variables and outcome in epilepsy surgery. *Journal of Neurosurgery* 1999; 90:998-1004.
38. Grigsby J, Kramer RE, Schneiders JL, Gates JR, Brewster SW. Predicting outcome of anterior temporal lobectomy using simulated neural networks. *Epilepsia* 1998; 39(1):61-66.
39. Berg AT, Walczak T, Hirsch LJ, Spencer SS. Multivariable prediction of seizure outcome one year after resective epilepsy surgery: development of a model with independent validation. *Epilepsy Res* 1998; 29(3):185-194.
40. Taylor DC, Falconer MA, Bruton CJ, Corsellis JA. Focal dysplasia of the cerebral cortex in epilepsy. *J Neurol Neurosurg Psychiatry* 1971; 34(4):369-387.
41. Gambardella A, Palmieri A, Andermann F, Dubeau F, da Costa JC, Quesney LF et al. Usefulness of focal rhythmic discharges on scalp EEG of patients with focal cortical dysplasia and intractable epilepsy. *Electroencephalogr Clin Neurophysiol* 1996; 98(4):243-249.
42. Avoli M, Bernasconi A, Mattia D, Olivier A, Hwa GG. Epileptiform discharges in the human dysplastic neocortex: in vitro physiology and pharmacology. *Ann Neurol* 1999; 46(6):816-826.
43. Sisodiya SM. Surgery for malformations of cortical development causing epilepsy. *Brain* 2000; 123(Pt 6):1075-1091.
44. Hong SC, Kang KS, Seo DW, Hong SB, Lee M, Nam DH et al. Surgical treatment of intractable epilepsy accompanying cortical dysplasia. *J Neurosurg* 2000; 93(5):766-773.
45. Hirabayashi S, Binnie CD, Janota I, Polkey CE. Surgical treatment of epilepsy due to cortical dysplasia: clinical and EEG findings. *J Neurol Neurosurg Psychiatry* 1993; 56(7):765-770.
46. Wyllie E. Children with seizures: when can treatment be deferred? *J Child Neurol* 1994; 9 Suppl 2:8-13.:8-13.
47. Keene DL, Jimenez CC, Ventureyra E. Cortical microdysplasia and surgical outcome in refractory epilepsy of childhood. *Pediatr Neurosurg* 1998; 29(2):69-72.
48. Kuzniecky R, Morawetz R, Faught E, Black L. Frontal and central lobe focal dysplasia: clinical, EEG and imaging features. *Dev Med Child Neurol* 1995; 37(2):159-166.

49. Kuzniecky R, Gilliam F, Morawetz R, Faught E, Palmer C, Black L. Occipital lobe developmental malformations and epilepsy: clinical spectrum, treatment, and outcome. *Epilepsia* 1997; 38(2):175-181.
50. Munari C, Lo RG, Minotti L, Cardinale F, Tassi L, Kahane P et al. Presurgical strategies and epilepsy surgery in children: comparison of literature and personal experiences. *Childs Nerv Syst* 1999; 15(4):149-157.
51. Otsubo H, Hwang PA, Jay V, Becker LE, Hoffman HJ, Gilday D et al. Focal cortical dysplasia in children with localization-related epilepsy: EEG, MRI, and SPECT findings. *Pediatr Neurol* 1993; 9(2):101-107.
52. Palmi A, Andermann F, Olivier A, Tampieri D, Robitaille Y. Focal neuronal migration disorders and intractable partial epilepsy: results of surgical treatment. *Ann Neurol* 1991; 30(6):750-757.
53. Palmi A, Gambardella A, Andermann F, Dubeau F, da Costa JC, Olivier A et al. Operative strategies for patients with cortical dysplastic lesions and intractable epilepsy. *Epilepsia* 1994; 35 Suppl 6:S57-71.:S57-S71.
54. Firlik KS, Spencer DD. Surgery for focal cortical dysplasia. *Neurosurg Clin N Am* 2002; 13(1):93-102, ix.
55. Lee BC, Schmidt RE, Hatfield GA, Bourgeois B, Park TS. MRI of focal cortical dysplasia. *Neuroradiology* 1998; 40(10):675-683.
56. Chan S, Chin SS, Nordli DR, Goodman RR, DeLaPaz RL, Pedley TA. Prospective magnetic resonance imaging identification of focal cortical dysplasia, including the non-balloon cell subtype. *Ann Neurol* 1998; 44(5):749-757.
57. Bastos AC, Comeau RM, Andermann F, Melanson D, Cendes F, Dubeau F et al. Diagnosis of subtle focal dysplastic lesions: curvilinear reformatting from three-dimensional magnetic resonance imaging. *Ann Neurol* 1999; 46(1):88-94.
58. Montenegro MA, Li LM, Guerreiro MM, Guerreiro CA, Cendes F. Focal cortical dysplasia: improving diagnosis and localization with magnetic resonance imaging multiplanar and curvilinear reconstruction. *J Neuroimaging* 2002; 12(3):224-230.
59. Woermann FG, Free SL, Koepp MJ, Ashburner J, Duncan JS. Voxel-by-voxel comparison of automatically segmented cerebral gray matter--A rater-independent comparison of structural MRI in patients with epilepsy. *Neuroimage* 1999; 10(4):373-384.

60. Kassubek J, Huppertz HJ, Spreer J, Schulze-Bonhage A. Detection and localization of focal cortical dysplasia by voxel-based 3-D MRI analysis. *Epilepsia* 2002; 43(6):596-602.
61. Zavaljevski A, Dhawan AP, Gaskil M, Ball W, Johnson JD. Multi-level adaptive segmentation of multi-parameter MR brain images. *Comput Med Imaging Graph* 2000; 24(2):87-98.
62. Held K, Kops ER, Krause BJ, Wells WM, III, Kikinis R, Muller-Gartner HW. Markov random field segmentation of brain MR images. *IEEE Trans Med Imaging* 1997; 16(6):878-886.
63. Gerig G, Martin J, Kikinis R, Kubler O, Shenton M, Jolesz FA. Unsupervised tissue type segmentation of 3D dual-echo MR head data. *Image and Vision Computing* 1992; 10(6):349-360.
64. Ozkan M, Dawant BM, Maciunas RJ. Neural-network-based segmentation of multi-modal medical images: a comparative and prospective study. *IEEE Transactions on Medical Imaging* 2002; 12:534-544.
65. Momenan R, Hommer D, Rawlings R, Ruttimann U, Kerich M, RioD. Intensity-adaptive segmentation of single-echo T1-weighted magnetic resonance images. *Human Brain Mapping* 1997; 5:194-205.
66. Schnack HG, Hulshoff Pol HE, Baare WF, Staal WG, Viergever MA, Kahn RS. Automated separation of gray and white matter from MR images of the human brain. *Neuroimage* 2001; 13(1):230-237.
67. Shattuck DW, Sandor-Leahy SR, Schaper KA, Rottenberg DA, Leahy RM. Magnetic resonance image tissue classification using a partial volume model. *Neuroimage* 2001; 13(5):856-876.
68. Rajapakse JC, Giedd JN, Rapoport JL. Statistical approach to segmentation of single-channel cerebral MR images. *IEEE Trans Med Imaging* 1997; 16(2):176-186.
69. Ruan S, Jaggi C, Xue J, Fadili J, Bloyet D. Brain tissue classification of magnetic resonance images using partial volume modeling. *IEEE Trans Med Imaging* 2000; 19(12):1179-1187.
70. MacDonald D, Kabani N, Avis D, Evans AC. Automated 3-D extraction of inner and outer surfaces of cerebral cortex from MRI. *Neuroimage* 2000; 12(3):340-356.
71. Fischl B, Dale AM. Measuring the thickness of the human cerebral cortex from magnetic resonance images. *Proc Natl Acad Sci U S A* 2000; 97(20):11050-11055.

72. Dale AM, Fischl B, Sereno MI. Cortical surface-based analysis. I. Segmentation and surface reconstruction. *Neuroimage* 1999; 9(2):179-194.
73. Magnotta VA, Andreasen NC, Schultz SK, Harris G, Cizadlo T, Heckel D et al. Quantitative in vivo measurement of gyrification in the human brain: changes associated with aging. *Cereb Cortex* 1999; 9(2):151-160.
74. A PDE approach for measuring tissue thickness.: 2001.
75. Heyden A, editor. A PDE approach for thickness, correspondance, and gridding of annular tissues. 02; Berlin: Springer-Verlag, 2002.
76. Ratnanather JT, Botteron KN, Nishino T, Massie AB, Lal RM, Patel SG et al. Validating cortical surface analysis of medial prefrontal cortex. *Neuroimage* 2001; 14(5):1058-1069.
77. Cook MJ, Free SL, Manford MR, Fish DR, Shorvon SD, Stevens JM. Fractal description of cerebral cortical patterns in frontal lobe epilepsy. *Eur Neurol* 1995; 35(6):327-335.
78. Julesz B. Visual pattern discrimination. *IRE Transactions on Information Theory* 1962; IT-8:84-92.
79. Julesz B. A theory of preattentive texture discrimination based on first-order statistics of textons. *Biological Cybernetics* 1981; 41:131-138.
80. Julesz B. Nonlinear and cooperative processes in texture perception. In: Werner TP, Reichardt E, editors. *Theoretical Approaches to Neurobiology*. Cambridge, MA: MIT Press, 1981: 93-108.
81. Julesz B. Textons, the elements of texture perception, and their interactions. *Nature* 1981; 290:91-97.
82. Julesz B. Experiments in the visual perception of texture. *Scientific American* 1975; 232:34-43.
83. Julesz B, Gilbert EN, Shepp LA, Frisch HL. Inability of humans to discriminate between visual textures that agree in second order statistics-revisited. *Perception* 1973; 2:391-405.
84. Haralick RM, Shanmugam K, Dinstein I. Textural features for image classification. *IEEE Transactions on Systems, Man, and Cybernetics* 1973; SMC-3(6):610-621.
85. James D, Clymer BD, Schmalbrock P. Texture detection of simulated microcalcification susceptibility effects in magnetic resonance imaging of breasts. *J Magn Reson Imaging* 2001; 13(6):876-881.

86. Kim JK, Park HW. Statistical textural features for detection of microcalcifications in digitized mammograms. *IEEE Trans Med Imaging* 1999; 18(3):231-238.
87. Nishikawa RM, Giger ML, Doi K, Vyborny CJ, Schmidt RA. Computer-aided detection of clustered microcalcifications on digital mammograms. *Med Biol Eng Comput* 1995; 33(2):174-178.
88. Mudigonda NR, Rangayyan RM, Desautels JE. Gradient and texture analysis for the classification of mammographic masses. *IEEE Trans Med Imaging* 2000; 19(10):1032-1043.
89. Sahiner B, Chan HP, Petrick N, Helvie MA, Goodsitt MM. Computerized characterization of masses on mammograms: the rubber band straightening transform and texture analysis. *Med Phys* 1998; 25(4):516-526.
90. Wei D, Chan HP, Petrick N, Sahiner B, Helvie MA, Adler DD et al. False-positive reduction technique for detection of masses on digital mammograms: global and local multiresolution texture analysis. *Med Phys* 1997; 24(6):903-914.
91. Chan HP, Sahiner B, Petrick N, Helvie MA, Lam KL, Adler DD et al. Computerized classification of malignant and benign microcalcifications on mammograms: texture analysis using an artificial neural network. *Phys Med Biol* 1997; 42(3):549-567.
92. Thiele DL, Kimme-Smith C, Johnson TD, McCombs M, Bassett LW. Using tissue texture surrounding calcification clusters to predict benign vs malignant outcomes. *Med Phys* 1996; 23(4):549-555.
93. Wei D, Chan HP, Helvie MA, Sahiner B, Petrick N, Adler DD et al. Classification of mass and normal breast tissue on digital mammograms: multiresolution texture analysis. *Med Phys* 1995; 22(9):1501-1513.
94. Gupta R, Undrill PE. The use of texture analysis to delineate suspicious masses in mammography. *Phys Med Biol* 1995; 40(5):835-855.
95. Zhang J, Chang CI, Miller SJ, Kang KA. A feasibility study of multispectral image analysis of skin tumors. *Biomed Instrum Technol* 2000; 34(4):275-282.
96. Murali A, Stoecker WV, Moss RH. Detection of solid pigment in dermatoscopy images using texture analysis. *Skin Res Technol* 2000; 6(4):193-198.
97. Ji Q, Engel J, Craine E. Texture analysis for classification of cervix lesions. *IEEE Trans Med Imaging* 2000; 19(11):1144-1149.

98. Chappard D, Chennebault A, Moreau M, Legrand E, Audran M, Basle MF. Texture analysis of X-ray radiographs is a more reliable descriptor of bone loss than mineral content in a rat model of localized disuse induced by the Clostridium botulinum toxin. *Bone* 2001; 28(1):72-79.
99. Cortet B, Bourel P, Dubois P, Boutry N, Cotten A, Marchandise X. CT scan texture analysis of the distal radius: influence of age and menopausal status. *Rev Rhum Engl Ed* 1998; 65(2):109-118.
100. Ferdeghini EM, Pinamonti B, Picano E, Lattanzi F, Bussani R, Slavich G et al. Quantitative texture analysis in echocardiography: application to the diagnosis of myocarditis. *J Clin Ultrasound* 1991; 19(5):263-270.
101. Bae RY, Belohlavek M, Greenleaf JF, Seward JB. Myocardial contrast echocardiography: texture analysis for identification of nonperfused versus perfused myocardium. *Echocardiography* 2001; 18(8):665-672.
102. Herlidou S, Rolland Y, Bansard JY, Le Rumeur E, de Certaines JD. Comparison of automated and visual texture analysis in MRI: characterization of normal and diseased skeletal muscle. *Magn Reson Imaging* 1999; 17(9):1393-1397.
103. Ferdeghini EM, Morelli G, Distanto A, Giannotti P, Benassi A. Assessment of normal testis growth by quantitative texture analysis of 2-D echo images. *Med Eng Phys* 1995; 17(7):523-528.
104. Gilles F, Gentile A, Le D, V, Kahn E. Use of texture parameters in the classification of soft tissue tumors. *Anal Quant Cytol Histol* 1994; 16(5):315-320.
105. Atlamazoglou V, Yova D, Kavantzias N, Loukas S. Texture analysis of fluorescence microscopic images of colonic tissue sections. *Med Biol Eng Comput* 2001; 39(2):145-151.
106. Esgiar AN, Naguib RN, Bennett MK, Murray A. Automated feature extraction and identification of colon carcinoma. *Anal Quant Cytol Histol* 1998; 20(4):297-301.
107. Jirak D, Dezortova M, Taimr P, Hajek M. Texture analysis of human liver. *J Magn Reson Imaging* 2002; 15(1):68-74.
108. Basset O, Sun Z, Mestas JL, Gimenez G. Texture analysis of ultrasonic images of the prostate by means of co-occurrence matrices. *Ultrason Imaging* 1993; 15(3):218-237.
109. van GB, Katsuragawa S, ter H, Doi K, Viergever MA. Automatic detection of abnormalities in chest radiographs using local texture analysis. *IEEE Trans Med Imaging* 2002; 21(2):139-149.

110. COST B11: Quantification of Magnetic Resonance Image Texture. 2002.
Ref Type: Internet Communication
111. Podo F, Orr JS, Bovee WMMJ, de Certaines JD, Leibfritz D. I. Introduction, objectives, and activities. *Magnetic Resonance Imaging* 1993; 11:809-815.
112. Freeborough PA, Fox NC. MR image texture analysis applied to the diagnosis and tracking of Alzheimer's disease. *IEEE Trans Med Imaging* 1998; 17(3):475-479.
113. Mathias JM, Tofts PS, Losseff NA. Texture analysis of spinal cord pathology in multiple sclerosis. *Magn Reson Med* 1999; 42(5):929-935.
114. Yu O, Mauss Y, Zollner G, Namer IJ, Chambron J. Distinct patterns of active and non-active plaques using texture analysis on brain NMR images in multiple sclerosis patients: preliminary results. *Magn Reson Imaging* 1999; 17(9):1261-1267.
115. Schad LR, Bluml S, Zuna I. MR tissue characterization of intracranial tumors by means of texture analysis. *Magn Reson Imaging* 1993; 11(6):889-896.
116. Lerski RA, Straughan K, Schad LR, Boyce D, Bluml S, Zuna I. MR image texture analysis--an approach to tissue characterization. *Magn Reson Imaging* 1993; 11(6):873-887.
117. Yu O, Mauss Y, Namer IJ, Chambron J. Existence of contralateral abnormalities revealed by texture analysis in unilateral intractable hippocampal epilepsy. *Magn Reson Imaging* 2001; 19(10):1305-1310.
118. Kjaer L, Ring P, Thomsen C, Henriksen O. Texture analysis in quantitative MR imaging. Tissue characterisation of normal brain and intracranial tumours at 1.5 T. *Acta Radiol* 1995; 36(2):127-135.
119. Kovalev VA, Kruggel F, Gertz HJ, von Cramon DY. Three-dimensional texture analysis of MRI brain datasets. *IEEE Trans Med Imaging* 2001; 20(5):424-433.
120. Bayes T. An essay towards solving a problem in the doctrine of chances. *Philosophical transactions of the royal society (London)* 1763; 53:370-418.
121. Mitchell TM. *Machine Learning*. Boston: WCB McGraw-Hill, 1997.
122. Duda RO, Hart PE, Stork DG. *Pattern Classification*. 2nd ed. New York: John Wiley & Sons, 2001.

123. Domingos P, Pazzani M. Beyond independence: Conditions for the optimality of the simple Bayesian classifier. Proceedings of the 13th International Conference on Machine Learning 1996;105-112.
124. Mehrubeoglu M, Kehtarnavaz N, Marquez G, Duvic M, Wang LV. Skin lesion classification using oblique-incidence diffuse reflectance spectroscopic imaging. Appl Opt 2002; 41(1):182-192.
125. Testi D, Cappello A, Chiari L, Viceconti M, Gnudi S. Comparison of logistic and Bayesian classifiers for evaluating the risk of femoral neck fracture in osteoporotic patients. Med Biol Eng Comput 2001; 39(6):633-637.
126. Kukar M, Kononenko I, Silvester T. Machine learning in prognosis of the femoral neck fracture recovery. Artif Intell Med 1996; 8(5):431-451.
127. Zelic I, Kononenko I, Lavrac N, Vuga V. Induction of decision trees and Bayesian classification applied to diagnosis of sport injuries. J Med Syst 1997; 21(6):429-444.
128. Raymond B, Taverner D, Nandagopal D, Mazumdar J. Classification of heart rate variability in patients with mild hypertension. Australas Phys Eng Sci Med 1997; 20(4):207-213.
129. Andersen MB, Gregersen H, Rosenfalck A, Stodkilde-Jorgensen H. Discrimination between artefacts and contractions in pressure signals from the gastrointestinal tract by pattern recognition method. Med Biol Eng Comput 1996; 34(2):127-132.
130. Gade J, Rosenfalck A, Bendtson I. Detection of EEG patterns related to nocturnal hypoglycemia. Methods Inf Med 1994; 33(1):153-156.
131. Schmitt HP, Oberwittler C. Computer-aided classification of malignancy in astrocytomas. II. The value of categorically evaluated histologic and non-histologic features for a numerical classifier. Anal Cell Pathol 1992; 4(6):409-419.
132. Welch AJ, Richardson PC, Mockford JN. Classification of sleep stage with period analysis features derived from the EEG. Aviat Space Environ Med 1978; 49(2):409-414.

The undersigned agree to waive the copyright for the following manuscript for the purposes of inclusion in the doctoral thesis of Samson Antel, Department of Biomedical Engineering:

Antel SB et al, "Automated detection of focal cortical dysplasia lesions using computational models of their MRI characteristics and texture analysis".

Authors:

SB Antel

DL Collins

N Bernasconi

R Shinghal

RE Kearney

DL Arnold

A Bernasconi

PERMISSIONS DEPARTMENT



March 13, 2003

Samson Ansel
Montreal Neurological Institute
3801 University St.
Montreal PQ H3A 2B4
Canada
VIA FACSIMILE: 514 398 2975

Dear Samson Ansel:

RE: Your February 27, 2003 request for permission to republish pages 770-775 from *Annals of Neurology* (2001) Vol. 49, No.6. This material will appear in your forthcoming dissertation, to be published by McGill University in 2003.

1. Permission is granted for this use, except that if the material appears in our work with credit to another source, you must also obtain permission from the original source cited in our work.
2. Permitted use is limited to your edition described above, and does not include the right to grant others permission to photocopy or otherwise reproduce this material except for versions made for use by visually or physically handicapped persons. Up to five copies of the published thesis may be photocopied by a microfilm company.
3. Appropriate credit to our publication must appear on every copy of your thesis, either on the first page of the quoted text, in a separate acknowledgment page, or figure legend. The following components must be included: Title, author(s) and /or editor(s), journal title (if applicable), Copyright © (year and owner). Reprinted by permission of John Wiley & Sons, Inc.
4. This license is non-transferable. This license is for non-exclusive English language print rights and microfilm storage rights by McGill University only, throughout the world. *For translation rights, please reapply for a license when you have plans to translate your work into a specific language.*

Sincerely,

Paulette Goldwaber
Senior Permissions Assn.

8 March 2003

Our ref: HW/vm/mar03.j123

Samson Antel

Email:

Dear Mr Antel

NEUROIMAGE, Vol 17, 2002, pp 1755-1760, Antel et al: "Computational models of MRI characteristics of focal cortical dysplasia ..."

As per your letter dated 27 February 2003, we hereby grant you permission to reprint the aforementioned material at no charge in your thesis subject to the following conditions:

1. If any part of the material to be used (for example, figures) has appeared in our publication with credit or acknowledgement to another source, permission must also be sought from that source. If such permission is not obtained then that material may not be included in your publication/copies.
2. Suitable acknowledgment to the source must be made, either as a footnote or in a reference list at the end of your publication, as follows:

"Reprinted from Publication title, Vol number, Author(s), Title of article, Pages No., Copyright (Year), with permission from Elsevier".
3. Reproduction of this material is confined to the purpose for which permission is hereby given.
4. This permission is granted for non-exclusive world English rights only. For other languages please reapply separately for each one required. Permission excludes use in an electronic form. Should you have a specific electronic project in mind please reapply for permission.
5. This includes permission for the National Library of Canada to supply single copies, on demand, of the complete thesis. Should your thesis be published commercially, please reapply for permission.

Yours sincerely

Helen Wilson
Rights Manager

Your future requests will be handled more quickly if you complete the online form at www.elsevier.com/homepage/questbook/?form=permis